

Structure determination of piezoelectric materials at extreme conditions

Dissertation

zur Erlangung des Doktorgrades
der Fakultät für Geowissenschaften
der Ludwig- Maximilians- Universität
München

vorgelegt von

Anzhela Pavlovska

München 2002

eingereicht am 15. April

Structure determination of piezoelectric materials at extreme conditions

Dissertation

zur Erlangung des Doktorgrades
der Fakultät für Geowissenschaften
der Ludwig- Maximilians- Universität
München

vorgelegt von

Anzhela Pavlovska

Berichterstatter:	Dr. S. Werner
Berichterstatter:	Prof. W. Moritz
Tag der Einreichung:	15. April
Tag der mündliche Prüfung:	04.Juli

München 2002

Zusammenfassung

Diese Arbeit präsentiert Ergebnisse an piezoelektrischen Materialien aus der Langasitfamilie, die unter extremen Bedingungen untersucht wurden. Die Einkristalle aus dieser Familie, vor allem $\text{La}_3\text{Nb}_{0,5}\text{Ga}_{5,5}\text{O}_{14}$ (LNG) und $\text{La}_3\text{Ta}_{0,5}\text{Ga}_{5,5}\text{O}_{14}$ (LTG), sind vielversprechende Materialien für Oberflächenwellen (OFW) –Substratmaterialien, die in der mobilen Kommunikationstechnik der Frequenzsteuerungsgeräte (mobile Kommunikation, Sensoren, usw.) und bei Hochtemperatur- OFW- Anwendung finden. Mit LNG und LTG OFW-Sensorelementen können physikalische Meßgrößen, wie Druck und Temperatur erfaßt werden. Aus diesem Grund sind die Strukturuntersuchungen an LNG und LTG bei verschiedenen Drucken und Temperaturen extrem wichtig.

Die Struktur von LNG und LTG ist unter normalen Bedingungen trigonal mit der Raumgruppe $P321$.

In der Struktur sind die schweren Atome polyedrisch von Sauerstoffatomen koordiniert. Vier Polyedertypen bilden decaedrisch-oktaedrische und tetraedrische Schichten. Diese sind in einer A-B- Stapelfolge senkrecht zur c -Achse angeordnet.

Die Kristallstrukturen von LNG und LTG wurden mittels Röntgenstrukturanalyse an LNG- und LTG- Einkristallen in Hochdruck- Diamant -Stempel Zellen unter Druck bis 23GPa untersucht. Die Proben für diese Forschungsarbeit wurden von den Forschungsgruppen von B. V. Mill (Rußland) und J. Bohm (Deutschland) freundlicherweise zur Verfügung gestellt. Als druckübertragende Medien wurden Alkohol und Helium benutzt. α - Quarz Kristalle und die Rubinfluoreszenzmethode wurden zur Druckmessung herangezogen. Die Experimente mit Röntgenstrahlung wurden im eigenen Labor und am Hamburger Synchrotronstrahlungslabor (HASYLAB, Beamline D-3) durchgeführt.

Die Gitterkonstanten und Reflexintensitäten von LNG und LTG wurden unter Drucken bis 22,8 beziehungsweise 16.7GPa gesammelt. Innerhalb des erforschten Druckbereichs nimmt das c/a - Verhältnis von 0,6232 bis 0,6503 für LNG und von 0,6227 bis 0,6350 für LTG zu. Folglich ist die a -Achse die an stärksten komprimierte Richtung in beiden Substanzen. Damit zeigen LNG und LTG unter Druck ein anisotropes Verhalten, das durch unterschiedliche Bindungsstärken in den Richtungen parallel zu den a - beziehungsweise c - Achsen bedingt ist. Unter hydrostatischem Druck ist die Komprimierung der c - Richtung (also zwischen den Schichten) steif, was wegen der weniger flexiblen Verknüpfung der Polyeder (gemeinsame Kanten) verständlich ist. Demgegenüber ist die Komprimierung innerhalb der ab - Ebene (also

innerhalb der Schichten) größer und kann hauptsächlich durch die abnehmenden Volumina und Verzerrungen der Polyeder erreicht werden.

Weil die Kristallstrukturen von LNG und LTG wegen der hohen Symmetrie und der Polyederkopplungen sehr steif sind, führt die Komprimierung dieser Strukturen zu einer Zunahme der internen Spannungen und endet bei einem Druck von 12.4(3)GPa für LNG und 11.7(3)GPa für LTG mit einem Phasenübergang in Strukturen mit niedrigerer Symmetrie. In dem untersuchten Druckbereich sind die Kompressibilitäten entlang der *c*-Achse fast identisch für LNG und LTG. Andererseits sind die Druckabhängigkeiten der *a* Gitterparameter dieser Materialien nur für die Ausgangsphase ähnlich, während die Achsenkompressibilitäten für die Hochdruckphasen von LNG und von LTG unterschiedlich sind. Die Volumenkompressibilitäten des trigonalen LNG und LTG sind 0.007GPa^{-1} , die entsprechenden Kompressionsmodule sind 145(3)GPa und 144(2)GPa.

Der Kompressionsmechanismus von LNG und LTG kann wie folgt beschrieben werden:

Eine Erhöhung des Drucks verursacht eine Reduzierung der Gittervolumina von LNG und LTG. Folglich verringern sich die Abstände zwischen den Ionen. Auf diese Weise werden die größten Kationen (La^{3+}) innerhalb der *ab*- Fläche verschoben, um die Abstände zwischen den positiv geladenen benachbarten Ionen ($\text{Ga}^{3+}/\text{Nb}^{5+}(\text{Ta}^{5+})$) zu maximieren. Auf die gleiche Weise bewegen sich die tetraedrisch koordinierten Ga^{3+} -Ionen. Wegen der Anionen-Kationenbindungsverkürzung versuchen die Polyeder zu rotieren. Nun werden diese Drehungen durch die gemeinsamen Ecken und/oder Kanten der benachbarten Polyeder behindert. Außerdem werden diese Bewegungen durch die geringe Flexibilität begrenzt, die durch die Symmetrie (zwei- und drei- zählige Achsen) verursacht wird. So resultiert die Komprimierung hauptsächlich aus Verkleinerungen der Polyedervolumina. Folglich steigen unter zunehmenden Druck die Spannungen innerhalb der Polyeder, vor allem innerhalb der kleinsten Polyeder (GaO_4 -Tetraeder), wegen deren geringer Flexibilität. Bei einem Druck von 12(1)GPa resultiert die Komprimierung von LNG und LTG in einer Transformation aus der Hochsymmetriephase in eine Niedersymmetriephase. Es kann gefolgert werden, daß dieser Phasenübergang durch die Zunahme der Spannungen innerhalb der Polyeder verursacht wird. Die Hochdruckphase ist verzerrter als die ursprüngliche Phase und beinhaltet mehr Freiheitsgrade für weitere Komprimierungen.

Die Hochdruckphasen von LNG und von LTG können in Strukturmodellen mit monokliner Symmetrie (Raumgruppe *A2*) verfeinert werden. Die Kompressionsmodule sind $B_0=93(2)\text{GPa}$ und $B_0=128(12)\text{GPa}$ für die Hochdruckphasen von LNG beziehungsweise von LTG. Die entsprechenden Kompressibilitäten der Hochdruckphasen sind 0.011GPa^{-1} für LNG und

0.008GPa^{-1} für LTG. Somit zeigen die Hochdruckphasen unterschiedliche Kompressibilität, die durch eine Nb^{5+} - Ta^{5+} Substitution gut erklärt werden kann. Die Kompressibilität der Hochdruckphase von LNG ist größer als der entsprechende Wert für das Hochdruckpolymorph von LTG. Dieses Phänomen kann durch die größere Verzerrung von NbO_6 - Polyedern im Vergleich zu TaO_6 - Polyedern gut erklärt werden, welche durch die höhere Polarisation der Sauerstoffanordnung bei Nb^{5+} -Kationen verursacht wird.

Außerdem sind die Kompressibilitäten der Hochdruckphasen größer als die entsprechenden Werte für die Ausgangsphasen von LNG und LTG. Die Beobachtung einer Zunahme der Kompressibilität weist auf zusätzliche Polyederverkippungen hin. In den meisten Fällen ergibt sich die zusätzliche Freiheit aus dem Symmetriebruch. Das erklärt eine (auf den ersten Blick ziemlich unerwartete) erhöhte Kompressibilität der Hochdruckphase. Zusätzlich kann sich durch ein anomales Elastizitätsverhalten eine Steigerung der Kompressibilität der Hochdruckphase ergeben.

Bei einer Zunahme des Druckes über 22GPa hinaus wird die Komprimierung der monoklinen Kristallstruktur von LGN vermutlich zu einer drastischen Strukturänderung führen, die von Änderungen der Koordinationszahlen begleitet ist. Wahrscheinlich werden ähnliche Prozesse auch im LTG statt finden, jedoch unter höherem Druck.

Im folgenden Teil dieser Arbeit wird die thermische Expansion der Gitterparameter von LNG, LTG und $\text{La}_3\text{SbZn}_3\text{GeO}_{14}$ (LSZG) dargestellt. Die Hochtemperaturmessungen wurden mit dem Pulverdiffraktometer im HASYLAB an der beamline B2 durchgeführt.

Die Temperaturabhängigkeit der Gitterparameter von LNG und von LTG wurde an polykristallinem Material bei Temperaturen von Raumtemperatur bis 850°C durchgeführt. Die thermischen Expansionen der Gitterparameter von LNG und LTG sind in diesem Temperaturbereich fast identisch. Die thermischen Expansionskoeffizienten des Gittervolumens a_v (24°C - 850°C) von LNG und LTG betragen $22.563(7)\times 10^{-6}\text{C}^{-1}$ beziehungsweise $20.651(7)\times 10^{-6}\text{C}^{-1}$. Deutliche Veränderungen der Temperaturabhängigkeit der Gitterparameter werden für die a - Richtung beobachtet. Folglich ist das Verhalten dieser Materialien bei thermischer Expansion ebenso wie bei Komprimierung anisotrop. Für einen Vergleich des Einflusses von Druck und Temperatur auf die Gitterparameter von LNG beziehungsweise LTG wurden die Druck und Temperatur- Abhängigkeiten des c/a -Verhältnisses gemeinsam aufgetragen. Es zeigt sich, dass eine lineare Abhängigkeit besteht. Daraus läßt sich ableiten, dass die Änderung der Gitterparameter von LNG (LTG) während der Abkühlung von 850°C auf Raumtemperatur einer Änderung der Gitterparameter von LNG (LTG) unter Zunahme des Drucks um 1.4GPa entspricht.

Die Substanz LSZG, welche in dieser Arbeit untersucht wurde, ist ein weiteres Mitglied der Langasitfamilie. LSZG kristallisiert in der monoklinen Symmetrie, Raumgruppe A2.

Die Temperaturabhängigkeit der Gitterparameter der monoklinen Phase von LSZG wurden mittels der Röntgenbeugung an polykristallinem LSZG bei Temperaturen von Raumtemperatur bis 800°C untersucht. Bei Temperaturen oberhalb 250(50)°C wurde ein Phasenübergang erster Ordnung festgestellt, welcher sich in Sprüngen der Temperaturabhängigkeiten der Gitterparameter des LSZG äußert.

Die monokline Struktur der bei Raumtemperatur und Normaldruck stabilen Phase des LSZG entspricht der der Hochdruckphase von LNG beziehungsweise LTG. Es ist bekannt, daß die Änderungen der Kristallstrukturen bei steigenden Drucken und Temperaturen gegenläufig sind. Aus diesem Grund wird vermutet daß sich die monokline Kristallstruktur des LSZG bei Temperaturen oberhalb von 250(50)°C in eine trigonale Kristallstruktur (Raumgruppe P321) umwandelt, welche der Normaldruckphase von LNG beziehungsweise LTG entspricht. Für eine detailliertere Beschreibung des Phasenübergang von LSZG bei einer Temperaturerhöhung über 250(50)°C hinaus werden weitere Experimente benötigt.

Zum Vergleich von strukturellen und physikalischen Eigenschaften seien auch die physikalischen Eigenschaften von LNG und LTG zusammenfassend dargestellt:

1. LNG- und LTG- Kristalle der enantiomorphen Kristallklasse 32 können im Gegensatz zu GaPO_4 mittels Züchtung nach der Czochralski- Methode mit ausreichend hoher struktureller Perfektion hergestellt werden.
2. DTA- Messungen von LNG und LTG zeigen keine Änderungen des thermischen Verhaltens bis zu Temperaturen von 1400°C [5]. Da LNG und LTG vermutlich keine Phasenübergänge bis zu ihren jeweiligen Schmelzpunkten bei ungefähr 1470(30)°C haben, sind sie für piezomechanische Anwendungen bei hohen Temperaturen gut geeignet.
3. Die Härte von LNG beziehungsweise LTG ist vergleichbar mit der von Quarz.
4. LNG und LTG sind chemisch inert und unlöslich in Säuren beziehungsweise Laugen.

5. Die Breite des Bandpassfilters von LNG oder LTG ist ungefähr dreimal größer als die von Quarz. Folglich sind LNG und LTG für Filter besser geeignet als Quarz.

Im Lichte der Ergebnisse aus dieser Forschungsarbeit können folgende Empfehlungen gemacht werden:

1. Bezüglich der hoher Qualität dieser Materialien (die Halbwertsbreite der Reflexionen beträgt 0.0008°) und wegen des großen Streuvermögens, kann empfohlen werden, diese Kristalle als Test- Kristalle für die Justage an Einkristall- Diffraktometer und für Experimente mit harter Röntgenstrahlung zu benutzen.
2. Ebenso wie α -Quarz- Einkristalle [58], können diese Kristalle als interner Druckstandard in Einkristallhochdruckexperimenten benutzt werden, weil diese Kristalle eine große Anzahl von starken unabhängigen Reflexen besitzen. Andererseits kann die niedrigere Kompressibilität von LNG beziehungsweise LTG, im Vergleich zu α -Quarz, zu einer niedrigeren Druckmessungspräzision führen. Dieser Nachteil wird wiederum durch große Streuvermögen kompensiert.
3. LNG oder LTG können als Materialien für Drucksensoren bis zu sehr hohen Drucken verwendet werden. Wegen des Phasenübergangs von LNG und LTG ist der Einsatz lediglich auf 12(1)GPa begrenzt.
4. Die Temperaturabhängigkeit der Gitterparameter dieser Materialien zeigt keine Anomalie innerhalb des untersuchten Temperaturbereiches ($24^\circ\text{C} - 850^\circ\text{C}$). Somit wurde die thermische Stabilität von LNG und LTG bestätigt. Auf diese Weise können LNG und LTG im Austausch für Quarz als Substratmaterialien für Temperatursensoren sehr empfohlen werden.

CONTENTS

1. INTRODUCTION	1
1.1. Background	1
1.2. The crystal structures of inorganic compounds in terms of polyhedral approach	2
1.3. Crystals at extreme conditions	5
1.3.1. Crystals at high pressure	5
1.3.1.1. Compression mechanism of compounds with GaO₄ tetrahedra	6
1.3.1.2. Decrease of the volume of LaO₈ decahedra under pressure	7
1.3.1.3. Compression of NbO₆ and TaO₆ octahedra	7
1.3.2. Crystals at high temperature	8
1.3.3. Features of polyhedral thermal expansion and compressibility	9
1.3.4. Strain and elasticity of crystalline materials at extreme conditions	10
2. EXPERIMENTS	13
2.1. Single crystal or powder diffraction ?	13
2.2. High pressure single crystal experiments	15
2.2.1. Preparation and loading of the diamond anvil cell	15
2.2.2. Pressure calibration	17
2.2.3. Pressure transmitting media	18
2.2.4. Equation of state	21
2.2.5. Reflection intensity data	22
2.2.6. Data reduction and structure refinement	24
2.3. High temperature experiments	28
2.3.1. X-ray powder diffraction experiments	28
2.3.2. Thermal expansion coefficients	32

3. RESULTS AND DISCUSSION	33
3.1. Compression mechanisms of LNG and LTG	33
3.1.1. Axial compressibilities	33
3.1.2. Bulk moduli	40
3.1.3. Compression mechanisms	44
3.1.4. High pressure phases of LNG and LTG	54
3.1.5. Broadening of reflections	62
3.2. Temperature dependencies of unit cell parameters of LNG, LNG and LGSZ	69
3.2.1. Thermal expansion of LNG and LTG lattices	69
3.2.2. Thermal expansion of LSZG lattice	74
4. CONCLUSIONS	82
5. ACKNOWLEDGEMENTS	86
6. REFERENCES	87
7. APPENDICES	94
7.1. APPENDIX A	95
7.2. APPENDIX B	96
7.3. APPENDIX C	97
7.4. APPENDIX D	98
7.5. APPENDIX F	99
7.6. APPENDIX G	101

1. INTRODUCTION

1.1. Background

The evolution of electronic technology towards higher frequencies and larger baud rates leads to an interest in finding new piezoelectric materials, which enable filters with large pass band widths and oscillators with larger shifts or larger frequency stability. To achieve the above-mentioned technical features, necessity has arisen to discover new piezoelectric crystals having superior properties to quartz, lithium tantalate or niobate (LiTaO_3 or LiNbO_3), *etc.* The crystals from the langasite family are current candidates for satisfying those requirements due to their unique acoustic characteristics [3].

As single- crystalline material, the langasite family, first of all langasite ($\text{La}_3\text{Ga}_5\text{SiO}_{14}$, LGS) langanite ($\text{La}_3\text{Nb}_{0.5}\text{Ga}_{5.5}\text{O}_{14}$, LNG) and langatite ($\text{La}_3\text{Ta}_{0.5}\text{Ga}_{5.5}\text{O}_{14}$, LTG) are of great interest because of the combination of a number of useful properties such as high piezoelectric coupling coefficients, temperature compensation and low acoustic loss. There are many publications providing information about crystal growth, crystal structure at normal condition, elastic and acoustic properties of compounds from this family [2-12]. Up to the present, especially LNG and LTG are taking a leading position in current research interest since they possess the best technical characteristics of all compounds in the langasite family.

Another very important property is that the compounds constituting the langasite family melt congruently so that large single crystals can be produced by the conventional Czochralski melt pulling technique. At present time, the production of high quality single crystals of these compounds is very reproducible. Otherwise, the crystals can form a number of defects such as twinning and domain structure. It requires special effort to optimize the growth condition in order to achieve the high quality single crystal growth. At present time, there is still a lot of problems to supply the material in production quantity with consistent crystal quality for mass production [4].

The possible use of langasite- type materials as temperature or pressure sensors, places a crucial importance on the investigations of the behaviour of these compounds under extreme conditions (such as pressure and temperature). Therefore this thesis contains two parts.

The first part of this thesis describes the high pressure structures of LNG and LTG crystals utilising diamond anvil cells. The investigations of the compression mechanisms of LNG and LTG at pressures up to 25GPa were undertaken in order to characterise the structural stability

of these compounds under pressure. Structure determinations of piezoelectric compounds should provide data to understand the influence of atomic arrangements on the piezoelectric effect. In contrast to investigations of compounds with different chemical compositions, varying pressure enables us to accomplish continuous structural changes within one experimental run.

The second part of this study was undertaken to analyse the changes of the lattice parameters of LNG and LTG under thermal expansion in order to confirm the structural stability under elevated temperature [11]. Furthermore in this part of study was investigated the changes of lattice parameters of another member of langasite family, $\text{La}_3\text{SbZn}_3\text{Ge}_2\text{O}_{14}$ (LSZG).

1.2. The crystal structure of inorganic compounds in terms of polyhedral approach

The crystal structure of inorganic compounds can be described in terms of cations (positively charged ions), which are surrounded by anions (negatively charged ions, most commonly oxygen). The cluster formed by a cation and its surrounding anions is usually quite regular in shape, with anions (most commonly oxygen) corresponding to the corners of a tetrahedron, an octahedron, a cube or some other simple polyhedral forms [24]. The representation of ionic clusters as cation-centered polyhedra simplifies the description of the complex crystal structures. Arrangements of many different atoms, which are difficult to depict if every atom is shown, are reduced to simple geometric forms. Common binary compounds, such as the oxides of a single metal, can be represented by a packing of one type of polyhedron. Silicates and multiple-metal oxides can be similarly treated, although they often call for two or more types of polyhedron.

Cation- centred polyhedra are more than just visual aids. Each type of polyhedron has its own distinctive set of properties, which can be helpful in predicting the behaviour of a crystal. This also depends on how the polyhedra are linked. In general, two polyhedra can be joined by a shared corner (one common anion), a shared edge (two common anions) or a shared face (three or more common anions). Furthermore, two polyhedra can be joined by weak atomic forces (no anions are shared). In the following, the example of crystal structure will be described by polyhedral approach of multiple-metal oxides $\text{La}_3\text{Nb}_{0.5}\text{Ga}_{5.5}\text{O}_{14}$ and $\text{La}_3\text{Ta}_{0.5}\text{Ga}_{5.5}\text{O}_{14}$.

LNG and LTG crystallise in the $\text{Ca}_3\text{Ga}_2\text{Ge}_4\text{O}_{14}$ trigonal structure-type(space group $P321$). This structure type was discovered in late 70's by Professor B. B. Mill and his associates [1]. There are 4 cation sites in this structure. The largest cation La^{3+} at position $3e$ is coordinated by 8 oxygen anions. $\text{Ga}(1)^{3+}$ and Nb^{5+} for LNG or Ta^{5+} for LTG share the octahedral site $1a$. Another two cations $\text{Ga}(2)^{3+}$ and $\text{Ga}(3)^{3+}$ are positioned at tetrahedral sites $2d$ and $3f$, respectively. The oxygen atoms O(1), O(2) and O(3) at positions $2d$, $6g$ and $6g$ are coordinated by 4,4 and 3 cations, respectively.

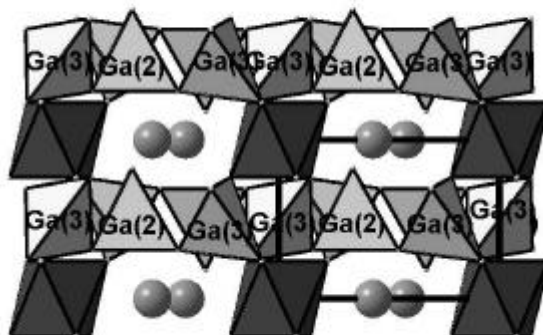


Fig.1.1: Crystal structure of LNG along b -axis; GaO_4 and Ga/NbO_6 polyhedra are shown.

Figure 1 displays a projection of the crystal structure of the LNG or LTG, which can be described as a mixed framework consisting of polyhedron layers. In other words, the structure of LNG or LTG consists of tetrahedral (GaO_4) chains arranged in layers perpendicular to the c axis, the layers being connected by octahedra (Ga/NbO_6 or Ga/TaO_6) and decahedra (LaO_8). Accordingly, tetrahedra are joined with decahedra and octahedra by shared edges or shared corners. Thus, the smallest of the two kind of tetrahedra at the $2d$ position is sharing half of its edges with decahedra. The other tetrahedra (position $3f$), surrounding the octahedra according to the triple axis law (Fig. 2), are joined with the octahedra and decahedra by shared corners. Within tetrahedron layers the tetrahedra are joined by shared corners. Most probably, the compressions of the tetrahedron layers (the layers of the smallest and strained polyhedra) will lead to possible phase transitions. Thus most likely, the $2d$ -tetrahedra are the structural element triggering a phase transition, whose central atoms are surrounded by one oxygen O(1)

(at $2d$ position) and by three oxygen O(2) according to the threefold axis, that will limit the flexibility of $2d$ -tetrahedra under extreme conditions. Finally, the octahedra are sharing three of their edges with decahedra. The largest polyhedra LaO_8 are sharing almost half of their edges with other polyhedra: one with octahedra, two with $2d$ -tetrahedra and four with neighbouring decahedra.

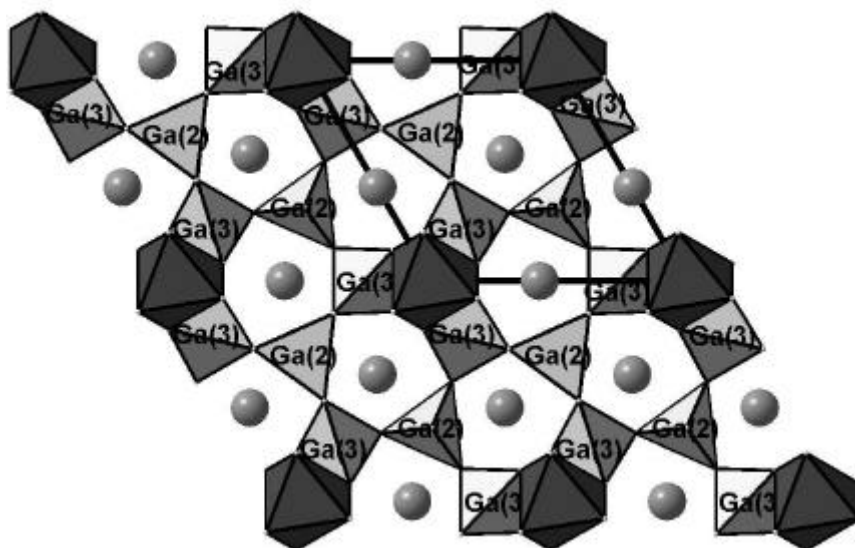


Fig.1.2: Crystal structure of LNG along c -axis; (GaO_4) and (Ga/NbO_6) polyhedra are shown.

Thus both compounds, LNG and LTG are isostructural. The only difference between both substances is the substitution of Nb^{5+} against Ta^{5+} ions. This gives rise to a slight deviation in cell and structural parameters. According to the literature [14-21], due to the Nb^{5+} Ta^{5+} substitution many compounds under extreme conditions (high- low temperature or high pressure) show comparative but characteristic behaviour, despite similar material properties. The difference in crystal chemical behaviour between niobium and tantalum lies in the greater polarisation of Nb^{5+} ions by neighbouring oxygen anions. This causes larger distortions of NbO_6 octahedra as compared to TaO_6 [14]. Actually, the polarisation of the oxygen environment around the atoms Nb or Ta was observed for several compounds. However, the high-temperature phases were always observed without any polarisation of the oxygen arrangements of these cations. In the case of LNG and LTG, the positions of the central cations of the octahedrons are shared by Nb^{5+} or Ta^{5+} with Ga^{3+} in a ratio 1:1. Furthermore, at normal conditions a characteristic polarisation of the oxygen arrangement was not observed neither for LNG [22] nor LTG [23]. A possible conclusion is that the tendency towards a

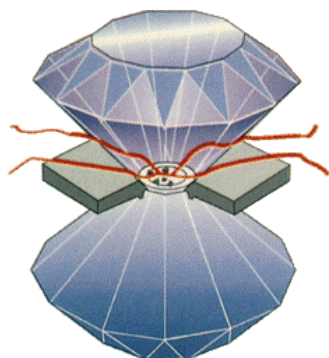
greater polarisation of the oxygen arrangements of Nb^{5+} as compared to Ta^{5+} will appear at certain pressures. This can lead to a phase transition with reduction of the symmetry and (or) to differences between the compressibilities of LNG and LTG.

1.3. Crystals at extreme conditions

A profound understanding of the crystalline state at extreme conditions of temperature and pressure is an integral part of solid state physics. The development of theoretical and experimental techniques is driven by the need to measure the equation of state of inorganic compounds, and to understand the mechanisms of isobaric changes under temperature or isothermal changes under pressure in crystals. However, studies of phenomena at high pressure, which are often technically demanding, usually follow detailed high-temperature investigations [40]. In contrast, this study is mainly focused on the high pressure behaviour of the structures of LNG and LTG. Complementary high-temperature investigations of these compounds were undertaken in order to characterise the temperature dependencies of the lattice parameters. Therefore a limited literature research has been focussed on high pressure investigations of analogous structures.

The first point in question was the change in the atomic structure of a crystal when external pressure is increased.

1.3.1. Crystals at high pressure



In the broadest sense the answer to this is obvious: the individual atoms move closer together, reducing the crystal's volume [24-26]. Studies of atomic arrangements of crystals are replaced by more detailed investigations of chemical bonding and electron distribution in order to describe the compression mechanisms.

Three kinds of changes and (or) their combination in the structural geometry of most crystals under compression can be distinguished: bond shortening, which is observed for polyhedra

with predominantly ionic types of bonding, tilting and distortion of polyhedra with covalent (atomic) kinds of bonding. Intermolecular compression is the principal response to increased pressure in condensed molecular substances. The compression mechanism is often complex and depends on how the polyhedra are linked.

Variations of polyhedral distribution in the structural geometry lead to differing behaviour in crystals under pressure. In the context of our study, the greater interest was placed in the investigations of compounds with GaO_4 , or NbO_6 , or TaO_6 , or LaO_8 polyhedra at high pressure. In such a way, the behaviour of GaPO_4 under pressure, whose structure consists of tetrahedral (GaO_4 and PO_4) chains, will be described in the following.

1.3.1.1. Compression mechanism of compounds with GaO_4 tetrahedra



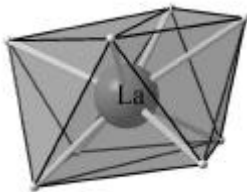
Single-crystalline GaPO_4 , gallium phosphate, is a piezoelectric material which is very similar to quartz in its crystal structure but has a much higher thermal stability, a higher piezoelectric effect, larger electromechanical coupling constants *etc.* It is a promising material for sensor applications in the temperature range up to 900 degrees C. The first products are already on the market: uncooled pressure sensors for combustion engines, with sensitivity and stability surpassing those attainable with quartz [31].

The crystal structure of the low-quartz modification of GaPO_4 is trigonal in symmetry (space group $P3_121$) and can be described as a holotetrahedral framework. Thus the tetrahedral chains consist of the two kinds of tetrahedra (GaO_4 and PO_4), sharing each corner with a neighbouring tetrahedron.

Like other quartz-type structures, GaPO_4 exhibits anisotropic behaviour under pressure [28]. The lattice parameter a is more compressible than c . The compression mechanism can be explained due to cooperative tilting and distortion of tetrahedra, because the tilting of GaO_4 and PO_4 requires much less energy than the shortening of covalent bonds (Ga-O or P-O). Accordingly, the compression in a -axis direction is dominated by corner sharing tetrahedra, which allows high flexibility (tilting of polyhedra). The c -axis compression is restricted due to the rather inflexible interconnectivities along the chains. At pressure around 9GPa GaPO_4 undergoes a phase transition, due to the stronger distortion of the GaO_4 tetrahedra. From powder diffraction diffraction studies it can be concluded that GaPO_4 becomes amorphous at about 9(2)GPa [28,32]. Contrary to this results, the investigations of GaPO_4 using Raman

spectroscopy clearly indicate that the high-pressure phase is crystalline and not amorphous [30]. A transformation of the quartz-type GaPO_4 to a monoclinic high-pressure phase was observed in a molecular dynamic simulation at 7GPa (experimental value is 9GPa). The same phenomenon was observed for the isostructural compound GaAsO_4 [37]. Thus at pressures about 12GPa GaAsO_4 is predicted to undergo a phase transition with changes in the coordination number, most likely for the Ga^{3+} cations.

1.3.1.2. Decrease of the volume of LaO_8 decahedra under pressure

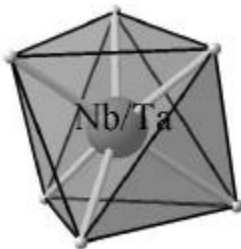


As a typical example, the crystal structure of LaNbO_4 (monoclinic distorted scheelite structure) can be used, which consists of LaO_8 and NbO_4 polyhedra [33]. The high-pressure behaviour of LaNbO_4 is very anisotropic due to differing bond strengths in different axis directions.

The monoclinic distortion increases with increasing pressure. The eight-coordinated La polyhedron undergoes significant compression under pressure, whereas the NbO_4 tetrahedron is comparatively incompressible. Thus the volume of LaO_8 decreases under pressure due to the lower bond strength of La-O (predominantly ionic character bonds), whereas the distortion of the neighbouring NbO_4 increases due to stronger Nb-O bonds (predominantly covalent character).

It may be concluded that large LaO_8 decahedra almost always decrease in volume with increase of pressure to a larger extent as compared to smaller polyhedra, due to shortening of La-O bonds with predominately ionic character.

1.3.1.3 Compression of NbO_6 and TaO_6 octahedra



Ferroelastic compounds of ABO_3 -type containing Nb^{5+} and Ta^{5+} ions may serve as an example of crystal structures with linked NbO_6 and TaO_6 octahedra [15, 19, 20]. According to the literature, bond types within these polyhedra can not be purely ionic and exhibit a large covalent part. Nb ions should be more polarizable than the Ta ions, which leads to the ferroelastic instability under temperature in compounds containing Nb

ions [36]. On the other hand, the compressions of NbO_6 and TaO_6 octahedra under high pressure are almost the same [14, 34]. Thus the compressions of these octahedra can not be described only in terms of polyhedral distortions, also changes in cation-anion distances (bonding shortening) must be taken into account. For example, in case of LiNbO_3 and LiTaO_3 crystals under anisotropic pressure, the deformation of the octahedral framework (neighbouring octahedra rotate in opposite directions) was observed as well as decreasing bond lengths and distortion of the octahedra. At pressures around 14(2)GPa both compounds undergo a phase transition [15].

It can be concluded from the above appointed investigations that the different bonding strengths within and between anion-cation polyhedra cause a varying crystal structure behaviour under pressure.

The second point of interest lies in the question of how the atomic structures of crystals change under thermal expansion in terms of the variation of cation-anion bond distances within polyhedra.

1.3.2. Crystals at high temperature

Information on the variation of the structural dimensions with temperature or pressure is deduced from two distinct types of studies[68]. Complete three-dimensional structure refinements are the most obvious sources of data, but it is also possible to derive this information from unit-cell dimensions alone in many constrained or simple structures. The structures of NaCl , CsCl , *etc.* are all fixed in that there are no variable positional parameters. Thermal expansion data on materials that crystallize in these structures thus provide information on bond thermal expansion as well. Other simple structures, including those of rutile (TiO_2), corundum (Al_2O_3), *etc.*, also have bulk expansions that are similar to expansions of cation-anion bonds.

Hazen & Finger (1982) calculated from several dozen studies of structures at high temperature linear expansion coefficients, \mathbf{a}_1 , for individual cation-anion bond distances, d , and the mean linear expansion coefficient, $\overline{\mathbf{a}}_1 \equiv \mathbf{a}_{poly}$, for the average bond length, \overline{d} , of all cation-anion bonds within a given polyhedron:

$$\mathbf{a}_1 = \frac{1}{d} \left(\frac{\Delta d}{\Delta T} \right), \quad (1.1)$$

$$\overline{\mathbf{a}}_1 = \frac{1}{d} \left(\frac{\Delta \overline{d}}{\Delta T} \right), \quad (1.2)$$

The thermal expansion coefficient for each type of polyhedron is assumed to be independent of the structural linkages of the polyhedron, presuming the site composition and topology of the structure do not change with temperature. Thus, for each type of cation-oxygen polyhedron there exists a value for an expansion coefficient that may be used to predict the behaviour at high temperature [83]. A second generalization is that all oxygen-based polyhedra with the same bond strength (cation charge divided by coordination number) have the same $\overline{\mathbf{a}}_1$. Therefore, if the bond strength is zero between two atoms, as in an inert gas, then thermal expansion is infinite. If bond strength is very large, then thermal expansion approaches zero. Thus the polyhedral volume thermal expansion is inversely proportional to bond strength of the cation –anion bonds within the polyhedra.

1.3.3. Features of polyhedral thermal expansion and compressibility

In general, the changes in the crystal structure under thermal expansion or compression, do not result only in changes of cation-anion distances[68]. The changes in angles between polyhedra must also be considered.

As pointed out above, two cation polyhedra may be linked by a shared face, a shared edge, a shared corner or Van der Waal's forces. The type and distribution of these polyhedral linkages are the most important factors in determining the influence of thermal expansion or compression on a given crystal structure [84].

The most rigid polyhedral linkage is one in which polyhedra share faces or edges in three dimensions. In this case, any change in the crystal structure must be accompanied by a change in metal-oxygen distance because of rigid polyhedral linkages. Thermal expansion or compression of these compounds is consequently small because it is similar in magnitude to the thermal expansion or compression of metal-oxygen polyhedra.

In contrast to these structures, some materials such as α -quartz consist of corner-linked polyhedra. In these structures volume changes may be effected by changes in angles between tetrahedra, without altering cation-anion bond distances. Thus the crystal structure of silica have relatively large thermal expansion and compressibility, even though individual tetrahedra may undergo no volume change with temperature or pressure. The tilting of polyhedra in expansion or compression of corner-linked materials may be treated as primarily metal-oxygen-metal angle bending, as opposed to metal-oxygen bond expansion or compression.

In addition, in most structures, including layer, chain, *etc.*, all polyhedra share edges with some adjacent polyhedra, link corners with other, and may have only weak Van der Waals attraction to still others. In these materials expansion or compression is due to a combination of polyhedral (metal-oxygen) bond distance variations and bond bending, and the net expansion or compression is greater than that of component polyhedra.

It may be concluded, that the cation polyhedron, a basic building block of most crystal structures, has physical properties, which are independent of structural linkage. These polyhedral properties include volume, shape, *etc.* The consistency of these parameters for a given polyhedron in different structures indicates the great influence of nearest-neighbour interactions in determining the atomic-scale properties of ionic compounds. Therefore, polyhedral volume changes with temperature or pressure may be predicted from the single bonding parameters: cation-anion bond distance, cation coordination number, cation radius *etc.* On the other hand, a knowledge of polyhedral expansion and compression does not lead directly to an understanding of crystal structure changes under extreme conditions. Additional information, such as how the polyhedra are linked and bond bending forces, is needed [44].

1.3.4. Strain and elasticity of crystalline materials at extreme conditions

In general, the compression or heating of the inorganic materials lead to structural changes, which may result in a phase transition. Many criteria (kinetic, thermodynamic, structural *etc.*) are used to classify phase transformations. However, the phase transition is a process consisting of shifts of atoms relative to each other, occasionally coupled with changes of size and direction of magnetic and electric moments and of electric charges of atoms. Almost any changes in the structure of a crystal, due to atomic displacements, atomic ordering *etc.*, is usually accompanied by changes in lattice parameters. The different types of phase transitions

found in inorganic compounds include displacive phase transitions, reconstructive phase transitions, cation ordering transitions, and orientational order-disorder phase transitions [43]. As a rule, the crystals turn to lower symmetry under pressure driven phase transitions with excess of free-energy. The heating of these compounds increases the energy of the crystals, and structures undergo phase transitions to higher symmetry, which is energetically more favourable.

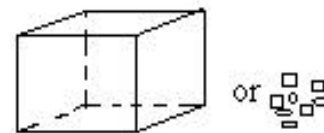
The crystal structure which undergoes phase transitions under pressure or temperature displays lattice-parameter variations that are subjected to constraints of symmetry, order parameter, *etc.* Lattice parameter variations can be described quantitatively as a combination of linear and shear strains [38-40]. Conversion from a purely geometrical description, in terms of lattice parameters, to a thermodynamic description, in terms of strain, leads through to the elastic properties. Thus variations of the elastic constants accompany phase transitions in many materials. And the elastic constant variations themselves also provide unique insights into the mechanisms of phase transitions. It must be expected that the elastic properties of crystals will display large variations if there is any possibility of a structural phase transition when pressure or temperature is applied. The dependencies of the elastic properties of LGS from temperature and from mechanical stresses are reviewed in order to predict the behaviour of isostructural materials (LNG and LTG), which were investigated in this study.

Sil'vestrova et al. (1986) and Sorokin et al. (1994) have obtained temperature and pressure dependencies of elastic properties of LGS. The elastic properties show no anomalies in the temperature range 77-373K [41]. Thus temperature dependencies of the elastic constants of LGS single crystal are monotonic and linear, this indicates the absence of phase transitions. It can be expected that other members from the langasite family such as LNG and LTG are thermally stable, and show no anomalies of elastic properties and no phase transition in the investigated temperature range (77-373K).

In contrast, anomalous elasticity under conditions of homogenous mechanical stresses in LGS single crystal was observed [42]. Thus, the application of pressure parallel to [100] and [010] direction lowers the effective symmetry of the LGS crystal to monoclinic (symmetry class 2) and triclinic symmetry, accordingly. In contrast, the application of pressure in [001] direction does not change the original symmetry of the crystal and results in quantitative changes of acoustic properties. Therefore an anomalous elasticity of LNG or LTG crystals under hydrostatic pressure can be expected. Furthermore, an anisotropic behaviour of LGS, LNG, LTG crystals under pressure can be predicted, due to anisotropic character of changes of elastic constants of LGS under homogenous mechanical stresses.

It can be concluded, that the behaviour of crystals under pressure or temperature can be described by the results of geometrical and thermodynamic analysis. Thus atomic arrangement or lattice parameters data provides essentially only geometrical properties, whereas the elastic properties can be related directly to thermodynamic quantities. In this way, this study represents the results of geometrical properties of LNG and LTG under extreme conditions (high pressure, high temperature).

2. EXPERIMENTS



2.1. Single crystal or powder diffraction?

Two kinds of experimental methods were applied in this study. The high-pressure experiments were performed by single crystal X-ray diffraction. The high-temperature experiments were performed by X-ray powder diffraction. The selection of the kind of experimental method can be explained in terms of expected results.

Some advantages and disadvantages of single crystal and powder diffraction methods are summarised in the following.

The advantages of the single crystal X-ray diffraction method:

1. The better peak to background ratio is advantageous in the single crystal method, as compared to powder diffraction technique. Thus the scattering intensity of a reflection is focused in a small ensemble of points, while for the same reflection the intensity (for a volume-same powder sample) is distributed on a diffraction ring (Debye ring).
2. The three-dimensional separation of individual reflections, which are symmetrically equivalent, makes it possible to record more independent observations (according to number of the reflections) using single crystal X-ray techniques. Therefore the intensity of the individual reflections can be determined more precisely. This gives an opportunity to refine or determine a large number of free parameters with high accuracy. On the other side, the structural refinement of powder-diffraction data can also give information about atomic positions under pressure or temperature. But this is possible with high accuracy only for a limited number of free parameters. Problematic are also uncontrolled and changing texture effects which are produced during pressure loading. Therefore the single crystal method is the more suitable for detailed investigations of complex structures.
3. The reflections from pressure standard, diamonds, *etc.* can be easily excluded from the collection of the reflections intensity data using single crystal X-ray diffraction method, whereas during X-ray powder diffraction experiment all possible reflections are registered, in most cases this leads to an overlap of diffraction lines of different phases.

The disadvantages of the single crystal X-ray diffraction method:

1. The experimental time for one data collection of reflection intensity by single crystal method is several times longer as compared to the duration of one X-ray powder diffraction experiment.
2. The high pressure crystal method is technically problematic as compared to powder experiment, because a large opening angle of the cell is necessary, but at the same time the stability of individual components is decreased under compression. Thus the stability and functionality of the cell may be affected. In this regard the X-ray powder diffraction experiment is advantageous. Thus, for example, the cell used in energy dispersive powder diffraction experiments does not require a large opening angle, therefore stable cell constructions are possible.
3. In the case of twinning domains due to phase transitions to lower symmetry, the crystal structure refinement using single crystal data can cause difficulties, whereas Rietveld refinements (provided excellent resolution) cause no troubles.
4. In the case of low symmetry, a given orientation of the single crystal in the diamond anvil cell does not allow a measurement of all symmetrically equivalent points of the reciprocal lattice (limited by the high pressure cell). Thus only one part of information is measured, depending on the orientation of crystal. In contrast, the powder diffraction measurements usually are limited only by the maximum diffraction angle. On the other hand, for the single-crystal experiment two or more single crystals can be used with different orientations, this can allow a measurement of all symmetrically equivalent reflection points of the investigated material.

Generally, it may be suggested, that X-ray powder diffraction method is the more preferable method for determination of the crystal structure changes under extreme conditions. On the other hand, the single crystal X-ray method gives an opportunity to refine or determine a large number of free parameters with high accuracy under extreme conditions. Therefore, for determination of the temperature dependencies of the unit cell parameters of LNG, LTG and LSZG the X-ray powder diffraction method was selected. For the detailed investigation of the complex crystal structures of LNG and LTG under pressure the single crystal X-ray diffraction method was selected.

2.2. High pressure single crystal experiments

The single crystals of LNG and LTG from a Czochralski-pulled boule were produced and kindly provided by research group of B. V. Mill (Moscow State University, Russia).

2.2.1. Preparation and loading of the diamond anvil cell

Figure 2.1 shows a schematic drawing of the diamond anvil cell (DAC) used in this experiments. The DAC consists essentially of a steel construction consisting of two halves, each containing a beryllium plate with conical hole in the centre. This allows visual inspection of the single crystal through the diamonds. The diamonds are pressed to beryllium plates by springs. Between the two diamonds, a metal gasket, with round hole in the centre, encloses sample and pressure standard. This pressure chamber is filled by a suitable pressure medium.

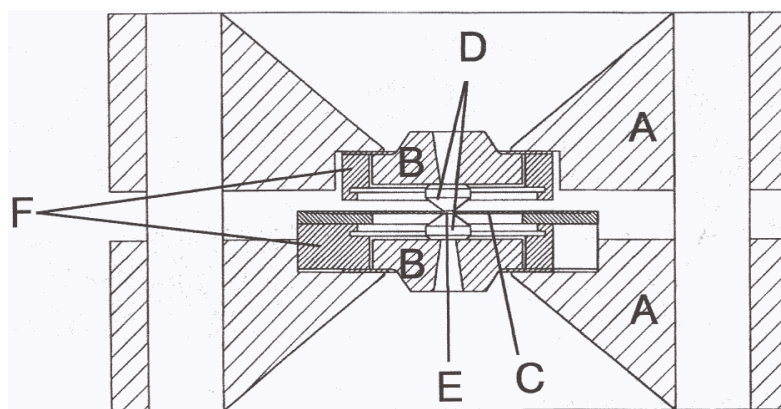


Fig. 2.1: The principle of a diamond anvil cell: A-steel matrix; B-beryllium plates; C-gasket; D-diamonds; E-pressure chamber for sample; F-support for beryllium plates.

In this study modified Merrill-Basset DACs [47] with opening angle 45° , specially designed to reach pressures above 20GPa [48, 49] utilising single crystals were used. Because diamonds are transparent to X rays, the crystals can be exposed to a narrow beam of X-rays, and the diffracted components of the beam can be measured by standard X ray detection equipment. All experiments under pressure were performed on a four-circle diffractometer (CAD4)

utilising monochromatized MoK α radiation (home laboratory) or at HASYLAB (beam-line D3) using synchrotron radiation ($0.55 < \lambda < 0.65 \text{ \AA}$).

The preparation of the DAC consists of two procedures:

- 1) adjustment of diamonds;
- 2) preparation of the gasket.

At first, the cell is closed without the gasket until the diamonds faces contact. Testing is simple to carry out visually by use an optic microscope. When the faces of diamonds are nearly in contact, the interference rings appear. One of the diamonds must be shifted relative to the other until full overlap the facets of their surfaces is reached. The next step is the tilting of the diamonds until their faces are positioned parallel to each other. The result can also be controlled by the distribution of interference rings. The faces of diamonds have a parallel position, when one of the rings covers the whole surface of diamonds.

The next step is the preparation of the gasket. As gasket material, spring steel (200 μm) or wolfram alloy (250 μm) were used. In order to prevent leakage of pressure fluid under compression, the gasket is pressed by diamond after the centring before a hole was drilled for the sample [50]. The thickness of the gasket between the faces of the diamonds is decreased down to about 60 μm . After the pre-indentation, a perfect round hole was made in the centre of the indentation by utilising a spark-eroding machine [49]. The hole must be placed in the centre or close to the centre of indentation, because the hole even after deformation should not contact with border of diamond surfaces, which will lead to leakage of pressure medium.

Before the gasket is mounted on the diamond, a crystal of LNG or LTG and pressure standard were put in the centre of the diamond face. Then the gasket was mounted. When this procedure is finished, the high pressure cell is prepared for loading the pressure medium and closing (Fig. 2.2).

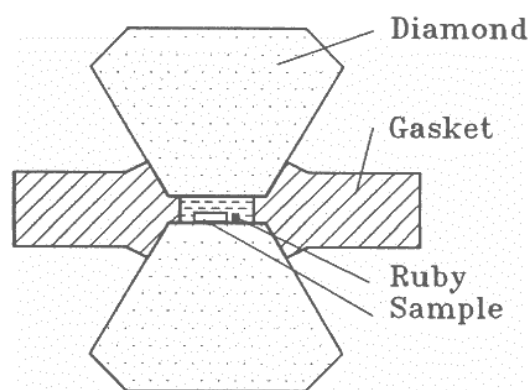


Fig. 2.2: Schematic diagrams showing the closed diamond anvil cell.

The size of the crystals is limited by the volume of the pressure chamber, which is formed by the faces of diamonds and the wall of the hole of the gasket [50]. In general, the hole must be at least three times sample crystal diameter in order to prevent shielding of X-rays at high inclination angles. The ratio of hole diameter to diamond face diameter depends on the stability of the gasket material used under compression. The size of the faces of the diamonds is selected according to pressure level. Therefore about 10 carefully selected crystals of LNG or LTG with different orientations and sizes of approximately $80 \times 80 \times 50 \mu\text{m}^3$ were used in experiments at pressure range from atmospheric up to 10GPa. Accordingly, for the higher pressures (above 20GPa) tiny crystals were used, one crystal of LTG and two crystals of LNG with sizes about $20 \times 30 \times 30 \mu\text{m}^3$. These experiments were performed in the pressure range from 3GPa up to 16(1)GPa (for LTG) and up to 23(1)GPa (for LNG).

As a final preparation, the selected pressure medium was loaded into the gasket hole and the two halves of the high pressure cell were put together and were pressed together by screws until an expected pressure was achieved.

2.2.2. Pressure calibration

The pressure calibration has been performed by using α -quartz as an internal pressure standard [58] or by the ruby- fluorescence method.

For single crystal diffraction at high pressures in DACs, the common solution is the ruby fluorescence technique presented by Forman *et. al.* [55] to determine the pressure. It utilises the fact that the wavelength for the ruby (Al_2O_3 with $\sim 0.5\text{wt}\%$ Cr^{3+}) R_1 fluorescence wavelength shifts almost linearly with pressure up to about 15GPa [56]. For higher pressures, up to 80GPa, the dependence of wavelength shifts on pressure shows a more complex character [57]:

$$p[\text{Mbar}] = \frac{A}{B} \left[\left(1 + \frac{\Delta\lambda}{\lambda_0} \right)^B - 1 \right] \quad (2.1),$$

where $A=19,04$ Mbar;

$B=7,665$;

λ_0 is the wavelength of the R_1 at atmospheric pressure;

$\Delta\lambda$ wavelength shift of the ruby fluorescence spectrum.

The ruby fluorescence technique is ideal because of its speed and ease of application [93]. Furthermore the ruby crystal used for pressure measurements needs only to be a few microns in size. Therefore it occupies only a very small proportion of the limited sample volume in a diamond-anvil cell. However, although the pressure induced wavelength shift can be readily measured to a precision equivalent to approximately 0.03GPa. On the other hand, an alternative calibration procedure of far greater potential precision is the use of internal X-ray standard single crystal. Thus the use of the oriented quartz single crystals improves the precision of pressure measurements (precision equivalent to approximately 0.009GPa) [58]. That is why α -quartz crystals were used as an internal pressure standard, in experiments with alcohol mixture as pressure transmitting medium, which allowed a volume of the pressure chamber large enough for samples. Accordingly, the ruby- fluorescence method was applied in investigations with helium pressure medium, because of the limited sample space in a diamond-anvil cell.

The measurements of the pressure by the ruby- fluorescence method were performed using a 25mW Argon laser installed at laboratory of beam-line F3 (HASYLAB).

2.2.3. Pressure transmitting media

The pressure generated in a DAC must be transmitted to a single crystal hydrostatically (that is, uniformly in all directions) by immersing the crystal in a fluid, which is confined by the metal gasket between the diamonds. It is possible to use many types of pressure media, such as gases, liquids or even solids [51]. For single crystals, a fluid pressure-transmitting medium is commonly used.

In this study experiments with four different pressure media were performed. The first one was the most widely used compressing medium, an alcohol mixture (methanol, ethanol and water in volume ratios 16:3:1). Alcohol was used in experiments within a pressure range up to 10GPa. Above this, it transforms into a very hard glass which leads to pressure gradients of 3GPa over 100 μ m. Thus above 10GPa the use of alcohol mixture as pressure transmitting medium results in non-hydrostatic conditions. Therefore the pressure range for experiments with alcohol mixture as pressure medium is limited to 10GPa.

Experimentally, four potential ways of studying the degree of hydrostaticity of a pressure medium are as follows [53]:

- 1) measuring the pressure at various points using ruby chips distributed within a pressure chamber and relating, if possible, the pressure gradient to the non-hydrostatic stress component;
- 2) knowing the effect of the non-hydrostatic component of stress on the full width at half maximum (FWHM) of the ruby fluorescence profile and measuring FWHM;
- 3) measuring the lattice parameter of, say, a cubic crystal within the medium, as a function of angle relative to the loading direction and relating this to the stress components;
- 4) knowing the effect of deviatoric stresses on the splitting between the ruby R_1 and R_2 fluorescence lines and measuring this shift.

The resultant pressure gradient can be related to the non-hydrostatic component of the stress [94]. Some pressure media, so far reported to be quasi-hydrostatic above the alcohol mixture limit (10GPa) are solid rare gases (Xe, Ar, Ne, and He), solid nitrogen, and solid hydrogen [53, 54, 95, 96]. Therefore for the following investigations under pressures above 10GPa argon, xenon and helium were selected as possible pressure transmitting media.

According to experiments of Kim-Zajonz [49] argon, which was loaded cryogenically, was successfully used for investigations of crystal structures of quartz and ruby under pressures up to 19(1)GPa and up to 30(1)GPa, respectively. On account of this, the high pressure cell was prepared in home laboratory with argon as pressure transmitting medium for the experiments with LNG [49]. It was observed, that reflections did not show significant changes up to 9(1)GPa, a broadening began to be noticeable with further increase in pressure. For example, the average value of the initial full width at half maximum (FWHM) for all reflections was about 0.008° , reflecting the extremely high crystal quality of our specimens. At pressures above 9GPa the FWHM increased fifty times, thus at a pressure of 9.5(5)GPa the FWHM of (h k l) reflections were about 0.4° . This effect can be well explained with non- hydrostaticity of the pressure medium, since no broadening was detectable under such pressures in experiments with alcohol pressure medium mixture. Thus argon can be applied as a hydrostatic pressure medium only up to 9GPa, the following increase in pressure (above 9GPa) leads to non-hydrostatic conditions [52].

For the following experiments xenon was selected as possible pressure medium. It was observed [53] that the splitting (peak-to-peak) between the R_1 and R_2 fluorescence lines of ruby within xenon pressure medium is almost constant up to 55GPa [53]. Furthermore the

FWHM of diffraction peaks of ruby, in case of xenon pressure medium, did not increase up to 33GPa [97]. These results indicate that xenon can be used as hydrostatic pressure medium up to 33GPa. In cooperation with R. Boehler at MPI of Chemistry (Mainz, Germany) we were able to load the DAC cryogenically with xenon as pressure medium. Our experiments with xenon as medium show, however, that already at pressures around 3(1)GPa, a broadening of reflections is observed. Thus at pressure 3.5(2)GPa the FWHM of (h k l) reflections were about 0.5° . It may be concluded that strains in the xenon matrix lead to non-hydrostatic conditions at even lower pressures than with argon.

For the next experiments helium was applied, which is known as the best hydrostatic pressure medium. Observations by single crystal X-ray diffraction suggest that the hydrostatic limit of He lies at around 35GPa at room temperature [54, 70]. On the other hand, the hydrostaticity of a helium-pressure medium has been evaluated with powder X-ray diffraction techniques up to 77GPa at room temperature. Unfortunately, it is also the most difficult gas to pressurize because of its high compressibility, and it is the most difficult to contain since its leak rate is the highest of all gases. The number of laboratories with respective gas-loading systems is very limited.

Luckily, in cooperation with R. Boehler at MPI of Chemistry (Mainz, Germany) the high pressure cells with single crystals of LNG or LTG and a pressure standard (ruby) were prepared. Helium was loaded to the DACs at room temperature at a gas pressure of 0.3GPa with the use of a gas-loading system [71]. The analysis of the profiles of reflections does not show any changes at pressures above 10GPa. This indicates that helium is the best of the tested pressure media. At pressures above 11(1)GPa helium crystallises. The noble gas atoms are held together by weak quasi Van-der-Waals bonds, therefore hydrostatic conditions are maintained at high pressures. Even though helium is known to provide perfect quasi-hydrostatic conditions at these pressures (above 11GPa), to exclude possible systematic errors, two differently orientated very small crystals of LGN were used in subsequent high pressure runs. The angle between the z-axis of these crystals was 32° . The full width at half maximum of the reflections of both crystals did not show significant changes up to 14(1)GPa. Above this pressure an equal broadening of reflections of both crystals of LGN was observed, which increased with further increase in pressure. This phenomenon was connected with structural changes in the LGN and will be described in the following. Thus helium was successfully applied as hydrostatic (or close to hydrostatic) pressure medium in pressure range from 3(1) up to 23(1)GPa.

2.2.4. Equation of state

The equation of state (EOS) of a system describes the relationships among the following thermodynamic variables: pressure, energy, temperature, and density, including changes of phase. Theoretical EOS studies are also concerned with the chemical bonding and atomic ordering of each phase encountered in the pressure-temperature phase diagram. These properties can be directly related to the forces between atoms by the methods of quantum and statistical mechanics [59].

The application of pressure offers a means by which the lattice constant or density may be varied, thus resulting in changes in properties, including transitions to new structures or phases and modifications in electronic configurations.

The EOS used in this study describes simply the pressure-volume relationship at constant temperature (commonly room temperature). Thus for our calculations we have used the semi-empirical Birch-Murnaghan EOS [60]:

$$p = \frac{3}{2} B_0 \left[\left(\frac{V_0}{V} \right)^{7/3} - \left(\frac{V_0}{V} \right)^{5/3} \right] \left\{ 1 - \frac{3}{4} (4 - B_0') \left[\left(\frac{V_0}{V} \right)^{2/3} - 1 \right] \right\} \quad (2.2)$$

V_0 : volume at atmospheric pressure;

V : volume at pressure p ;

B_0 : isothermal bulk modulus;

B_0' : pressure derivative of the isothermal bulk modulus.

By fitting this equation to the experimental pressure (p) and unit cell volume (V) or unit cell parameters (a , c) data, two constants were determined: isothermal bulk modulus (B_0) and its derivative (B_0'). These constants were used as a measure of the compressibility of the structure. A low value of the bulk modulus, B_0 , corresponds to higher compressibility of the structure or axis, and a high value indicates a higher stiffness.

2.2.5. Reflection intensity data

All measurements were carried out on an Enraf - Nonius automated four-circle diffractometer (CAD4) using monochromatized MoK α radiation ($\lambda = 0.7107\text{\AA}$) at our own laboratory or on a Huber-diffractometer installed at beam-line D3 at HASYLAB ($0.55 < \lambda < 0.65\text{\AA}$). The adjustments of high pressure cells were controlled by the profile of the primary X-ray beam, which was measured in six different positions, two positions for each freedom of movement of the pressure cell on diffractometer (x, y, z). The difference between intensities or centres of gravity of two profiles, with regard to the diffractometer axes, indicated how the position of the pressure cell must be changed. When the adjustment was completed, the orientation matrix of the crystal in the high pressure cell was determined.

Lattice parameters of a number of crystals of LGN and LGT were obtained by a least-squares fit to θ values ($20^\circ \leq |2\theta| \leq 36$) of automatically centred 16-24 reflections.

Conditions for the data collection for LGN and LGT can be seen in Table 2.1 and 2.2, respectively. The crystals with different orientations are appointed by letters A_1 , B_1 , *etc.* for LNG and A_2 , B_2 , *etc.* for LTG single crystals.

With the help of a program of S. Werner ("Miss") according to the orientation matrix and required value of $2\theta_{\max}$ angles, all accessible reflections were calculated and sorted taking into account necessary movements of diffractometer circles. Therefore measurement time could be optimized. For measurements on the CAD4 program all accessible reflections were calculated for space group $P321$ utilising the "Miss" program. Due to limited time for measurements at HASYLAB, the suitable reflections were calculated for higher symmetry (space group $\bar{P}3m1$), that required less time for one data collection. The maximum value of 2θ angle was usually set at 60° . For some experiments with helium as pressure transmitting medium under pressures below 15GPa this value was 80° , for $60^\circ < 2\theta < 80^\circ$ only the strong reflections were measured. The reflection list for data collection on LGT under pressure 16.7GPa was calculated for $2\theta = 40^\circ$, and all reflections were measured. Thus the different numbers of reflections for measurements were calculated with regard to experimental conditions.

Table 2.1. Details of data collection for LNG

p [GPa]	0.8	1.8	3.3	4.5	4.8	5.2	6.8	7.8
X-ray	MoK α	synchrotr	synchrotr	Synchrotr	synchrotr	MoK α	MoK α	MoK α
pressure medium	alcohol mixture	alcohol mixture	helium	Alcohol mixture	helium	alcohol mixture	alcohol mixture	alcohol mixture
crystal	A ₁	B ₁	E ₁	B ₁	E ₁	C ₁	A ₁	C ₁
sinq/l_{max}	0.74	0.71	0.74	0.65	0.99	0.74	0.74	0.66
N_{measured}	1602	837	1667	528	1563	1602	1608	1553
N_{averaged}	424	403	425	344	759	412	408	400

Table 2.1. Details of data collection for LNG (continued)

p [GPa]	9.67	9.9	11.7	13.1	15.6	18.5	21.85	22.85
X-ray	synchrotr							
pressure medium	helium							
crystal	D ₁	D ₁	E ₁	E ₁	D ₁	D ₁	D ₁	D ₁
sinq/l_{max}	1.04	0.80	0.81	0.81	1.02	0.90	0.90	0.88
N_{measured}	1406	1027	1146	1090	702	445	485	435
N_{averaged}	656	456	508	473	419	305	283	218

Table 2.2. Details of data collection for LTG

p [GPa]	0.7	2.3	3.3	3.4	5.1	6.1	6.64
X-ray	MoK α	synchrotr	MoK α	synchrotr	MoK α	MoK α	MoK α
pressure medium	alcohol mixture	alcohol mixture	alcohol mixture	helium	alcohol mixture	alcohol mixture	alcohol mixture
crystal	A ₂	B ₂	C ₂	D ₂	A ₂	A ₂	C ₂
sinq/l_{max}	0.66	0.74	0.74	0.69	0.74	0.74	0.74
N_{measured}	1967	790	1624	1784	1737	1685	1685
N_{averaged}	367	412	433	759	438	424	427

Table 2.2. Details of data collection for LTG (continued)

p [GPa]	7.7	8.15	9.5	11.57	13.2	14.4	16.7
X-ray	synchrotr	MoK α	synchrotr	synchrotr	synchrotr	synchrotr	synchrotr
pressure medium	helium	alcohol mixture	helium	helium	helium	helium	helium
crystal	D ₂	A ₂	D ₂	D ₂	D ₂	D ₂	D ₂
sinq/l_{max}	0.69	0.74	0.69	0.69	0.69	0.69	1.05
N_{measured}	1208	1208	1212	1210	1297	1131	1659
N_{averaged}	449	449	426	434	483	450	841

During data collection, ω -scans were performed and the ψ -angles were optimised according to the geometry of the DAC so that the beam path through the beryllium backing plates and diamonds is minimised [61]. In each data collection, four symmetrically equivalent sets of reflections were collected in order to eliminate diffractometer calibrations and to compensate for crystal-offset effects.

2.2.6. Data reduction and structure refinement

Data reduction was carried out with program REDA [62]. The absorption caused by the cell components (diamonds and beryllium backing plates) was taken into account. During the data reduction the measured blocks of reflections (from one standard reflections to next one) were accepted with trend factor $\leq 15\%$. Symmetry equivalent reflections were averaged as follows:

$$\langle I \rangle = \sum (w * I) / \sum w \quad (2.3);$$

$$R_{av} = \left(\sum |\langle I \rangle - I| \right) / \sum |I| \quad (2.4);$$

where I is the integral intensity of a reflection.

Absorption corrections were accounted for by the program Jana98 [63]. Anomalous atomic scattering factors and X-ray absorption coefficients were taken from references [64] and [65], respectively.

Structure refinements were carried out with program SHELXL97 [66]. All refinements were based on $|F|^2$ (structure factor). Details of data reduction and structure refinement of LGN and LGT can be seen in Tables 2. 3 and 2.4. The weighted and non-weighted values of R1 and wR2 as well as *goodness of fit* (GooF) were calculated in SHELXL97 with regard to following equations:

$$wR2 = \left\{ \sum [w(F_o^2 - F_c^2)^2] / \sum [w(F_o^2)^2] \right\}^{1/2} \quad (2.5);$$

$$R1 = \sum ||F_o| - |F_c|| / \sum |F_o| \quad (2.6);$$

$$GooF = S = \left\{ \sum [w(F_o^2 - F_c^2)^2] / (N - P) \right\}^{1/2} \quad (2.7);$$

where F_o and F_c are the structural factors of measured and calculated integral intensity of reflections, respectively. N is the number of reflections and P is the total number of parameters refined.

For the high pressure phases of LNG and LTG all data were transformed from trigonal to monoclinic Laue-symmetry group with the program Jana98. The following refinements of the structures of the high pressure phases of LNG and LTG were carried out with the program SHELXL97.

Table 2.3. Details of the data reduction and structure refinements of LNG

p [GPa] sp. gr.	0.8 (P321)	0.8 (A2)	1.8 (P321)	3.3 (P321)	4.5 (P321)	4.8 (P321)	5.2 (P321)	6.8 (P321)
N_{used}	424	937	403	425	344	759	412	408
$R_{\text{av.}}$	5.5	2.8	5.2	5.0	3.5	5.0	6.3	4.2
P	39	75	39	39	30	39	39	39
R1, %	3.9	4.1	3.3	3.0	3.3	4.4	3.9	3.1
Flack x	0.04(11)	0.00(8)	0.02(4)	0.02(7)	0.06(5)	0.07(7)	0.19(11)	0.01(7)
wR2, %	11.02	12.57	7.30	8.90	8.90	13.15	12.86	8.00
Goof	1.1	1.2	0.9	1.0	1.0	1.0	1.0	1.0

Table 2.3. Details of the data reduction and structure refinements of LNG (continued)

p [GPa] sp. gr.	7.8 (P321)	9.67 (P321)	9.67 (A2)	9.9 (P321)	11.7 (P321)	11.7 (A2)	13.1 (P321)	13.1 (A2)
N_{used}	400	656	848	456	508	708	473	661
$R_{\text{av.}}$	6.2	5.3	5.0	5.5	5.2	4.26	6.0	4.9
P	39	39	75	39	39	75	28	74
R1, %	4.5	3.9	4.3	4.1	3.8	4.0	4.5	5.0
Flack x	0.06(11)	0.01(7)	0.02(7)	0.09(9)	0.10(9)	0.03(8)	0.00(11)	0.07(10)
wR2, %	10.81	8.86	12.20	11.22	11.57	10.80	13.08	12.97
Goof	1.0	0.9	1.0	1.0	1.0	1.0	1.1	1.1
TWIN, %	-	-	44:23:23	-	-	34:32:34	-	38:31:31

Table 2.3. Details of the data reduction and structure refinements of LNG (continued)

p [GPa] sp. gr.	15.6 (P32I)	15.6 (A2)	18.5 (P32I)	18.5 (A2)	21.85 (P32I)	21.85 (A2)	22.85 (P32I)	22.85 (A2)
N_{used}	419	481	305	393	283	341	218	295
R_{av.}	7.1	6.2	6.1	5.4	7.3	7.2	9.2	7.1
P	38	74	28	75	28	67	28	67
R1, %	7.0	6.2	9.4	7.8	14.9	12.5	14.0	12.3
Flack x	0.12(18)	0.11(14)	0.1(3)	0.1(3)	0.0(6)	0.1(4)	0.3(5)	0.4(5)
wR2, %	18.36	15.44	24.05	19.62	35.60	29.99	34.86	30.00
GooF	1.4	1.2	1.7	1.5	2.34	2.1	2.6	2.4
TWIN, %	-	35:37:28	-	49:37:14	-	75:11:14	-	35:40:25

Table 2.4. Details of the data reduction and structure refinements of LTG

p [GPa] sp. gr.	0.7 (P32I)	0.7 (A2)	2.3 (P32I)	3 (P32I)	3.3 (P32I)	5.1 (P32I)	6.1 (P32I)	6.64 (P32I)	7.7 (P32I)
N_{used}	367	795	412	759	433	438	424	427	449
R_{av.}	7	3.7	6.8	4.4	5.6	6.0	5.5	5.5	4.6
P	39	75	39	39	39	39	39	28	39
R1, %	4.2	4.9	3.9	4.0	3.8	3.4	4.1	4.0	4.7
Flack x	0.10(5)	0.30(7)	0.13(7)	0.16(7)	0.01(6)	0.00(4)	0.03(6)	0.08(5)	0.1(1)
wR2, %	9.71	11.92	10.69	13.64	10.88	7.38	9.84	10.75	13.90
GooF	0.9	1.2	1.0	1.1	1.0	0.7	0.9	1.0	1.2

Table 2.4. Details of the data reduction and structure refinements of LTG (continued)

p[GPa] sp. gr.	8.15 (P32I)	9.5 (P32I)	9.5 (A2)	11.57 (P32I)	11.57 (A2)	13.2 (P32I)	13.2 (A2)	14.4 (P32I)	14.4 (A2)	16.7 (P32I)	16.7 (A2)
N_{used}	449	426	577	434	667	483	757	450	700	841	1265
R_{av.}	4.6	6.6	4.07	5.7	5.3	6.9	6.9	3.8	4.3	5.4	4.06
P	39	39	75	39	75	39	75	39	75	28	75
R1, %	5.5	4.7	4.8	4.9	4.9	4.6	4.7	4.9	4.6	8.9	7.3
Flack x	0.0(1)	0.1(1)	0.1(1)	0.1(1)	0.0(1)	0.1(1)	0.0(1)	0.2(1)	0.1(1)	0.3(2)	0.2(1)
wR2, %	12.67	12.92	13.31	15.00	12.30	13.18	12.66	15.26	13.18	25.73	21.23
GooF	1.1	1.3	1.2	1.3	1.2	1.2	1.1	1.3	1.1	1.7	1.5
TWIN,%	-	-	49:30:21	-	22:31:47	-	23:31:46	-	26:37:37	-	29:33:48

The crystal structures of LNG and LTG were refined by the full-matrix method (using SHELXL97), which gives good convergence per cycle, and allows esd's (errors) to be estimated. In order to obtain good esd's on all geometric parameters [66], the final cycle was performed with no applied shifts (for reducing the number of parameters, the anisotropic displacement parameters were held fixed).

Geometrical calculations were performed with the program "VOLCAL" of Hazen et al. [67]. This program calculates polyhedral volumes for all coordination groups, but polyhedral distortion indices are generated only for tetrahedral and octahedral cases. The distortion parameters characterise the deviations of polyhedra from regular geometrical forms. Two kinds of polyhedral distortion indices were calculated, such as quadratic elongation (Q. E.) and bond angle variance (B. V.), which are based on values of bond distances and bond angles, respectively [68].

Quadratic elongation, $\langle I \rangle$, is defined as:

$$\langle I \rangle = \sum_{i=1}^n [(l_i / l_0)^2 / n] \quad (2.8);$$

where l_0 is the centre-to-vertex distance of a regular polyhedron of the same volume, n is the coordination number of the central atom, and l_i is the distance from the central atom to the i th coordinating atom. A regular polyhedron has a quadratic elongation of 1, whereas distorted polyhedra have values greater than 1.

Bond angle variance, σ^2 , is defined as:

$$\sigma^2 = \sum_{i=1}^n [(\theta_i - \theta_0)^2 / (n-1)] \quad (2.9);$$

where θ_0 is the ideal bond angle for the regular polyhedron (e.g. 90° for an octahedron or 109.47° for a tetrahedron), n is the coordination number, and θ_i is the i th adjacent bond angle from outer, to central atoms. Angle variance is zero for a regular polyhedron and positive for a distorted polyhedron.

2.3. High temperature experiments

The LNG and LTG samples used in this part of study were produced and kindly provided by research group of J. Bohm (Freiberg University of Mining and Technology, Germany). The LGSZ samples were produced and kindly provided by research group of B. V. Mill (Moscow State University, Russian).

2.3.1. X-ray powder diffraction experiments

The high temperature measurements were carried out on the powder diffractometer at the beamline B2, HASYLAB [85]. A STOE-high-temperature-chamber for Debye-Scherrer geometry was used [86, 87]. The diffraction patterns were recorded with an image plate in a 2θ range of $7-38^\circ$. The wavelength of $1.1200(2)\text{\AA}$ and the step size of 0.01° were employed, which were determined by current technical conditions at measuring place B2. For determination of 2θ the reflection positions of Si powder standard was recorded at first and last references for each temperature experiments. The obtained image patterns were read by image plate scanner (Fig. 2.3) and by software image program "Quart".

We have used a temperature program with steps of 60° for investigation of the expansion of the unit cell parameters of LNG and LTG. In case of LSZG this step was set at 100° in temperature range from 24°C (room temperature) up to 400°C . Above these temperatures the step was decreased to 50°C in order to detect a possible phase transition at temperatures around 500°C [88].

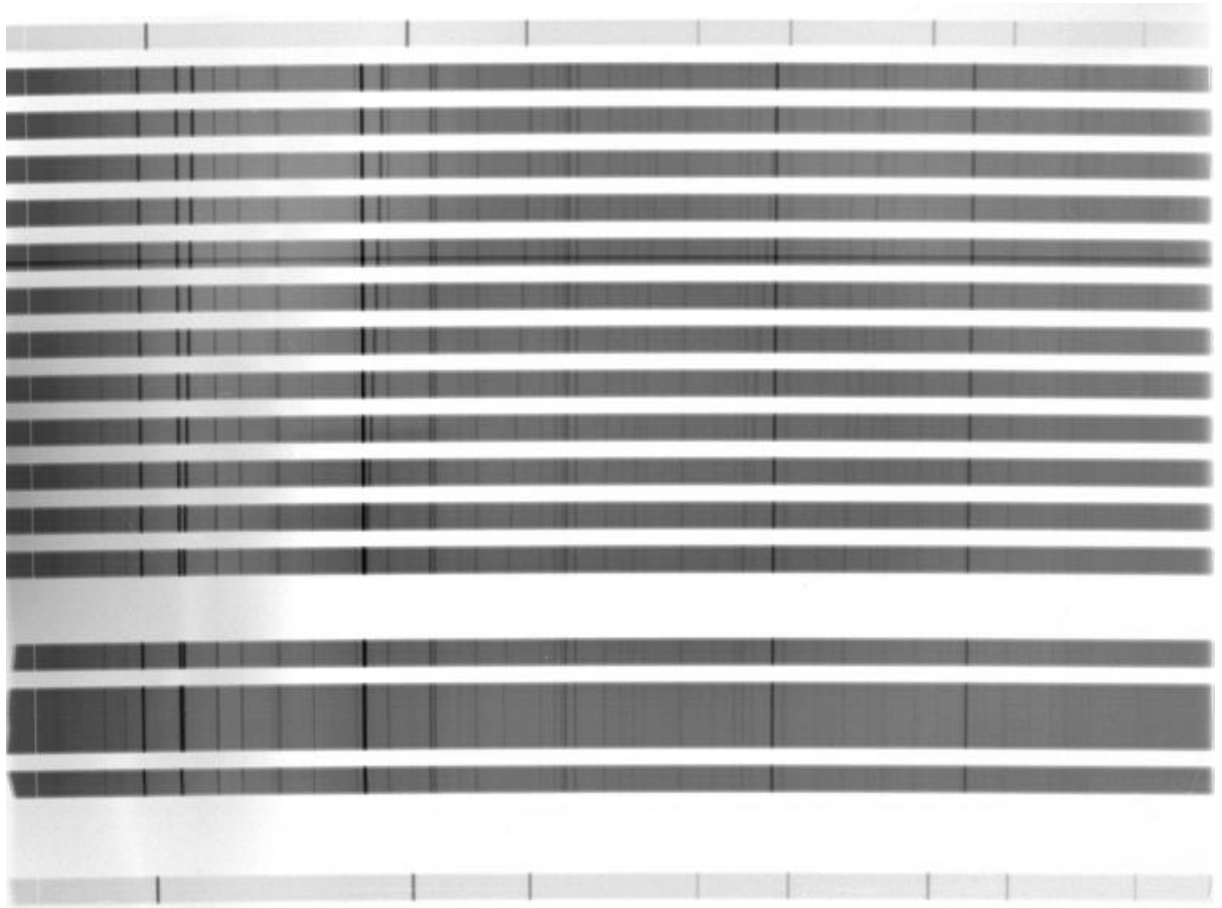


Fig. 2.3: The image plate recorded for mixture LNG, NaCl and diamond powder in ratio 1:1:3 at different temperatures. The first and last records correspond to Si powder standard at room temperature.

The samples powder mixed with NaCl powder and diamond powder in ratio 1:1:3 was contained in a 0.3mm diameter quartz capillary which was inserted into the heating element. NaCl was used as internal temperature standard [90]. The diamond powder was applied in order to minimise the absorption effects.

The cell parameters were refined by use of the PC-Rietveld package WYRIET3 [87, 89]. The atom positions and isotropic temperature factors were set accordingly to refinements at room temperatures for LNG [22], LTG [23] and LSZG [88], respectively. The agreement index R_{Bragg} shown in Tables 2.4, 2.5 and 2.6 is defined as

$$R_{Bragg} = \sum_j |I_{oj} - I_{cj}| / \sum_j I_{oj} \quad (2.10);$$

where I_{oj} and I_{cj} are the observed and calculated integrated intensities of reflections j , respectively. Although the program minimizes the quantity $\sum_i w_i (y_{oi} - y_{ci})^2$ where $w_i = 1/y_{oi}$ and y_{oi} and y_{ci} designate the observed and calculated intensities of data points i , respectively. R_{Bragg} is much more sensitive to subtle differences of the refined structural models. This is due to the fact that the usual profile R -factor

$$R_{wp} = \left[\left(\sum_i w_i (y_{oi} - y_{ci})^2 / \sum_i w_i y_{oi}^2 \right)^{1/2} \right] \quad (2.11);$$

also includes background data points outside the reflection profiles.

Table 2.5. Results of Rietveld refinements of LSZG X-ray data at different temperatures

T [°]	R_{Bragg}	R_{wp}	a	b	c	β
24	27.73	2.16	5.1272(9)	8.249(2)	14.259(4)	90.18(2)
100	25.90	2.26	5.1310(9)	8.257(2)	14.264(4)	90.16(2)
200	26.23	2.34	5.135(1)	8.262(3)	14.24784	90.16(2)
300	29.80	2.57	5.1386(12)	8.248(3)	14.345(4)	90.08(5)
400	25.99	2.96	5.1431(12)	8.254(2)	14.345(4)	90.06(6)
450	25.03	3.03	5.1456(12)	8.257(2)	14.354(4)	90.04(8)
500	25.27	3.02	5.1479(12)	8.263(2)	14.362(4)	90.08(5)
550	26.43	2.91	5.1514(11)	8.266(3)	14.372(4)	90.11(3)
600	25.73	2.83	5.1542(11)	8.270(2)	14.380(3)	90.11(3)
650	42.42	2.86	5.1564(13)	8.279(3)	14.379(5)	90.07(7)
700	26.38	2.92	5.1581(11)	8.280(2)	14.392(4)	90.12(3)
800	34.52	2.97	5.162(3)	8.296(6)	14.400(11)	90.11(8)

Table 2.6. Results of Rietveld refinements of LNG X-ray data at different temperatures

T [°]	R_{Bragg}	R_{wp}	a	c
24	8.99	2.33	8.2274(5)	5.1261(4)
60	10.03	2.30	8.2291(5)	5.1270(4)
120	10.60	2.40	8.2321(5)	5.1284(4)
180	11.20	2.27	8.2356(5)	5.1298(3)
240	10.90	2.26	8.2392(5)	5.1311(4)
300	10.45	2.30	8.2422(5)	5.1325(4)
360	9.98	2.38	8.2469(5)	5.1348(4)
420	11.18	2.53	8.2513(5)	5.1365(4)
480	9.05	2.49	8.2543(5)	5.1380(4)
540	10.23	2.59	8.2591(6)	5.1402(5)
600	8.94	2.41	8.2634(5)	5.1421(4)
660	7.24	2.21	8.2663(5)	5.1434(6)
720	8.12	2.45	8.2705(6)	5.1452(5)
780	7.68	2.15	8.2760(5)	5.1421(4)
850	12.29	2.28	8.2827(6)	5.1522(5)

Table 2.7. Results of Rietveld refinements of LTG X-ray data at different temperatures

T [°]	R_{Bragg}	R_{wp}	a	c
24	12.73	2.40	8.2322(5)	5.1254(4)
60	10.98	2.28	8.2330(5)	5.1258(4)
120	12.00	2.36	8.2372(5)	5.1268(4)
180	11.42	2.39	8.2395(5)	5.1278(3)
240	12.25	2.57	8.2436(5)	5.1295(4)
300	12.16	2.53	8.2473(5)	5.1313(4)
360	13.23	2.57	8.2511(5)	5.1336(4)
420	12.67	2.64	8.2543(5)	5.1348(4)
480	12.77	2.45	8.2582(5)	5.1368(4)
540	11.54	2.68	8.2126(6)	5.1384(5)
600	12.22	2.95	8.2672(5)	5.1406(4)
660	11.94	2.87	8.2690(5)	5.1420(6)
720	11.68	3.28	8.2758(6)	5.1449(5)
780	9.46	3.59	8.2799(5)	5.1460(4)
850	12.21	2.48	8.2836(6)	5.1480(5)

The large values of R_{Bragg} and R_{wp} are due to fixed atom positions and large absorption effects in the whole temperature range.

2.3.2 Thermal expansion coefficients

When heat is added to a material so that there is a change in temperature, T_0 to T_1 , there is a corresponding change in volume, V_0 to V_1 . To describe this change the mean coefficient of volumetric thermal expansion of the material is defined by

$$\mathbf{b}_m = \frac{V_1 - V_0}{V_0(T_1 - T_0)} \quad (2.12).$$

The coefficient of thermal expansion is not measured directly but it is either calculated directly from consecutive observations of expansion or by differentiating an equation that represents the expansion. The mean thermal expansion coefficient [91]:

$$\mathbf{a}_L = \frac{1}{L_0} * \frac{L_T - L_0}{T - T_0} \quad (2.13);$$

is used throughout this study to characterize thermal expansions of selected parameters. The term L_0 and L_T are the values of cell parameters at room temperature (or some initial temperature) and at some higher temperature T .

3. RESULTS AND DISCUSSION

3.1. Compression mechanisms of LNG and LTG single crystals

In this part the influence of hydrostatic pressure on lattice parameters and crystal structures of a single crystals of $\text{La}_3\text{Nb}_{0.5}\text{Ga}_{5.5}\text{O}_{14}$ and $\text{La}_3\text{Ta}_{0.5}\text{Ga}_{5.5}\text{O}_{14}$ will be reported.

The unit cell and structural parameters of LNG and LTG at normal conditions were reported by Molchanov et al. (2001) and Takeda et al. (1997), respectively (see also APPENDIX A).

3.1.1 Axial compressibilities

Figure 3.1 and 3.2 depict the dependencies of the lattice parameters a and c of LNG from pressure. To maintain a simple description of these dependencies it is necessary to divide each of data sets into two parts. This leads to the assumption of the existence of a phase transition. Thus the changes in the lattice parameters of LNG under pressure reveal that a phase transition occurs at pressure 12.4(3)GPa. It can be seen that in a - direction the high-pressure phase of LGN is even more compressible than for the low-pressure polymorph. In contrast, a decrease of compressibility of the lattice parameter c after phase transition pressure is observed. Furthermore at pressure about 12.4(3)GPa there is a small but significant discontinuity in the c parameter evolution, that is characteristic for the first-order nature of the phase transition. The c cell edge change at the phase transition is rather small and has been estimated to $\Delta c=0.16\%$.

The lattice parameter dependencies from pressure of LTG single crystals are represented in Figure 3.3 and 3.4. In this case the division of the data sets into two parts were needed, again. This must be caused by phase transition of LTG at pressures around 11.7(3)GPa. As it can be seen in Figure 3.1 or 3.3, the a parameter of LNG or LTG decreases continuously across the phase transition pressure, this can demonstrate the second order character of transition. At the same time, discontinuity in the c parameter evolution of LNG or LTG may indicates a phase transition of the first-order. The change of the c unit parameter of LTG $\Delta c=0.11\%$ is calculated at pressure about 11.7(3)GPa.

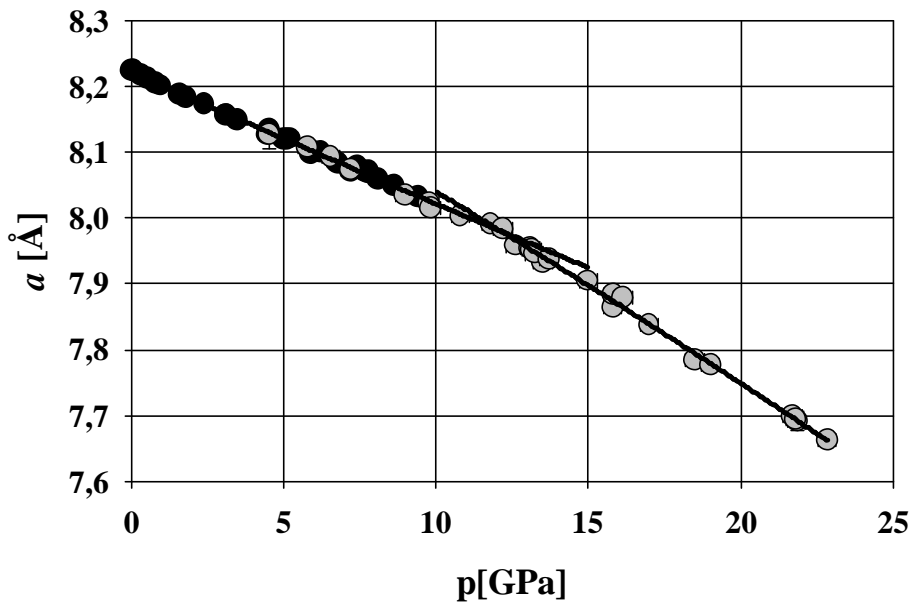


Fig. 3.1: Unit –cell parameter a of LNG at pressures. The colour of the symbols corresponds to the used pressure medium (black-alcohol mixture, grey- He).

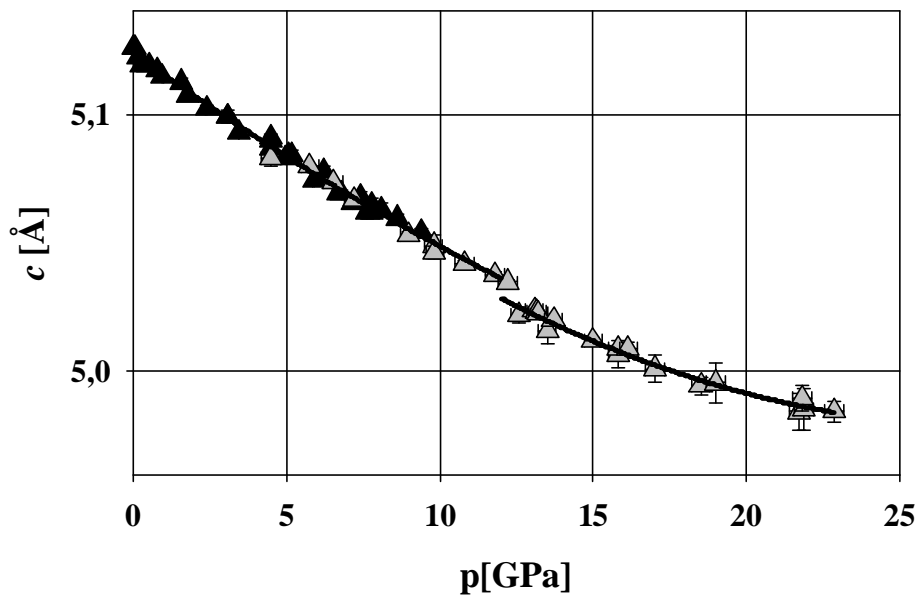


Fig. 3.2: Unit –cell parameter c of LNG at pressures. The colour of the symbols corresponds to the used pressure medium (black-alcohol mixture, grey-He).

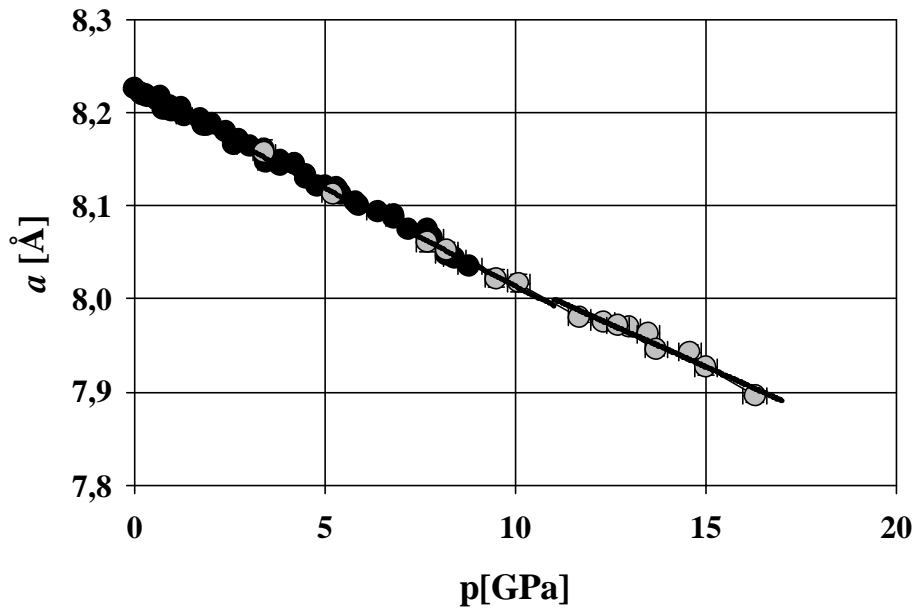


Fig. 3.3: Unit –cell parameter a of LTG at pressures. The colour of the symbols corresponds to the used pressure medium (black-alcohol mixture, grey-He).

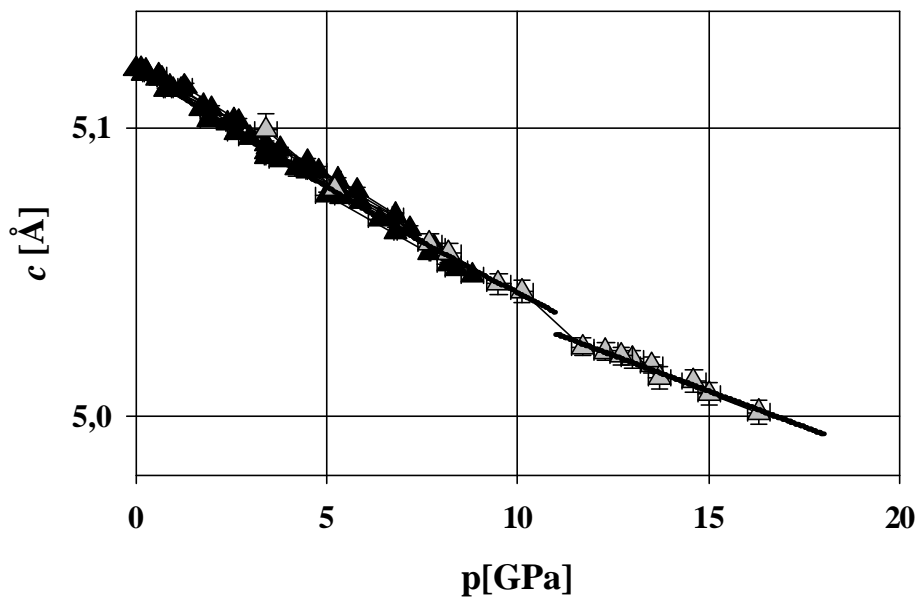


Fig. 3.4: Unit –cell parameter c of LTG at pressures. The colour of the symbols corresponds to the used pressure medium (black-alcohol mixture, grey-He).

In addition, the precision and number of measurements of the cell parameters of LNG or LTG at pressures about 12GPa are not enough for conclusion about a nature of phase transition. Therefore it can be suggested rather a first order nature of the phase transition of LNG or LTG, in respect with the pronounced discontinuity in the c parameter evolution of LNG or LTG across the pressure of phase transition.

To simplify the analysis of the axial compressibilities of LNG and LTG the dependencies of the relative lattice parameters (a/a_0 and c/c_0) from pressure are plotted in Fig.3.5. It can be seen that the compressibilities along c axis are almost the same for LNG and LTG in the whole investigated pressure range. In contrast, the pressure dependencies of a axis of these materials are similar for low-pressure form, whereas the compressibilities in a -axis direction for the high-pressure polymorphs of LNG and LTG are significant different to each other.

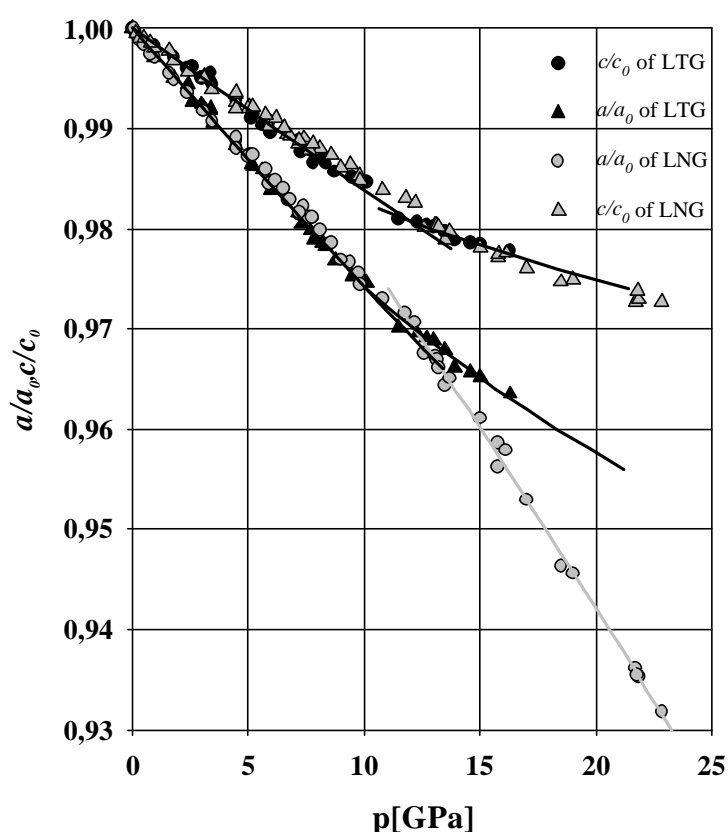


Fig. 3.5: The variations of a/a_0 and c/c_0 as functions of pressure for LGN and LGT

The isothermal bulk moduli and their derivatives (B_0 and B_0') were calculated by fits of Birch-Murnaghan equations of state to the data for a and c parameters of LNG and LTG under pressure. Accordingly, axial compressibilities were obtained as $\beta=1/B_0$. The results are listed in Table 3.1.

Table 3.1. The compressibilities of the a and c parameters of LGN and LGT

Compound	Low- pressure phase		High- pressure phase	
	β_a [GPa ⁻¹]	β_c [GPa ⁻¹]	β_a [GPa ⁻¹]	β_c [GPa ⁻¹]
LNG	2.61×10^{-3}	1.87×10^{-3}	4.69×10^{-3}	1.26×10^{-3}
LTG	2.71×10^{-3}	1.97×10^{-3}	1.89×10^{-3}	1.12×10^{-3}

Thus the values from Table 3.1 indicate that compressibilities of LNG and LTG in c -axis direction are similar in whole pressure range, and decrease after pressures phase transitions. The compressibilities of a axis of these compounds are comparable for low pressure phase, whereas after pressure phase transition these values increases for LNG and decrease in case of LTG.

These results for axial compressibilities can be well explained in terms of crystal structures of LNG and LGT, which are similar in the pattern of their cation arrangement. As it can be seen (Fig. 3.5 and 3.6), the a axis is the most compressible direction for both compounds. The compressional anisotropy is typical for a layered structure, and can be explained through the differing character of interconnectivities across and within the layers. The increase of the c/a -ratio (Fig. 3.6) under pressure indicates that the compression mechanism of LNG and LTG operates mostly on the ab -plane. Thus within the layers (in the ab plane) these structures can compress more readily due to cation-anion bond shortening, that causes a decrease of volume of large polyhedra (first of all the largest LaO₈ dodecahedra with predominantly ionic character of bonding). This is accompanied by slight tilting and distortions of corner sharing tetrahedra within the tetrahedral layers. On the other hand, the compression in c direction is more rigid due to less flexible interconnectivities of polyhedrally coordinated cations (shared edges etc.) between the layers. The differing behaviour of c/a ratio under pressure between high pressure polymorphs of LNG and LTG can be well explained due to Nb⁵⁺ and Ta⁵⁺ substitution. Presumably, the polarisation of the oxygen arrangement by Nb⁵⁺ ion is increased within the high pressure polymorph of LNG, whereas TaO₆ octahedra still stay almost regular.

The compression mechanism of this compounds will be described more detailed in the following.

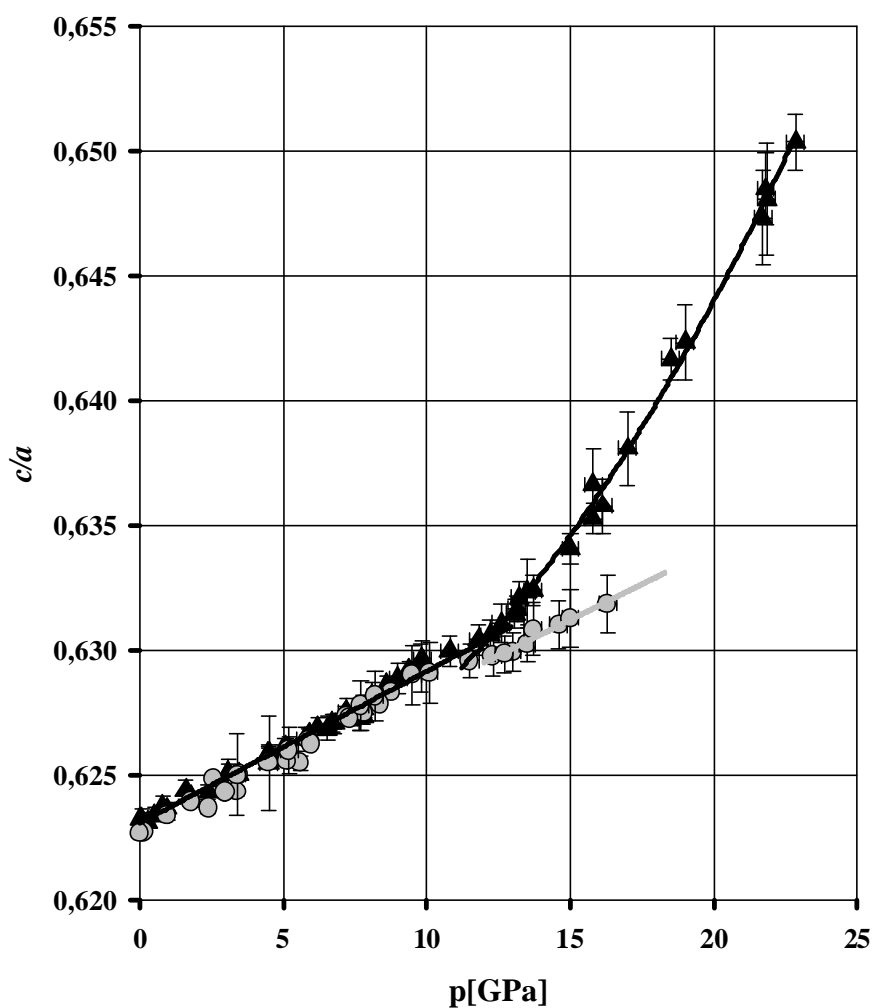


Fig. 3.6. Axial ratios c/a_0 of LGN (triangle up) and LGT (circle) vs. pressure.

Since LNG and LTG belong to the same crystal class as quartz (trigonal symmetry), it will be of interest to compare the effect of high hydrostatic pressure on the lattice of LNG, LTG single crystals with α -quartz and isostructural materials like GaPO_4 [28]. These compounds, LNG or LTG and α -quartz or GaPO_4 , are to be described in enantiomorphous acentric space groups. Otherwise, the quartz structure is simple and can be described by consideration of

tetrahedral chains, whereas the structure of LNG or LTG has a mixed framework consisting of polyhedron layers. It is well known, that under hydrostatic pressure the a axis of quartz-type structures is more compressible than the c axis. Thus α -quartz [58] or GaPO_4 [28] display an anisotropic behaviour as a function of pressure, as well as LNG or LTG. In spite of the similar compressional anisotropy of these materials under pressure, the mechanism of the axial compression has to be explained by various concepts.

Thus the higher compression in the a -axis direction of α -quartz or GaPO_4 is dominated by tilting of corner sharing tetrahedra along the tetrahedral chains. Contrary to this, the tilting of GaO_4 tetrahedra within the tetrahedral layers of LNG or LTG (along a -axis) are hampered due to shared edges and (or) corners with other polyhedra. Therefore the compression within the polyhedral layers is dominated by cation-anion bond shortening. The lower compression of the crystal structure of α -quartz or GaPO_4 along c -axis is caused mainly by less vacancies between the tetrahedral chains. Thus the compressibility along c axis direction is rigid due to repulsive interaction between these chains. Similar to this the compression in c -axis direction in the case of LNG or LTG is rigid interaction between the layers and by less flexible interconnectivities between the layers (shared edges of polyhedrally coordinated cations etc.). Furthermore the reduction of cell volume of the LNG or LTG crystals can only be explained through complex changes in the structural geometry, whereas the compressions of α -quartz and GaPO_4 mainly lead to tilting of the tetrahedra [28]. Especially, the existence of octahedral-dodecahedral layers in the crystal structure of LNG or LTG causes the difference to the compression mechanisms of α -quartz type structures.

On the other hand, the anisotropic behaviour of the crystals can be predicted by anomalous elasticity, which is characterized by variations of elastic constants [38, 39, 46]. As pointed out above (chapter 1.3.4.), nonlinear behaviour of elastic constants under homogenous mechanical stresses of $\text{La}_3\text{Ga}_{5.5}\text{SiO}_{14}$ (LGS) crystals was observed, which are a structural isomorph to LGN or LTG [42]. Thus, the application of pressure parallel to a - and c -axis causes differing effects on the crystal symmetry of LGS. Therefore the extraordinary behaviour of a axis as compared to c in case of LNG or LTG under hydrostatic pressure can be well explained with regard to anomalous elasticity.

3.1.2 Bulk moduli

The pressure dependencies of the relative volumes of LNG and LTG are shown in Figure 3.7. To find a simple description of these dependencies, the division of the data sets of LNG as well as of LTG into two parts is necessary. This fact provides further evidence for the assumption of a phase transition at pressures above 12.4(3)GPa for LNG and 11.7(3)GPa for LTG. Furthermore, no well pronounced discontinuities, characteristic for a first order phase transition, can be observed for the pressure dependencies of the relative volumes of LNG and LTG at pressures around 12(1)GPa. This phenomenon can be well explained due to differing axial compressibilities. As pointed out above (chapter 3.1.1.), the decreasing of the a parameter of LNG or LTG across the phase transition pressure suggests second order character of transition. The first-order character of phase transition, indicated by a jump of the c -axis across pressures around 12(1)GPa, presumes reconstructive changes between polyhedral layers with possible changes of the coordination number. The dominant influence of the second-order nature on the phase transitions of LNG and LTG could be expected, which manifests the absence of a significant volumes jumps of LNG or LTG at pressure phase transition. In terms of these phenomena, the phase transitions of LNG and LTG presumably will have displacive character.

For the analysis of the volume compressibilities of low- and high- pressure phases of LNG and LTG, the bulk modulus B_0 and pressure derivative B_0' were obtained by fitting Birch-Murnaghan equations of state. In the pressure range from atmospheric up to 12(1)GPa the pressure contraction of LNG and LTG are almost the same and close to linear, demonstrated by the extraordinarily small value of B_0' (1.4(8) for LNG and 0.5(5) for LGT). Compression is uniform up to this pressure, with calculated bulk modulus of 145 ± 3 GPa and 144 ± 2 GPa for LNG and LTG respectively. Accordingly, the calculated compressibilities of low pressure phases of both compounds are around 0.007GPa^{-1} . Thus the substitution of Nb^{5+} against Ta^{5+} causes almost no difference of compressibilities of low pressure phases of LNG and LGT.

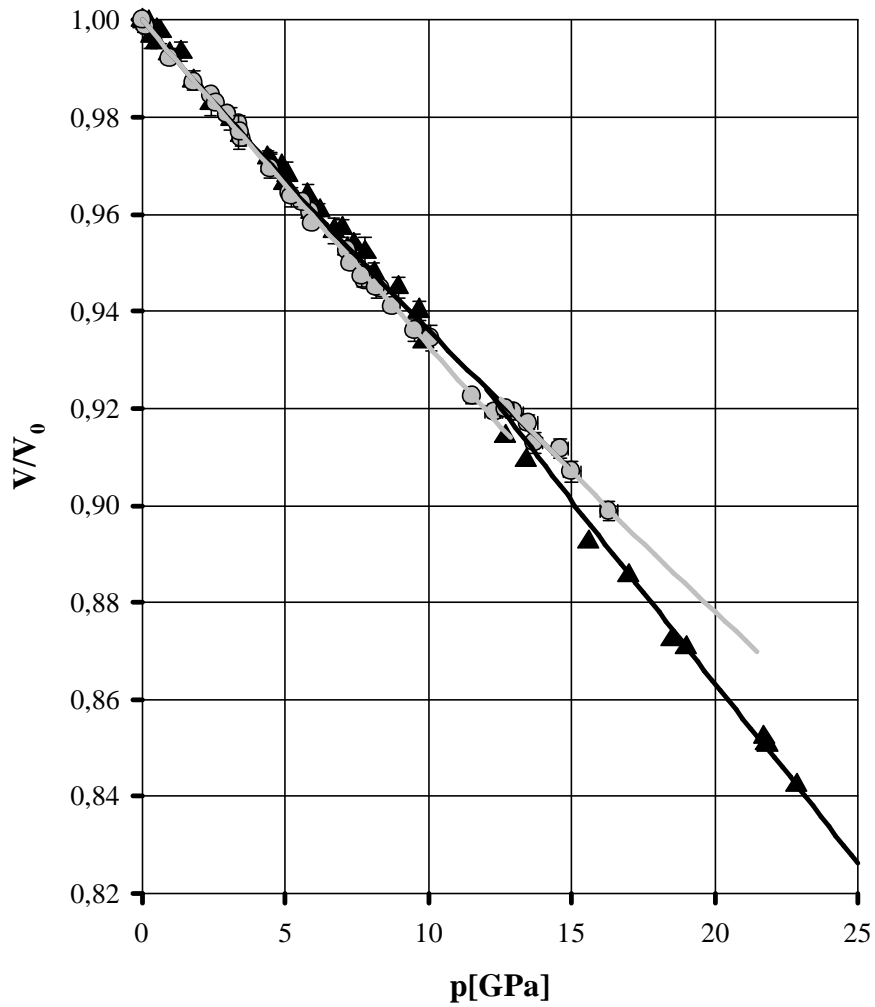


Fig. 3.7: Relative volume compressions of LGN (triangle up) and LGT (circle) vs. pressure

The initial phase of LNG or LTG crystals is less compressible as compared to α -quartz and GaPO_4 with bulk moduli 37.12(9)GPa ($B_0'=5.99(4)$) and 39.9(9)GPa ($B_0'=3.7(3)$), respectively. This difference might be explained by closer packing of the layered structure.

Thus, the packing coefficients (c_i) can be estimated by means of the following equation [74]:

$$c_i = \sum V_a / V_c, \quad (3.1),$$

where $\sum V_a$ is the sum of volumes of the atoms or anions contained in the elementary cell of volume V_c .

Thus the packing coefficient of LTG as well as of LNG is 0.63, due to the equal ionic radiuses of Nb and Ta (0.64Å). The c_i calculated for α -quartz and GaPO₄ at ambient conditions are 0.41 and 0.32, respectively. Whereas within α -quartz or GaPO₄ the space is filled only to about 40% at normal conditions, the structure of LNG or LTG is filled about 60%. Thus the less filled space within unit cell of α -quartz or GaPO₄ allows higher compressibility of these materials as compared to LNG or LTG. Nevertheless, the different compression mechanisms of appointed compounds do affect the different compressibilities.

On the other hand, the difference between bulk moduli of α -quartz structures and LNG or LTG can be well explained by different interconnectivities of polyhedra of these structures. As pointed out above the crystal structure of α -quartz or GaPO₄ consist of corner sharing tetrahedra. This allows the higher compression of low quartz structures as compared to that of LNG or LTG, which compression is rigid due to sharing edges of tetrahedra.

The high-pressure phase of LNG has a bulk modulus of 93(2)GPa (B_0' =1.9(9)). The cell constants of the high pressure polymorph of LTG were investigated in a considerably smaller pressure range (11.7-16.7GPa) as compared to experiments with LNG (from pressure phase transition up to 23GPa). Thus with six data points, the fitting of the data of LTG resulted in large errors, making it difficult to get meaningful results for B_0 and B_0' . Furthermore, the hypothetical V_0 of the high-pressure phases were calculated. Thus the determination of the pressure derivative of the bulk modulus or hypothetical V_0 of high pressure modifications from compression experiments are hampered by the fact of correlation of these two variables in the P - V equation of state, and by extrapolation over a large pressure range (from pressures of phase transition 12(1)GPa to atmospheric conditions). Therefore the bulk modulus B_0 for high pressure phase of LTG was calculated by fits of Birch-Murnaghan equations of state to the data sets with B_0' constrained to 1.9, with respect to the high-pressure phase of LNG. The obtained bulk modulus for high-pressure phase of LTG is B_0 =128(12)GPa. Accordingly, the calculated compressibilities are 0.011GPa⁻¹ for high pressure polymorph of LNG and

0.008GPa⁻¹ for LTG, respectively. Thus a difference between compressibilities of investigated compounds appears only above pressures of the phase transitions.

Nevertheless a higher compressibility of the high-pressure polymorph of LNG, as compared to the low-pressure phase, is clearly observed. In contrast, the compressibility of LTG after pressure phase transition slightly increases. Furthermore, whereas the hypothetical V_0 of high pressure phase of LNG is 4(2)% larger than the initial one, the value of V_0 of high pressure phase of LTG stay almost the same within the error (0.9(8)%).

Generally, an increase in compressibility is typical for polyhedral tilt [25, 26]. In most cases, the additional freedom due to the symmetry breaking and thus increasing flexibility of individual structural rigid units within framework- type structures gives sufficient explanation for the (in first glance rather unexpected) higher compressibility of the high pressure polymorph. In contrast to LNG, in case of LTG it can be assumed that a high pressure polymorph does not obtain enough degrees of freedom for a pronounced increase of compressibility due to soft Ta-O bonding. Presumably, the difference between behaviours of high pressure polymorphs of LNG and LTG is caused by increase of polarisation of the oxygen arrangement by Nb⁵⁺ ions, whereas the octahedra forming by Ta⁵⁺ still stay almost regular.

On the other hand, for various compounds, a higher compressibility of the high-pressure phase has been characterised through anomalous elasticity [46]. Most recent experiences with high-pressure phase transitions using high-resolution single crystal measurements reveal the occurrence of nonlinear elasticity on approaching the critical pressures for several independent systems [38,77]. In particular transformations of displacive structural transitions can show, with respect to the given structural flexibility quite large anomalies. Thus, due to elastic softening the evolution of both lattice parameters and unit-cell volumes can be affected over a quite broad range in pressure, showing a typical and more pronounced softening for the low-symmetry form [38]. According to this, the increase of compressibility of high pressure polymorph and extraordinary behaviour of a axis as compared to c in case of LGN crystals under hydrostatic pressure can be well explained in terms of anomalous elasticity. Probably, the Nb –Ta substitution causes a stronger effect on elastic constants of high pressure polymorphs (lower symmetry phases) of LNG and LTG as compared to the initial ones.

3.1.3. Compression mechanisms

The crystal structures of LNG and LTG have following variable positional parameters:

La ($x; 0; 0$), Ga(2) ($1/3; 2/3; z$), Ga(3) ($x; 0; 1/2$), O(1) ($1/3; 2/3; z$), O(2) ($x; y; z$) and O(3) ($x; y; z$). Ga(1) and Ta or Nb share the position ($0; 0; 0$) in ratio 1:1. The results from refinements in trigonal symmetry using intensity data collected for LNG and LTG at investigated pressures are listed in Tables 3.2 and 3.3

Table 3.2. Structural parameters of LNG refined in the trigonal space-group $P321$

p [Gpa]	La-3e ($x;0;0$)	Ga(2)-2d ($1/3;2/3;z$)	Ga(3)-3f ($x;0;1/2$)	O(1)-2d ($1/3;2/3;z$)	O(2)-6g ($x;y;z$)			O(3)-6g ($x;y;z$)		
	x	z	x	z	x	y	z	x	y	z
0	.42459(2)	.53124(7)	.76176(4)	.1784(5)	.4563(3)	.3088(3)	.3054(3)	.2188(3)	.0773(3)	.7627(3)
0.8	.42528(12)	.5307(8)	.7624(2)	.182(5)	.4557(14)	.3083(14)	.300(3)	.2128(13)	.0708(18)	.760(3)
1.8	.42575(18)	.5310(2)	.76283(17)	.177(2)	.4548(8)	.3082(10)	.3064(10)	.2186(8)	.0765(10)	.7621(11)
3.3	.42652(8)	.5308(5)	.76405(16)	.181(4)	.4546(9)	.3067(9)	.302(2)	.2145(9)	.0720(9)	.759(2)
4.5	.42700(11)	.5305(3)	.7644(2)	.179(2)	.4570(13)	.3093(13)	.3052(15)	.2205(10)	.0735(11)	.7613(14)
4.8	.42746(10)	.5307(4)	.76376(19)	.182(3)	.4542(13)	.3089(14)	.3023(18)	.2201(11)	.0750(12)	.7602(19)
5.2	.42755(14)	.5298(9)	.7647(3)	.182(7)	.4533(18)	.3083(13)	.304(4)	.2159(11)	.0691(15)	.760(4)
6.8	.42868(8)	.5291(6)	.76526(18)	.184(4)	.4574(10)	.3072(12)	.308(3)	.2180(11)	.0722(11)	.759(3)
7.8	.42902(13)	.5294(6)	.7657(3)	.173(4)	.4535(17)	.307(2)	.317(3)	.217(2)	.0721(14)	.757(3)
9.67	.43162(9)	.5252(5)	.76729(16)	.173(3)	.4537(16)	.306(2)	.311(3)	.2180(11)	.0714(15)	.760(3)
9.9	.43207(11)	.5250(5)	.7672(2)	.171(3)	.4538(18)	.305(2)	.309(3)	.2196(13)	.0719(18)	.760(3)
11.7	.43306(11)	.5231(4)	.7679(2)	.168(3)	.4530(16)	.3045(18)	.310(2)	.2191(17)	.0698(19)	.761(2)
13.1	.43418(15)	.5190(6)	.7666(3)	.168(4)	.447(2)	.295(2)	.302(3)	.2200(19)	.069(2)	.761(3)
15.6	.4361(3)	.5125(9)	.7661(4)	.160(7)	.445(4)	.295(7)	.319(5)	.221(4)	.074(4)	.766(4)
18.5	.4390(5)	.5075(17)	.7650(8)	.168(8)	.439(8)	.279(8)	.332(8)	.228(7)	.074(7)	.765(6)
21.8	.4372(8)	.505(3)	.7681(13)	.15(3)	.435(7)	.287(9)	.379(13)	.239(7)	.072(7)	.760(14)
22.8	.4405(10)	.501(2)	.7652(17)	.118(17)	.443(14)	.29(2)	.355(17)	.247(12)	.067(13)	.784(12)

Table 3.3. Structural parameters of LTG refined in the trigonal space-group $P321$

P. Gpa	La-3e ($x;0;0$)	Ga(2)-2d ($1/3;2/3;z$)	Ga(3)-3f ($x;0;1/2$)	O(1)-2d ($1/3;2/3;z$)	O(2)-6g ($x;y;z$)			O(3)-6g ($x;y;z$)		
	x	z	x	z	x	y	z	x	y	z
0	.42492(7)	.4689(2)	.7617(1)	.822(2)	.4568(7)	.3089(8)	.694(1)	.2194(8)	.0787(8)	.241(1)
0.7	.42586(11)	.4687(6)	.7618(2)	.824(4)	.4518(14)	.3056(16)	.704(3)	.2172(13)	.0731(14)	.243(2)
1.4	.4260(2)	.4698(12)	.7622(5)	.838(7)	.460(2)	.307(2)	.693(3)	.215(2)	.077(2)	.235(3)
2.3	.42651(11)	.4691(3)	.7628(3)	.824(2)	.4566(16)	.3095(16)	.6958(14)	.2195(13)	.0766(16)	.2389(11)
3	.42713(10)	.4694(4)	.7634(2)	.822(2)	.4568(12)	.3077(15)	.6969(17)	.2188(13)	.0749(14)	.2404(14)
3.3	.42707(11)	.4696(7)	.7636(2)	.833(5)	.4536(13)	.3064(11)	.704(3)	.2188(12)	.0742(12)	.239(2)
5.1	.42799(8)	.4693(5)	.76424(15)	.827(3)	.4539(9)	.3052(9)	.703(2)	.2188(8)	.0736(9)	.2426(18)
6.1	.42883(14)	.4695(6)	.7643(3)	.834(4)	.455(16)	.3062(18)	.694(3)	.2166(16)	.0719(18)	.239(2)
6.64	.42912(10)	.4709(6)	.7649(2)	.832(4)	.4575(14)	.3059(14)	.703(3)	.2209(12)	.0749(13)	.243(2)
7.7	.43055(13)	.4742(6)	.7656(3)	.828(4)	.454(2)	.304(3)	.697(4)	.2178(18)	.072(2)	.242(3)
8.15	.43038(17)	.4715(8)	.7651(4)	.840(6)	.455(2)	.302(3)	.688(3)	.2165(2)	.071(2)	.239(3)
9.5	.43218(15)	.4738(5)	.7668(3)	.838(4)	.451(3)	.300(3)	.685(4)	.2170(17)	.071(3)	.241(2)
11.57	.43463(19)	.4795(5)	.7659(4)	.838(3)	.453(4)	.296(3)	.691(3)	.225(2)	.077(3)	.238(2)
13.2	.43528(17)	.4800(4)	.7660(3)	.834(3)	.452(2)	.293(4)	.695(3)	.225(2)	.076(3)	.238(2)
14.4	.4362(2)	.4810(6)	.7660(3)	.837(4)	.443(4)	.277(5)	.698(4)	.220(3)	.071(3)	.235(3)
16.7	.4381(2)	.4879(9)	.7661(4)	.831(6)	.459(6)	.303(9)	.689(6)	.226(4)	.077(5)	.234(5)

Compression mechanisms of LNG and LTG are quite complex and can be described as follows. The changes of bonding distances and angles under pressure are caused by the reduction of the unit cell volume, by the variation of the c/a -ratio and by shifts of atomic position parameters. Thus with increase of the pressure, the distances between cations decrease. The cations are shifted in order to maximize the distances between the positively charged centres. Thus the largest cation La^{3+} is shifted within the ab plane (Fig. 3.8). This leads first of all to a displacement of tetrahedrally coordinated Ga(2) ions, which share half of their edges (O2-O2) with LaO_8 dodecahedra. Accordingly, neighbouring Ga(3) ions try to shift in similar manner. These displacements within ab -plane are hampered because the polyhedra share corners (first of all due to shared corners with octahedra, which are surrounded by Ga(3)O_4 tetrahedra according to the triple axis law). Therefore the following compression leads to a decrease of anion-cation bonds.

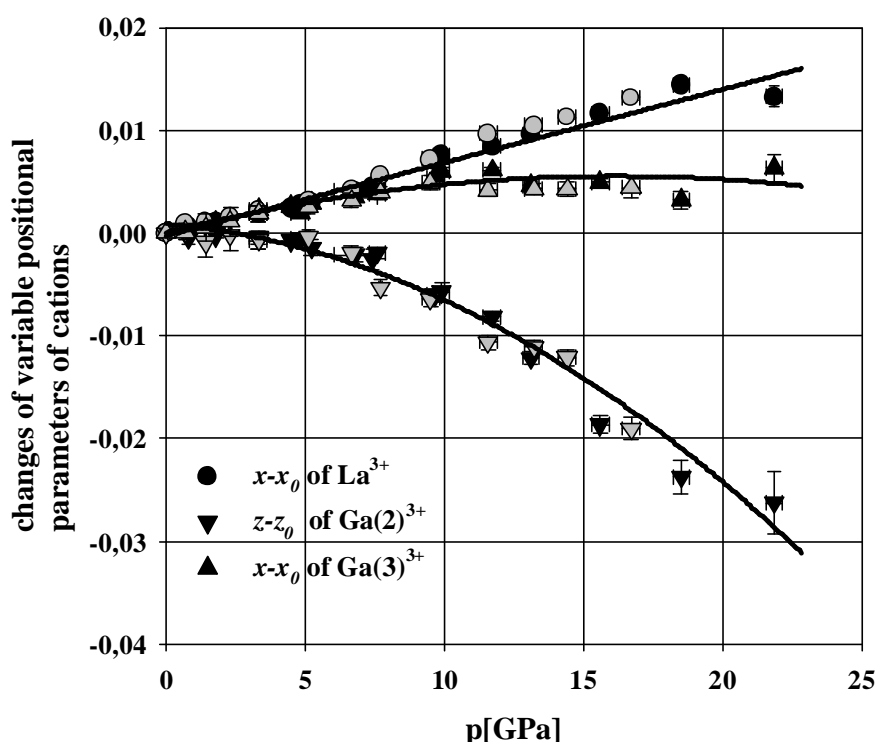


Fig. 3.8. Changes of variable coordinates of the cations vs. pressure of trigonal LNG (black symbols) and LTG (grey symbols).

Selected interatomic distances (bond lengths) and polyhedral volumes are listed in Table 3.4 for LNG and in Table 3.5 for LGT.

Table 3.4. Interatomic distances [\AA], polyhedral volumes [\AA^3], quadratic elongation (Q. E.) and angle variance (A. V.) for polyhedra of LGN.

Pressure	0	1.8	3.3	5.2	6.8	7.6	9.67	11.7
La-3e decahedron								
La-O3x2	2.413(3)	2.411(6)	2.420(8)	2.392(14)	2.393(8)	2.404(10)	2.392(9)	2.375(10)
La-O1x2	2.6189(9)	2.603(3)	2.598(7)	2.587(12)	2.579(8)	2.554(7)	2.535(5)	2.516(5)
La-O2x2	2.464(2)	2.455(7)	2.436(8)	2.418(16)	2.424(9)	2.446(14)	2.410(11)	2.398(12)
La-O2'x2	2.882(2)	2.877(6)	2.847(8)	2.859(17)	2.843(11)	2.874(14)	2.842(17)	2.827(17)
Volume	28.7	28.4	28.0	27.7	27.5	27.7	26.9	26.4
Ga-1a octahedron								
Ga-O3x6	1.994(2)	1.988(5)	1.970(8)	1.972(13)	1.977(9)	1.976(11)	1.964(9)	1.964(10)
Volume	10.20	10.11	9.76	9.70	9.86	9.83	9.67	9.40
Q. E.	1.02	1.02	1.03	1.03	1.03	1.03	1.03	1.03
A. V.	75.0	79.3	102.0	110.7	100.5	107.8	104.4	111.1
Ga-2d tetrahedron								
Ga-O1	1.809(3)	1.811(9)	1.79(2)	1.77(3)	1.75(2)	1.80(2)	1.780(14)	1.784(16)
Ga-O2x3	1.840(2)	1.840(6)	1.842(7)	1.846(15)	1.798(9)	1.802(12)	1.813(10)	1.812(10)
Volume	3.10	3.08	3.04	3.04	2.84	3.03	2.92	2.90
Q. E.	1.02	1.02	1.02	1.02	1.02	1.01	1.02	1.01
A. V.	78.2	74.0	90.6	82.3	84.4	56.6	80.8	78.0
Ga-3f tetrahedron								
Ga-O3x2	1.838(2)	1.831(6)	1.827(9)	1.840(16)	1.815(10)	1.799(12)	1.805(9)	1.812(11)
Ga-O2x2	1.873(2)	1.859(6)	1.873(8)	1.853(16)	1.865(9)	1.815(13)	1.832(12)	1.830(10)
Volume	3.11	3.00	3.09	3.07	3.03	2.87	2.91	2.94
Q. E.	1.04	1.04	1.03	1.03	1.03	1.03	1.04	1.04
A. V.	154.1	158.2	139.0	144.5	153.1	145.5	165.5	176.2

Table 3.5. Interatomic distances [\AA], polyhedral volumes [\AA^3], quadratic elongation (Q. E.) and angle variance (A. V.) for polyhedra of LGT.

Pressure	0	2.3	3.3	5.1	7.7	8.15	9.5	11.57
La-3e decahedron								
La-O3	2.428(7)	2.404(9)	2.412(8)	2.403(8)	2.407(16)	2.398(15)	2.403(12)	2.376(14)
La-O1	2.618(3)	2.595(4)	2.567(8)	2.569(5)	2.547(7)	2.528(9)	2.516(6)	2.499(5)
La-O2	2.464(6)	2.436(10)	2.436(12)	2.411(8)	2.401(11)	2.453(15)	2.45(2)	2.430(19)
La-O2'	2.885(6)	2.868(9)	2.832(12)	2.818(8)	2.82(2)	2.823(19)	2.82(2)	2.77(2)
Volume	28.8	28.0	27.3	27.2	26.9	26.9	27.0	26.0
Ga-1a octahedron								
Ga-O3	2.007(6)	1.993(8)	1.979(11)	1.993(7)	1.976(13)	1.959(13)	1.959(11)	1.979(16)
Volume	10.45	10.17	10.06	10.11	9.80	9.57	9.57	10.02
Q. E.	1.02	1.02	1.03	1.03	1.03	1.03	1.03	1.02
A. V.	74.2	79.7	88.8	96.9	103.1	103.1	106.6	80.7
Ga-2d tetrahedron								
Ga-O1	1.810(8)	1.804(12)	1.88(2)	1.821(15)	1.79(2)	1.86(3)	1.836(18)	1.801(17)
Ga-O2	1.836(6)	1.830(9)	1.846(11)	1.846(8)	1.826(16)	1.790(15)	1.800(17)	1.793(16)
Volume	3.06	3.04	3.18	3.08	2.97	2.72	2.97	2.88
Q. E.	1.02	1.02	1.02	1.02	1.02	1.05	1.01	1.02
A. V.	74.2	83.9	108.3	108.9	74.3	144.3	64.8	110.7
Ga-3f tetrahedron								
Ga-O3	1.819(6)	1.825(9)	1.826(11)	1.812(8)	1.858(17)	1.821(14)	1.800(13)	1.793(12)
Ga-O2	1.874(6)	1.872(11)	1.864(11)	1.876(8)	1.805(12)	1.838(17)	1.812(18)	1.835(15)
Volume	3.07	3.06	3.1	3.06	2.99	3.1	2.87	2.86
Q. E.	1.03	1.04	1.04	1.03	1.03	1.04	1.03	1.04
A. V.	158.4	160.4	160.3	155.3	153.3	174.9	150.2	190.4

As it can be seen, the volume changes of polyhedra are quite the same for LNG and LTG. The LaO_8 dodecahedra undergo the largest decreasing of volume (Fig. 3.9). The volumes of polyhedra forming by Ga ions (GaO_6 and GaO_4) decrease obviously less as compared to that of dodecahedra.

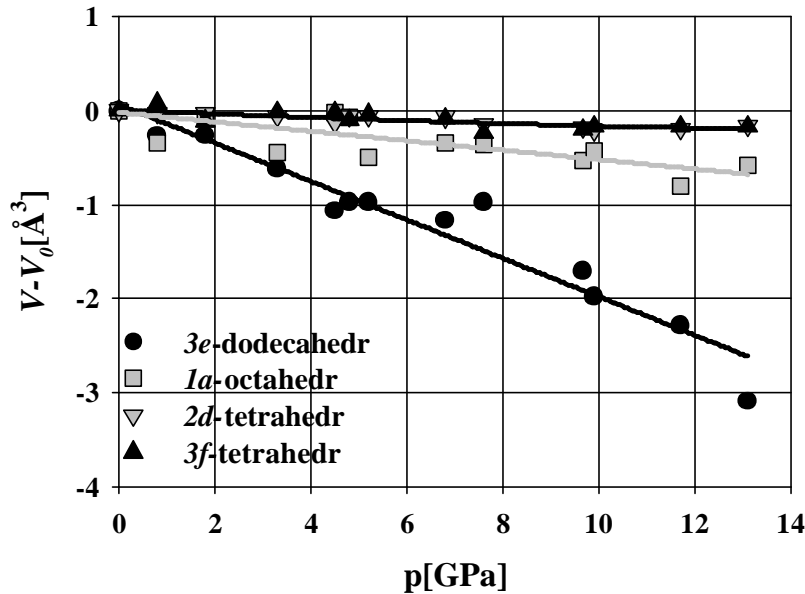


Fig. 3.9 Changes of the volume of polyhedra of LNG as a function of pressure

Otherwise, percentage changes of volumes of polyhedra indicate the following (Fig. 3.10). The volumes of dodecahedra and octahedra decrease in similar manner and almost regular within the investigated pressure ranges, whereas the volumes of tetrahedra start to decrease significantly only at pressures above 6GPa. Thus at pressures around 5(1)GPa the volumes of dodecahedra and octahedra decrease by 6(1)%, whereas the volumes of tetrahedra stay almost the same. These phenomena can be well explained by differences in bonding strengths in cation-anion polyhedra. Thus, the largest La^{3+} ions are coordinated by eight oxygen, which are forming the dodecahedra with a predominantly ionic character of bonding. The volumes of these weakly bonded dodecahedra decrease rapidly due to La-O bonds shortening. Accordingly, the bonding types within octahedra (Ga(1)/NbO_6 or Ga(1)/TaO_6) are partly ionic and covalent. Therefore, compressions of these octahedra could result in bond shortening as well as in slight polyhedral distortion. Finally, the smallest polyhedra (GaO_4 tetrahedra) are

rigid due to the strongest cation-anion (Ga-O) bonding types with apparently covalent characteristics. For this reason the compression within tetrahedral chains (layers of corner sharing GaO_4 tetrahedra) at pressures up to 5(1)GPa may lead to tilting and distortions of tetrahedra, because the tilting requires much less energy than the shortening of a covalent bond. Nevertheless, the further compression (above 5GPa) causes also decrease of the covalent Ga-O bonds. Thus in case of LNG at pressure 11.7(3)GPa the volume of dodecahedra and octahedra decrease around 8%, whereas the decreasing of volume of smaller tetrahedra reaches 6%.

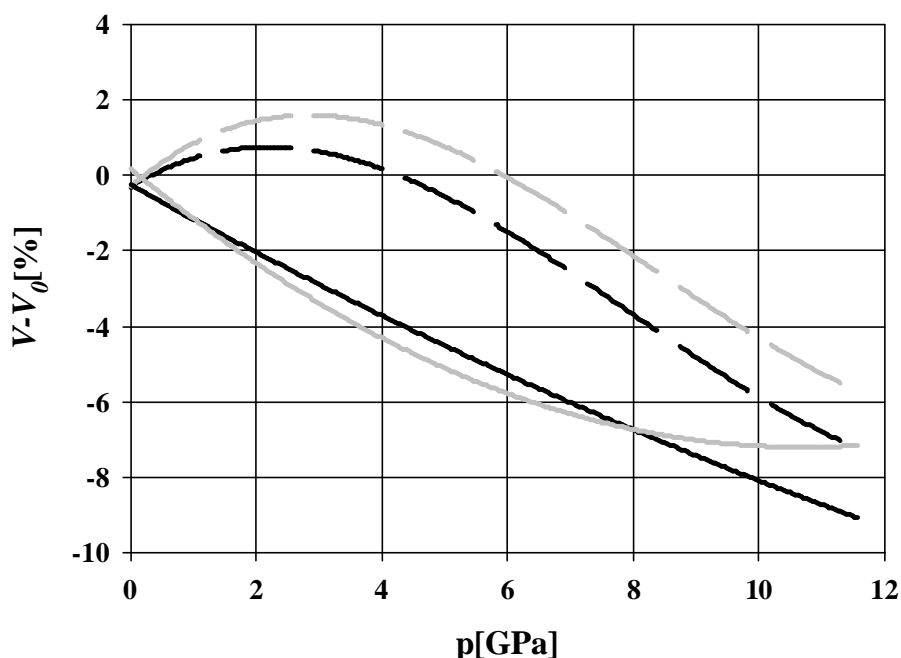


Fig. 3.10: Percentage changes of the volume of polyhedra of LTG as a function of pressure. The line styles appropriate to following polyhedra:
 grey dash – $2d$ tetrahedra;
 black dash – $3f$ tetrahedra;
 black solid – $3e$ dodecahedra;
 grey solid – $1a$ octahedra.

To compliment the analysis of compression mechanisms of investigated crystals, a figure will be useful, which demonstrates the typical representation of the crystal structures of LNG or LTG at different pressures. Thus Figure 3.11 shows the crystal structure of LNG along c - and

b-axis at pressures 1.8, 9.67 and 11.7GPa. As it can be seen, despite of increasing compressions, the crystal structures at different pressures look like nearly identical. This phenomenon can be well explained through high symmetry of the crystal structures of LNG and LTG. As pointed out above, all polyhedra are sharing several corners or(and) edges with neighbouring polyhedra, that limits the flexibility of these structure. Because geometrical changes within these layered structures are hampered, internal strains are increasing. Therefore the tilting of tetrahedra and distortions of polyhedra are rather small and could not be observed by visual analysis.

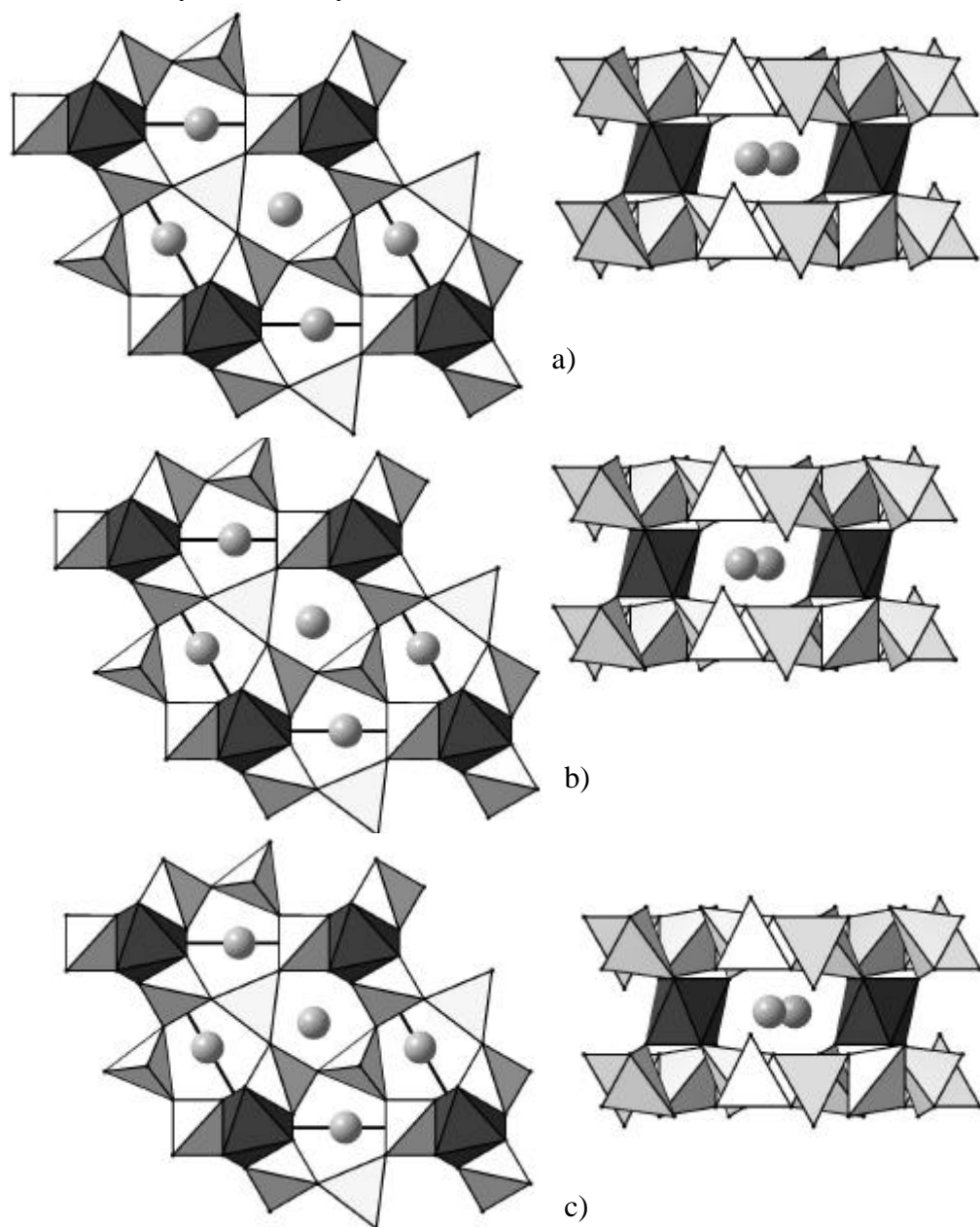


Fig. 3.11: Projection of the unit cell of LNG along the *c*- and *b*- axis at different pressures; the GaO_4 and Ga/NbO_6 polyhedra are shown:
a) $p=1.8\text{GPa}$; b) $p=9.67\text{GPa}$; c) $p=11.7\text{GPa}$.

From all these observations it follows that the compressions of crystal structures of LNG and LTG cause the increasing internal strains and must result in break of high symmetry. The nature of these transitions can be understood in terms of changes of ionic arrangement within and between polyhedral layers of LNG and LTG under increasing pressure:

- 1) The increasing pressure up to 5GPa causes decreasing of the unit cell volumes of LNG or LTG. Accordingly, the distances between ions are decreasing. The largest cations La^{3+} are shifted within the ab plane in order to maximize the distances between the positively charged neighbouring ions $\text{Ga}^{3+}/\text{Nb}^{5+}(\text{Ta}^{5+})$. This leads to displacements of tetrahedrally coordinated Ga^{3+} ions. Due to anion-cation bonds shortening polyhedra try to rotate, these rotations are hampered because of shared connectivities (corners or/and edges) with neighbouring polyhedra. Thus the compressions leads mostly to decrease of volume of weakly bonded polyhedra, such as LaO_8 dodecahedra with a predominantly ionic character of bonding and Ga/NbO_6 (Ga/TaO_6) octahedra with partly ionic and covalent types of bonds. With regard to behaviour of these polyhedra, the neighbouring tetrahedra try to tilt and distort.
- 2) The following compressions (at pressures above 5GPa) cause more significant changes of the crystal structures of LNG and LTG. The volumes of the largest polyhedra continue to decrease in similar manner, with these the volumes of the smallest polyhedra (GaO_4 tetrahedra) also start to decrease. Thus the covalent Ga-O bonds within tetrahedra significantly decrease at pressures above 5GPa. Moreover the distortion of polyhedra tries to increase, despite of small flexibilities, which are imposed by two- and three-fold axis laws. The least flexible polyhedra are $2d$ -tetrahedra. As pointed out above, the central cations $\text{Ga}(2)^{3+}$ of these tetrahedra are surrounded by oxygen O(1) (at special $2d$ position) and by three oxygen O(2) (at general position) according to the threefold axis law. Therefore, due to rigid flexibility the strains within $\text{Ga}(2)$ -tetrahedra increase with increasing pressure. This leads to redistribution of Ga-O bonds at pressures above 12(1)GPa. Thus at pressures around 12(1)GPa it was observed for LNG as well as for LTG, that oxygen O(2) takes a split position (O21-O22). Figures 3.12 and 3.13 show the pressure dependencies of the positional parameters of oxygen O(2) with regard to determined split positions at pressures above 11(1)GPa for LNG and LTG, respectively. These positions (O21-O22) are approximately 0.8\AA apart. With increasing pressure the distance between O21 and O22 increases (Fig.3.14). This phenomenon may be explained as a result of breaks in the high symmetry of the crystal structure of LNG or LTG,

presumably the three-fold axes (according to the triple axis law the oxygen O2 surrounding the Ga2- tetrahedra).

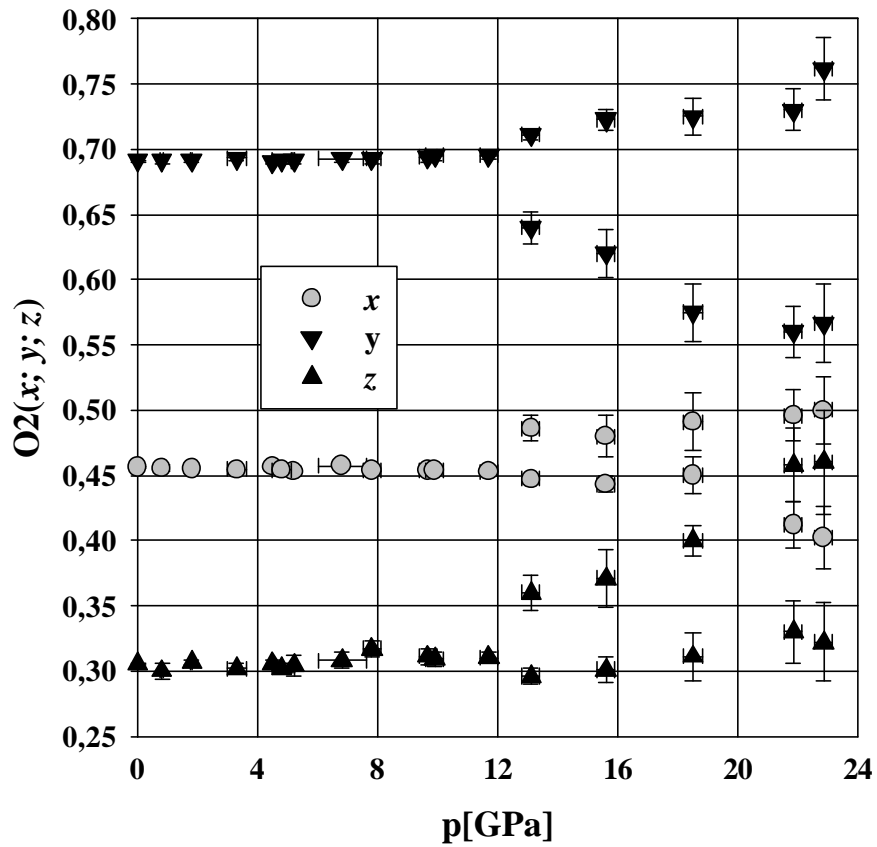


Fig. 3.12: Variations of position parameters of oxygen O(2) of LNG with pressure. At pressures above 11(1)GPa the coordinations of split positions are depicted.

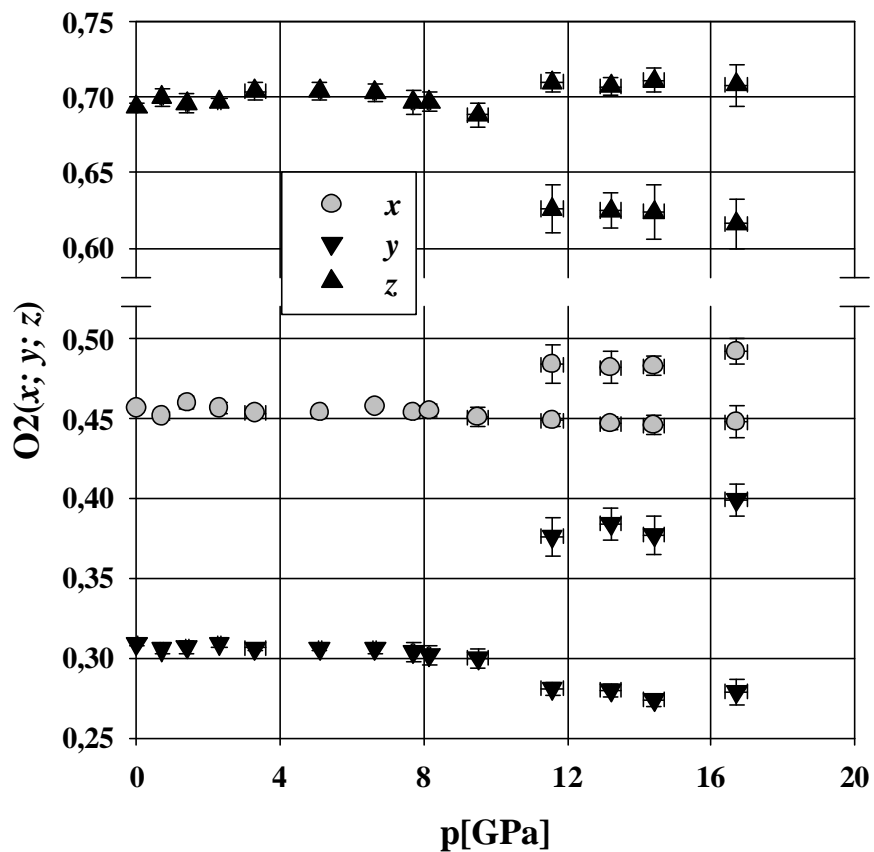


Fig. 3.13: Variations of position parameters of oxygen O(2) of LTG with pressure. At pressures above 11(1)GPa the coordinations of split positions are depicted.

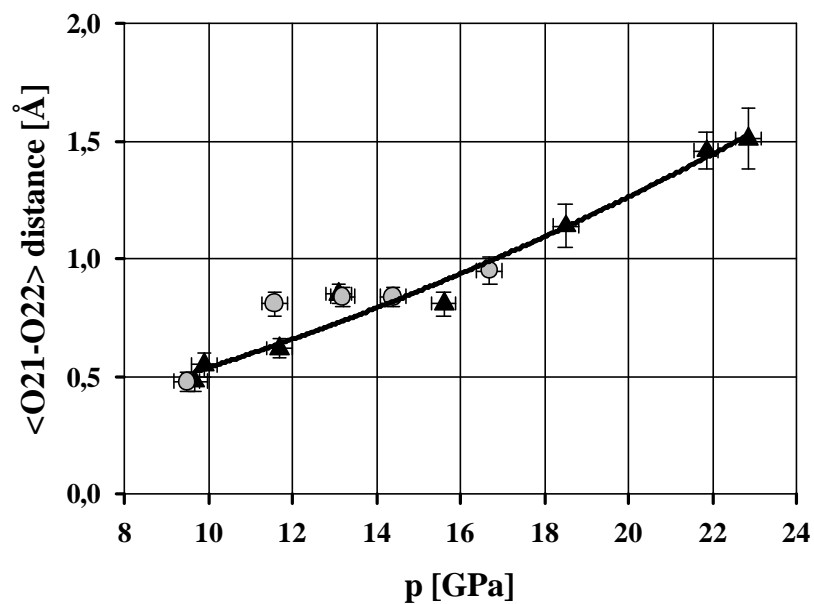


Fig. 3.14: Distance O21-O22 in split position vs. pressure, refined in trigonal space group for LGN (triangle up) and LGT(circle), respectively.

It may be concluded that the hampered flexibility of tetrahedra, especially at pressures above 7GPa, are the main driving forces for the transformation from higher-symmetry to lower symmetry, which is necessary for increase of compression capability within tetrahedral layers. Thus the strong polyhedral distortions (first of all GaO₄ 2*d*-tetrahedra) under high pressures cause the transformation to a higher distorted low-symmetry form, which involves more degrees of freedom for subsequent compression.

Similar to GaPO₄ or α -quartz, the crystal structures of LNG and LTG under pressure undergo a phase transition, whereas the driving forces for these transitions are differing. Thus the compression of GaPO₄ leads to tilting and distortion of tetrahedra [28]. At pressures above 7GPa (experimental value 9GPa) the GaO₄ tetrahedra are so strongly distorted (the O-Ga-O angle distribution shows two maxima) that a phase transition to lower symmetry occurs. The existence of octahedra and dodecahedra, which are sharing edges and (or) corners with neighbouring tetrahedra, causes the main difference between compression mechanisms of the crystal structures of LNG or LTG and of GaPO₄. Thus the compressions of LNG and LTG are mainly achieved by decreasing volume of polyhedra. The tilting and distortion of polyhedra are hampered due to shared interconnectivities and high symmetry. This leads to increasing internal strains (especially within the layers of GaO₄ tetrahedra with atomic bonding). Finally, this results in break of high symmetry of the crystal structures of LNG and LTG.

3.1.4 High pressure phases of LNG and LTG

As pointed out above (chapters 3.1.1. and 3.1.3), the changes of the lattice parameters of LNG and LTG, as well as the structures refinements indicate the existence of phase transitions in both cases at pressures around 12(1)GPa. The maximal non-isomorphic subgroups for $P321$ are the space groups $P3$ and $C2$. The refinements of the crystal structures of LNG or LTG in the space group $P3$ did not yield satisfying results. Thus choose of trigonal symmetry without two-fold axis for high pressure polymorph (space group $P3$) does not lead to significant improvement of the refinements parameters, moreover the split position for O(2) oxygen was still observed. This leads to assumption of break of three-fold axis in the crystal structure of LNG and LTG under pressures above 12(1)GPa. Therefore all reflection intensity data of LGN and LGT was transformed to monoclinic symmetry with the help of the program Jana98 by following transformation matrix:

$$\begin{vmatrix} 0 & 0 & 1 \\ 1 & 1 & 0 \\ 1 & 1 & 0 \end{vmatrix}$$

The monoclinic angle was set $\beta=90^\circ$ in both cases due to the fact that possibly existing small (about 0.02°) deviations from this value could not be sufficient determined (see also chapter 3.1.5.). The refinements of the crystal structure of LNG and LTG in monoclinic symmetry (space group $A2$) allowed to improve the R factors and, in contrast to the attempts to refine the crystal structures in $P3$, no split positions for oxygen were observed. The details of these refinements, including appropriate treatment of twinning following the former triad in trigonal symmetry, are listed in Table 2.3 and 2.4 for LNG and LTG, respectively. The twin law with respect to broken triad axis is following:

$$\begin{vmatrix} 1 & 0 & 0 \\ 0 & -0.5 & -0.5 \\ 0 & 1.5 & -0.5 \end{vmatrix}$$

As usual, twin domains, which are characteristic for transitions from high to low symmetry, causes complications of the determination of positional parameters of light elements from intensity data collected on single crystals (especially the refinements of parameters of anisotropic displacements are problematic). For this reason, only isotropic temperature factors

for oxygen of the crystal structures of LNG and LTG were refined, whereas the determinations of anisotropic displacement parameters were still possible in case of cations. Correspondingly, the standard deviations of positional parameters of oxygen are more essential than those of La³⁺, Ga³⁺ or Nb⁵⁺/Ta⁵⁺ cations. Positional parameters of cations and anions in monoclinic symmetry are listed in Table 3.6 and 3.8 for LNG as well as in Table 3.7 and 3.9 for LTG. There are two kinds of coordinations listed at each pressure in these tables. The first one are the positional parameters, which were transferred to monoclinic cell from results of refinements in trigonal symmetry (space group *P321*). The next are the coordinations refined in monoclinic symmetry (space group *A2*).

Table* 3.6. Positional parameters of cations for monoclinic crystal structure of LNG at different pressures

p[GPa]	La1 (x;y;z)			La2 (0;y;0)	Ga/Nb (0;y;0)	Ga(2) (x;y;z)			Ga(3) (0.5;y;0)	Ga(4) (x;y;z)		
13.1	0	.2171	.7829	.4342	0	.4808	.5	.1667	.2334	0.5	.3833	.3833
	.002(2)	.217(1)	.783(1)	.434(1)	.002(3)	.481(1)	.498(2)	.166(1)	.233(4)	.502(3)	.381(2)	.384(1)
15.6	0	.2182	.7818	.4363	0	.4874	.5	.1667	.2332	.5	.3834	.3834
	.004(2)	.217(1)	.781(1)	.436(1)	.002(4)	.488(1)	.498(2)	.166(1)	.236(6)	.500(3)	.384(2)	.384(1)
18.5	0	.2195	.7805	.4390	0	.4925	.5	.1667	.235	.5	.3825	.3825
	.008(3)	.219(2)	.779(1)	.438(2)	.009(4)	.491(3)	.498(4)	.165(2)	.236(5)	.512(4)	.385(2)	.384(1)
21.85	0	.2186	.7814	.4372	0	.495	.5	.1667	.2319	.5	.384	.384
	.001(5)	.220(1)	.782(2)	.439(3)	.005(6)	.496(5)	.491(3)	.168(3)	.235(3)	.500(7)	.379(3)	.385(3)
22.85	0	.2203	.7797	.4405	0	.499	.5	.1667	.2348	.5	.3826	.3826
	.003(4)	.220(2)	.779(2)	.439(4)	.011(6)	.498(3)	.498(4)	.168(3)	.230(7)	.50(1)	.384(6)	.383(3)

Table* 3.7. Positional parameters of cations for monoclinic crystal structure of LTG at different pressures

p[GPa]	La1 (x;y;z)			La2 (0;y;0)	Ga/Ta (0;y;0)	Ga(2) (x;y;z)			Ga(3) (0.5;y;0)	Ga(4) (x;y;z)		
11.57	0	.7827	.2173	.4346	0	.4795	.5	.1667	.7659	0.5	.6171	.3829
	.002(1)	.783(1)	.218(1)	.434(1)	.002(3)	.480(1)	.499(4)	.167(1)	.763(3)	.496(3)	.618(3)	.385(1)
13.2	0	.7824	.2176	.4353	0	.4800	.5	.1667	.7660	.5	.6170	.3830
	.000(2)	.781(1)	.218(1)	.433(1)	.003(3)	.480(1)	.497(3)	.166(1)	.763(4)	.495(3)	.616(3)	.383(1)
14.4	0	.2181	.2181	.4362	0	.4810	.5	.1667	.234	.5	.617	.383
	.002(2)	.781(1)	.219(1)	.433(1)	.000(2)	.482(1)	.496(3)	.165(2)	.771(2)	.495(5)	.615(3)	.381(1)
16.7	0	.2191	.2191	.4372	0	.4879	.5	.1667	.2340	.5	.617	.383
	.005(3)	.219(1)	.220(1)	.437(1)	.005(2)	.497(2)	.500(3)	.166(2)	.230(4)	.500(2)	.616(1)	.381(1)

*The first row at each pressure appropriate to transformed coordinates from trigonal symmetry, the second row lists positional parameters refined in monoclinic symmetry (space group *A2*)

Table* 3.8. Positional parameters of anions for monoclinic crystal structure of LNG at different pressures

p[GPa]	O(1) (x;y;z)			O(2) (x;y;z)			O(3) (x;y;z)			O(4) (x;y;z)		
	<i>13.1</i>	.168 .167(5)	.5 .51(1)	.1667 .172(6)	.3 .28(1)	.37 .372(8)	.076 .092(3)	.3 .39(1)	.071 .14(1)	.777 .761(6)	.3 .290(8)	.299 .286(5)
<i>15.6</i>	.170 .17(1)	.5 .51(1)	.1667 .173(8)	.312 .29(2)	.3645 .38(1)	.0765 .078(0)	.312 .30(2)	.0675 .051(8)	.7795 .717(5)	.312 .40(3)	.297 .27(2)	.144 .20(1)
<i>18.5</i>	.168 .16(1)	.5 .50(2)	.1667 .17(1)	.332 .35(3)	.359 .35(2)	.08 .06(1)	.332 .30(3)	.0595 .05(2)	.7805 .74(1)	.332 .41(2)	.2995 .27(1)	.1395 .219(9)
<i>21.85</i>	.15 .17(3)	.5 .53(11)	.1667 .18(1)	.379 .39(3)	.3595 .33(1)	.0725 .10(1)	.379 .37(3)	.071 .13(1)	.784 .79(1)	.379 .43(4)	.2885 .31(1)	.1435 .13(1)
<i>22.85</i>	.118 .14(2)	.5 .53(2)	.1667 .17(2)	.355 .31(3)	.3665 .33(2)	.0765 .08(1)	.355 .38(4)	.0685 .17(2)	.7785 .75(1)	.355 .36(4)	.298 .33(2)	.145 .16(1)

Table* 3.8. Positional parameters of anions for monoclinic crystal structure of LNG at different pressures (continued)

p[GPa]	O(5) (x;y;z)			O(6) (x;y;z)			O(7) (x;y;z)		
	<i>13.1</i>	.762 .746(9)	.1444 .123(6)	.9246 .914(3)	.238 .207(8)	.0409 .006(6)	.1099 .115(3)	.762 .736(18)	.1853 .191(13)
<i>15.6</i>	.768 .75(2)	.1525 .125(14)	.9215 .917(9)	.232 .21(3)	.0415 .03(2)	.1155 .112(12)	.768 .80(3)	.193 .20(2)	.963 .938(13)
<i>18.5</i>	.765 .764(17)	.151 .132(11)	.923 .952(10)	.235 .235(17)	.040 .029(12)	.114 .129(10)	.765 .81(3)	.191 .205(18)	.963 .996(13)
<i>21.85</i>	.760 .79(3)	.1555 .136(10)	.9165 .935(15)	.240 .23(3)	.0475 .057(11)	.1195 .124(14)	.760 .69(4)	.203 .233(10)	.965 .910(16)
<i>22.85</i>	.784 .82(3)	.157 .117(18)	.910 .897(13)	.216 .21(4)	.0565 .050(17)	.1235 .129(15)	.784 .71(3)	.2135 .197(17)	.9665 .926(17)

*The first row at each pressure appropriate to transformed coordinates from trigonal symmetry, the second row lists positional parameters refined in monoclinic symmetry (space group A2)

Table* 3.9. Positional parameters of anions for monoclinic crystal structure of LTG at different pressures

p[GPa]	O(1) (x;y;z)			O(2) (x;y;z)			O(3) (x;y;z)			O(4) (x;y;z)		
11.57	.162	0	.3333	.309	.6255	.0785	.309	.0695	.7735	.309	.305	.148
	.164(5)	.01(1)	.334(8)	.29(1)	.64(1)	.089(7)	.30(1)	.06(1)	.776(5)	.38(2)	.28(2)	.182(9)
13.2	.1660	0	.3333	.305	.6275	.0795	.305	.0670	.7730	.305	.3055	.1465
	.167(6)	.01(2)	.326(7)	.28(1)	.648(8)	.093(4)	.30(1)	.073(9)	.779(5)	.36(1)	.29(1)	.192(6)
14.4	.163	.0	.3333	.302	.640	.083	.302	.0555	.7795	.302	.3045	.1385
	.166(8)	.01(2)	.330(9)	.30(3)	.64(2)	.079(4)	.30(2)	.043(9)	.78(1)	.35(2)	.28(1)	.19(1)
16.7	.168	0	.3333	.309	.629	.077	.309	.070	.776	.309	.301	.147
	.17(1)	.01(1)	.336(9)	.35(4)	.64(2)	.08(1)	.39(2)	.16(1)	.756(6)	.28(4)	.31(2)	.14(1)

Table* 3.9. Positional parameters of anions for monoclinic crystal structure of LTG at different pressures (continued).

p[GPa]	O(5) (x;y;z)			O(6) (x;y;z)			O(7) (x;y;z)		
11.57	.238	.849	.926	.238	.9645	.1125	.238	.1865	.9615
	.254(15)	.857(15)	.920(9)	.206(8)	.986(9)	.120(4)	.26(2)	.18(2)	.978(8)
13.2	.238	.8495	.9255	.238	.9635	.1125	.238	.1870	.9620
	.266(12)	.885(10)	.921(6)	.198(9)	.989(11)	.118(4)	.249(11)	.191(11)	.964(4)
14.4	.235	.8545	.9255	.235	.961	.110	.235	.1845	.9645
	.276(14)	.896(10)	.917(6)	.204(13)	.988(8)	.120(4)	.226(16)	.194(11)	.968(5)
16.7	.232	.847	.926	.232	.9655	.1135	.232	.1875	.9615
	.23(3)	.847(13)	.919(9)	.19(4)	.991(18)	.129(10)	.27(3)	.175(14)	.975(8)

As it can be seen, the crystal structures of the high pressure phases of LNG and LTG reveal, as expected, the pseudo-hexagonal nature. Thus the positional parameters of cations in high pressure polymorphs of LNG (Tab.3.6) and LTG (Tab. 3.7) only slightly deviate from the values obtained in trigonal symmetry. The large errors for positional parameters of oxygen complicate sufficient analysis of their behaviours. Therefore, for more detailed description of the high pressure polymorphs of LNG or LTG ongoing investigations are necessary.

To compliment the description of high pressure polymorphs of LNG and LTG the illustration of monoclinic crystal structures will be useful. Figure 3.15 shows two kind of projections of the monoclinic cell of LNG along *a*-axis at pressure 15.6GPa. The first part of this figure

*The first row at each pressure appropriate to transformed coordinates from trigonal symmetry, the second row lists positional parameters refined in monoclinic symmetry (space group A2)

demonstrates trigonal structure transformed to monoclinic cell (a) and the second one shows monoclinic cell of LNG with refined structural parameters in space group $A2$ (b).

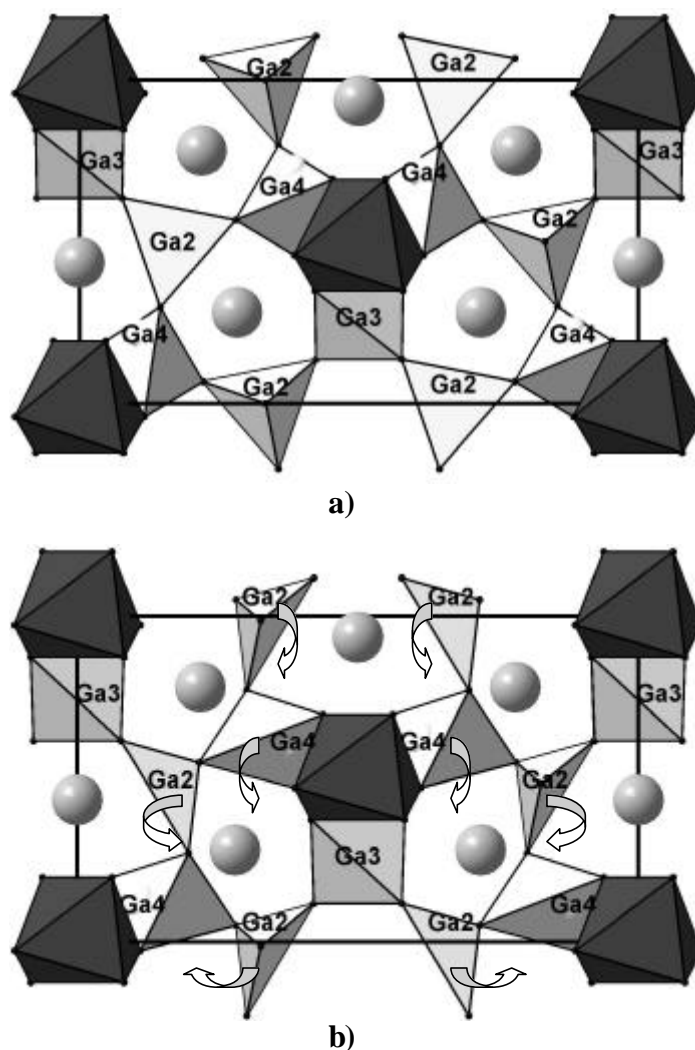


Fig. 3.15: Projection of the monoclinic unit cell of LNG along the *b* axis at pressure 15.6GPa, the GaO₄ and Ga/NbO₆ polyhedra are shown:

- a) crystal structure refined in trigonal symmetry represented in monoclinic cell;
- b) crystal structure refined in monoclinic symmetry (space group $A2$).

As it can be seen, the distortion of polyhedra, first of all the distortion of tetrahedra significantly increases for monoclinic high pressure polymorph. The tilting of tetrahedra is clearly observed too. This can be well explained due to decreasing symmetry of high pressure polymorph as compared to the initial phase. Thus the crystal structure obtains more degrees of freedom. This results in increasing distortion and tilting of polyhedra. The crystal structure of LTG undergoes almost the same changes under pressure. Otherwise the Nb⁵⁺ Ta⁵⁺ substitution causes some difference between high pressure polymorphs of LNG and LTG, whereas the

initial phases of these compounds are similarly compressible. This phenomenon is caused by decreasing symmetry during the phase transition. Thus the central cations of octahedra of the initial phases of LNG or LTG are surrounded by oxygen according to three- and two- fold axis laws. Therefore all bonding distances Ga(1)/Nb-O or Ga(1)/Ta-O are the same. Due to decrease of symmetry (break of three-fold axes) the bonding distances within the octahedra of monoclinic high pressure phase of LNG and LTG are containing three pairs. Therefore due to more degrees of freedom the bonding distances within the octahedra can deviate from each other. Accordingly, the polarisation of the oxygen arrangement of Nb⁵⁺ ions increases, whereas the TaO₆ octahedra stay almost regular. Figure 3.16 shows the NbO₆ and TaO₆ polyhedra of high pressure phases of LNG and LTG. The higher distortion of NbO₆ octahedra can be clearly seen. The bonding distances within octahedra are listed in Tables 3.10 for LNG and 3.11 for LTG. At pressures around 16(1)GPa, the variation of bonding distances within NbO₆ is from 1.88(6)Å to 2.03(6)Å, whereas the bonding distances Ta-O are about 1.98(5)Å within the errors. As pointed out above the difference in crystal chemical behaviour between niobium and tantalum causes the greater polarisation of Nb⁵⁺ ions by neighbouring oxygen anions[14]. Therefore the larger distortion of NbO₆ octahedra as compared to TaO₆ in high pressure polymorphs of these compounds is clearly observed. In this way the compressibility of monoclinic structure of LNG is significantly higher as compared to the initial trigonal phase of LNG or low- and high- pressure phases of LTG. Obviously the further compression (at pressures above 18GPa) of LTG could lead to similar phenomena.

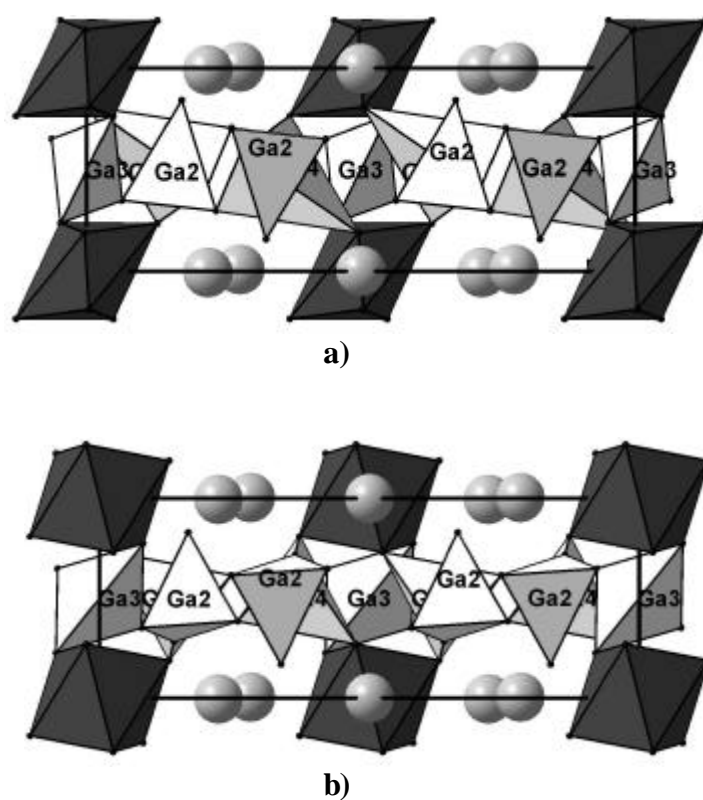


Fig. 3.16: Projection of the monoclinic unit cell along the b axis, the GaO_4 and Ga/NbO_6 or Ga/TaO_6 polyhedra are shown:

a) crystal structure of LNG at pressure 18.5(3)GPa;

b) crystal structure of LTG at pressure 16.7(3)GPa.

Table 3.10. Interatomic distances [\AA] within octahedra of high pressure polymorph LNG

p[GPa]	Ga(1)/Nb-O(7)x2	Ga(1)/Nb-O(5)x2	Ga(1)/Nb-O(6)x2
13.1	1.97(6)	2.03(6)	1.96(2)
15.6	2.03(6)	1.97(4)	1.88(6)
18.5	1.80(8)	1.74(7)	2.12(6)
21.85	2.63(14)	1.75(14)	2.07(10)
22.85	2.37(11)	1.83(13)	2.02(11)

Table 3.11. Interatomic distances [\AA] within octahedra of high pressure polymorph LTG

p[GPa]	Ga(1)/Ta-O(7)x2	Ga(1)/Ta-O(5)x2	Ga(1)/Ta-O(6)x2
11.57	1.97(6)	2.03(6)	1.96(2)
13.2	1.95(4)	2.04(3)	1.91(3)
14.4	1.96(4)	1.97(4)	1.94(3)
16.7	1.98(4)	1.97(5)	2.00(5)

In addition, the phase transitions of LNG and LTG from trigonal to monoclinic symmetry under compressions are in agreement with expected results [73]. Thus Eysel et al (1992) described a structural family with the summarizing formula $M_{5-p}T_{4+p}O_{14}$ with $p=0$ or $p=1$, which comprises the structure types I ($P321$, trigonal phases isostructural to LNG or LTG), II ($I2/a$, monoclinic symmetry) and III ($P2_1$, or $P2_1/m$, or Pm , monoclinic symmetry). The basic unit of all structures is a folded tetrahedral single chain with Ge or Ga as predominant tetrahedral ions. Thus the crystal structures of these materials are comparable, the differences between their structures lie in different sizes of the cations M. The substitutions of different sized cations at structural positions cause rearrangement of the oxygen atoms and accordingly some changes in the positions and coordination of the cations. For example, for compound $Pb_3CuGe_5O_{14}$, a monoclinic structure was determined, and its structural relation to langasite was described [73]. Moreover, the monoclinic structure was determined for the high-pressure phase of $Ca_3Mn_2Si_4O_{14}$ [78], which structure is trigonal at normal conditions and isostructural to langasite [2]. Thus it may be assumed that LNG and LTG under high pressures undergo similar polymorphic transitions and the further compression of these structures can lead to more dramatic reconstructive transformations.

In addition, the trigonal-monoclinic structural transformations was observed for α -quartz and $GaPO_4$ as well as for LNG and LTG. Thus α -quartz, which has been reported to undergo pressure-induced amorphisation [80, 81], was found to transform to a monoclinic, crystalline phase when compressed to 45GPa at room temperature in a close to hydrostatic condition (with helium pressure medium) [79]. Likewise, the investigation of $GaPO_4$ using Raman spectroscopy clearly indicates that the high-pressure phase is crystalline [30], whereas the powder diffraction or X ray diffraction studies it can be concluded that $GaPO_4$ becomes amorphous at about 9(2)GPa [28,32]. However the theoretical study of a transformation of the quartz-type $GaPO_4$ leads to monoclinic high-phase [29,37].

3.1.5. Broadening of reflections

In addition to all described phenomena, it was observed that the reflections of LNG as well as LTG broaden with the increase in pressure after the phase transition, in spite of perfect trigonal metric within the whole pressure range (no deviations from trigonal lattice parameters could be observed within the experimental errors). The triclinic lattice parameters at selected pressures after pressure phase transitions (above 12(1)GPa) are listed in Tables 3.12 and 3.13 for LNG and LTG, respectively.

Table 3.12. The variations of the lattice parameters of LNG at pressures.

p[GPa]	a [Å]	b [Å]	c [Å]	α [°]	β [°]	γ [°]
15.6(3)	7.8662(84)	7.8626(103)	5.0066(54)	90.009(97)	90.019(87)	119.997(72)
18.5(3)	7.7854(50)	7.7813(57)	4.9943(33)	90.036(57)	90.007(53)	119.966(43)
22.8(3)	7.6631(53)	7.6553(70)	4.9844(40)	89.973(70)	90.074(61)	120.030(54)

Table 3.13. The variations of the lattice parameters of LTG at pressures.

p[GPa]	a [Å]	b [Å]	c [Å]	α [°]	β [°]	γ [°]
13.7(3)	7.9475(49)	7.9441(78)	5.0134(39)	90.006(72)	89.991(57)	119.988(51)
14.8(3)	7.9263(51)	7.9253(81)	5.0080(41)	90.000(76)	90.001(60)	119.995(53)
16.7(3)	7.8729(49)	7.8715(78)	4.9990(40)	90.007(73)	89.995(59)	119.995(52)

The full width at half maximum (FWHM) of a reflection is known to be a function of a number of different effects, for example, the divergence of the beam, the deviation of the wavelength and size of the aperture of the detector [82]. Given that experimental parameters are not changed, the tendency for a reflection to become broader might well be explained by structural changes of LNG and LTG. Figures 3.17, 3.18 and 3.19, 3.20 show the profiles of reflections (5 0 2) and (4 0 0) of LNG and LTG, respectively.

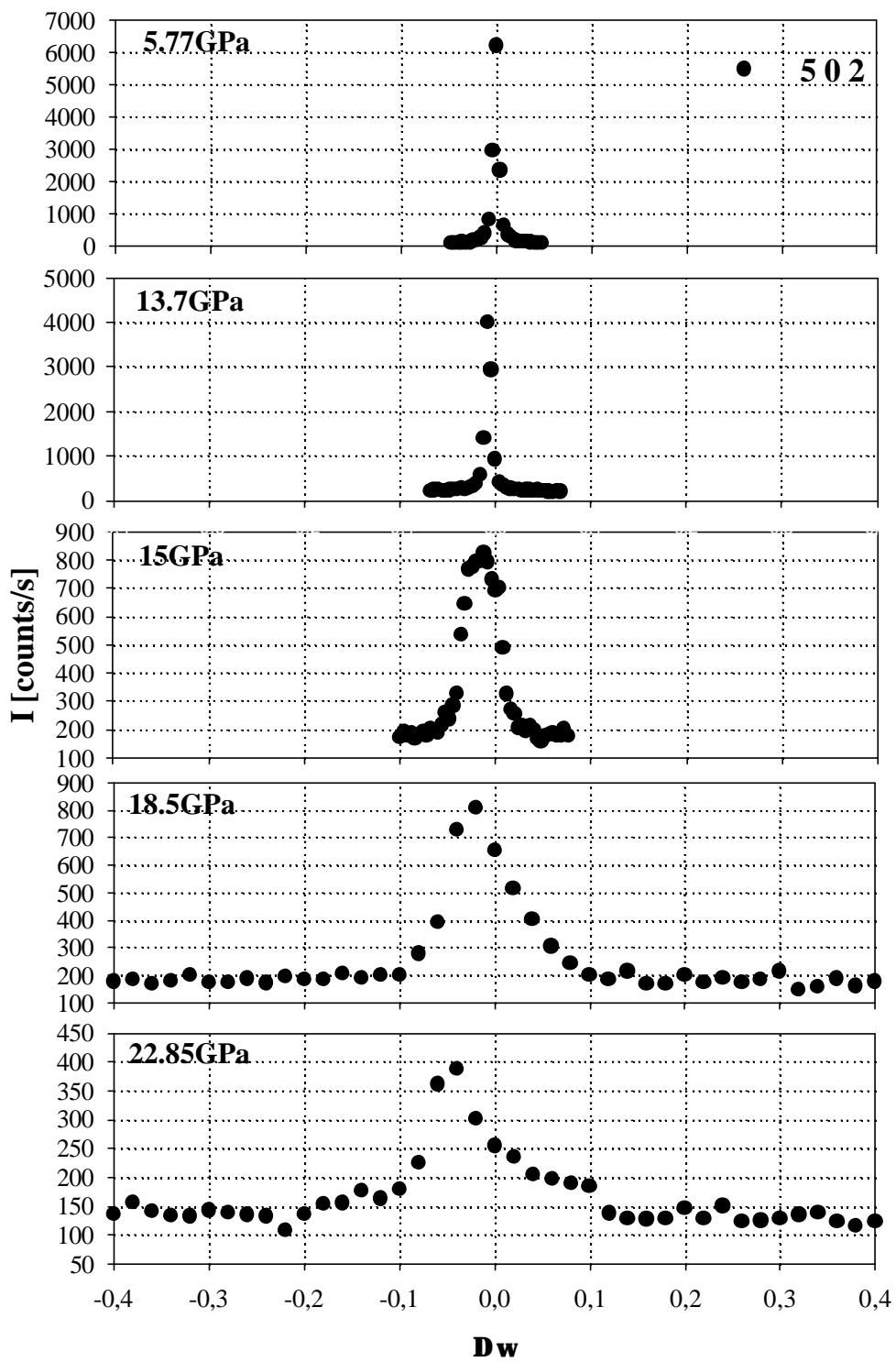


Fig.¹ 3.17: The profiles of reflection (5 0 2) of LNG at different pressures.

¹ The different reflection intensity could be caused by different X-ray intensity at the beam-line D3

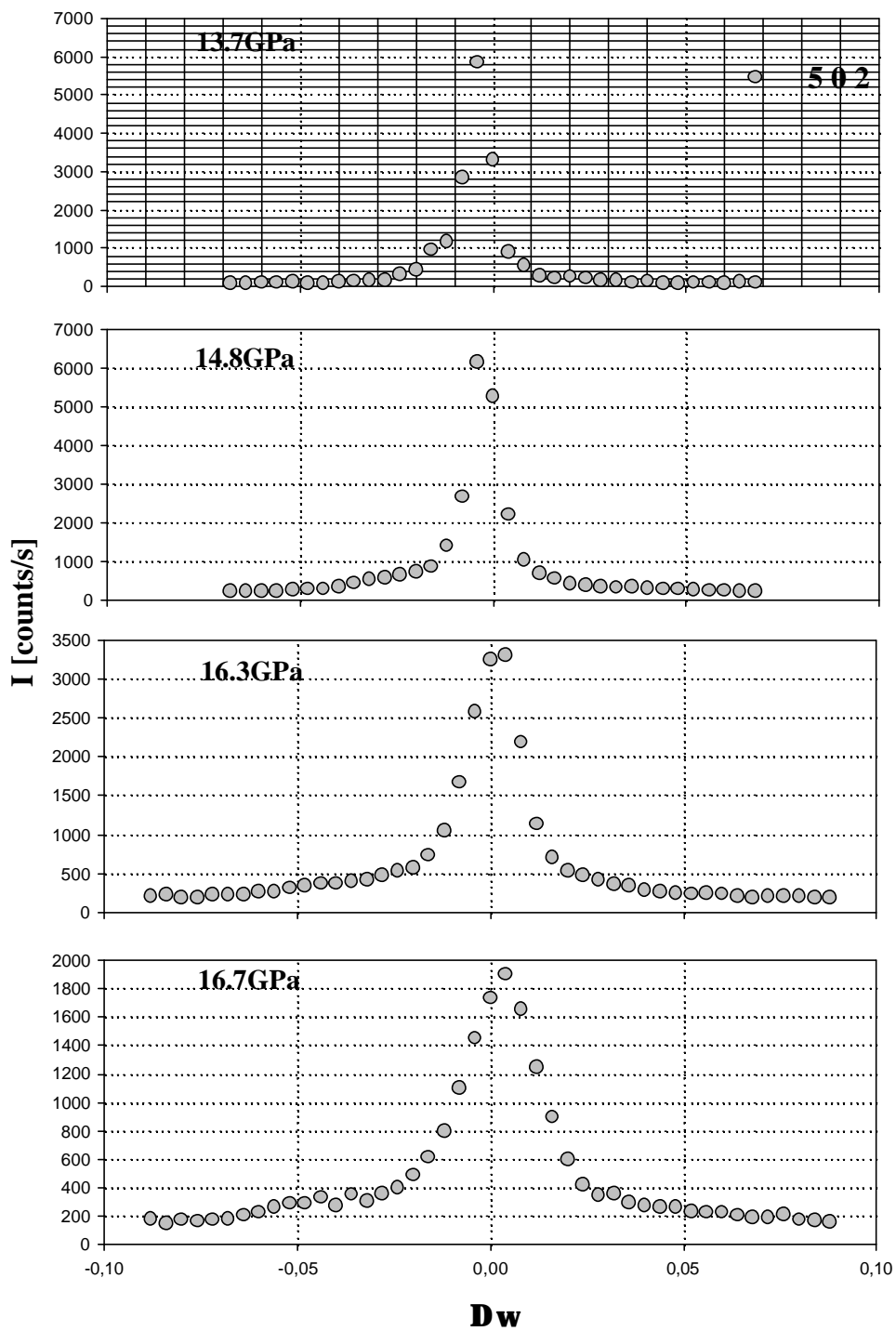


Fig.² 3.18: The profiles of reflection (5 0 2) of LTG at different pressures.

² The different reflection intensity could be caused by different X-ray intensity at the beam-line D3

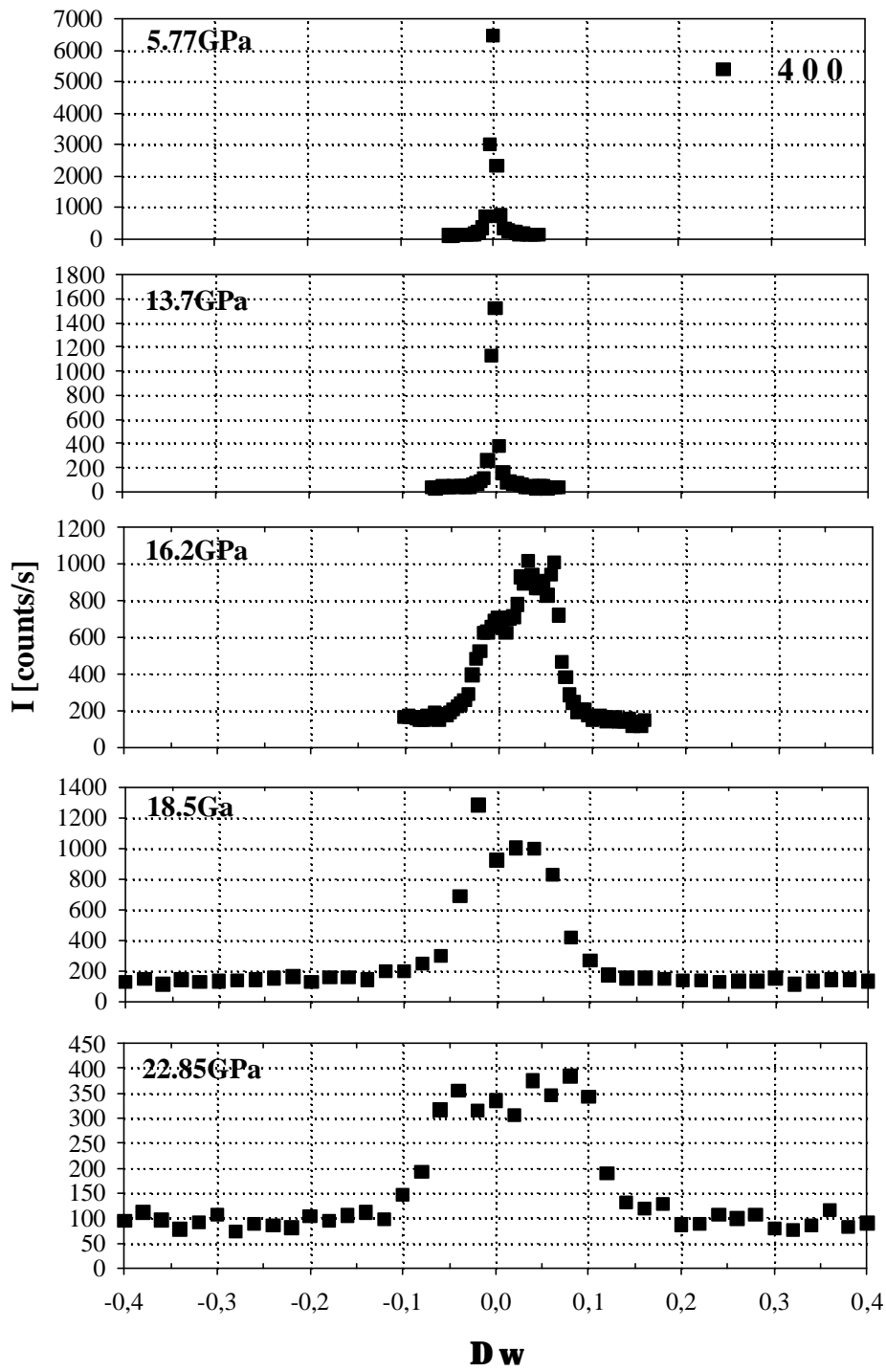
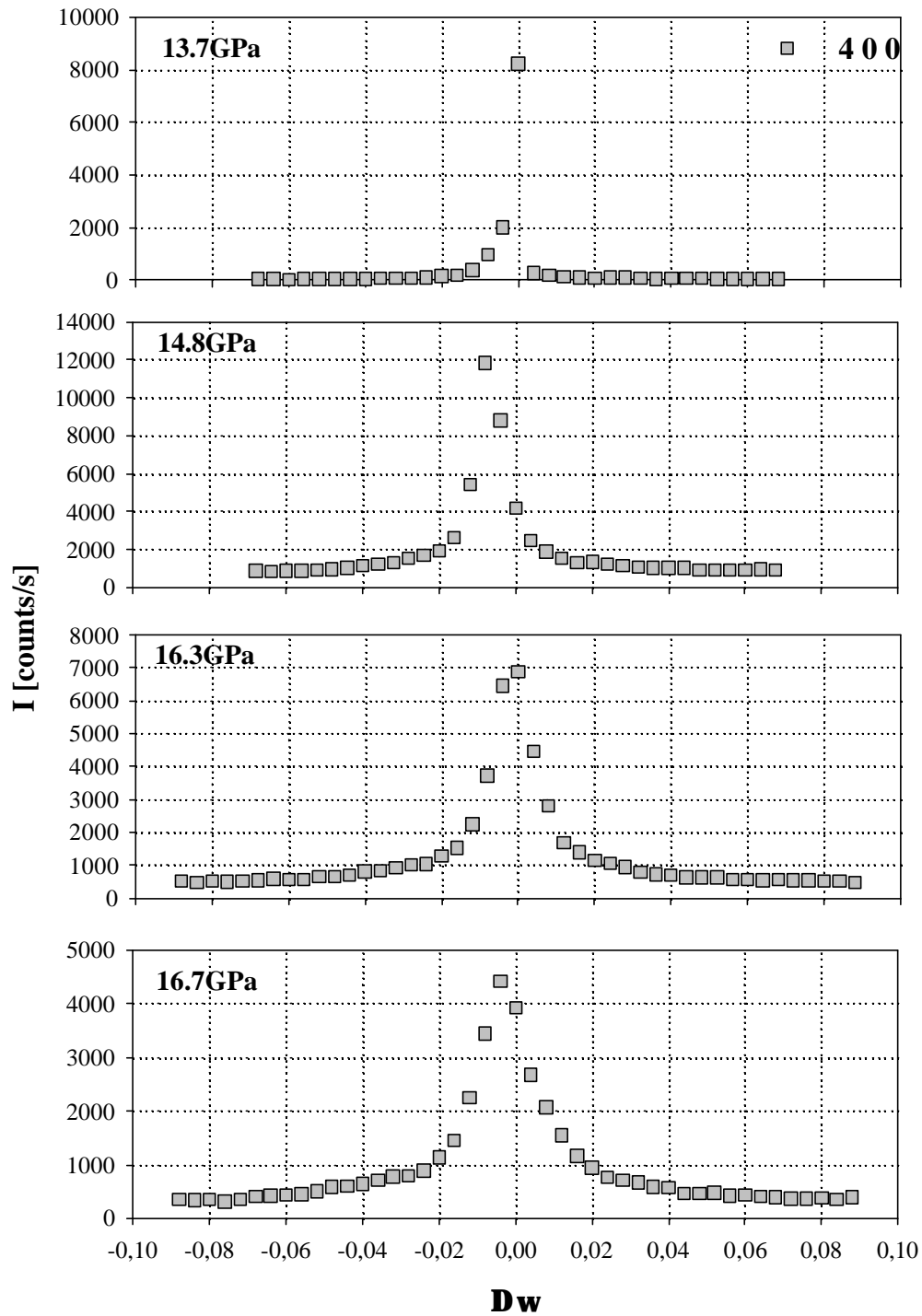


Fig.³ 3.19: The profiles of reflection (4 0 0) of LNG at different pressures.

³ The different reflection intensity could be caused by different X-ray intensity at the beam-line D3



Figure⁴ 3.20: The profiles of reflection (4 0 0) of LTG at different pressures.

⁴ The different reflection intensity could be caused by different X-ray intensity at the beam-line D3

As it can be seen, the full width at half maximum (FWHM) of the reflections does not show significant changes up to 14(1)GPa, the broadening increases with further increase in pressure. As pointed out above, the lattice parameters of LNG and LGT were found to obey trigonal symmetry constraints within the experimental errors in whole pressure range. Therefore the tendency for a reflection to become broader might well explained by deviations of the β angle from 90° or (and) deviation from $a=b$ in monoclinic domains, which have directly after transition from trigonal to monoclinic symmetry $\beta \approx 90^\circ$. A broadening of reflection profiles due to non-hydrostatic conditions can be excluded, as the same broadening effect was observed for two single crystals with totally different orientations. Furthermore the broadening of reflections does not depend on diffractometer angles (Fig. 3.21). This confirms assumption of deviations of the β angle from 90° .

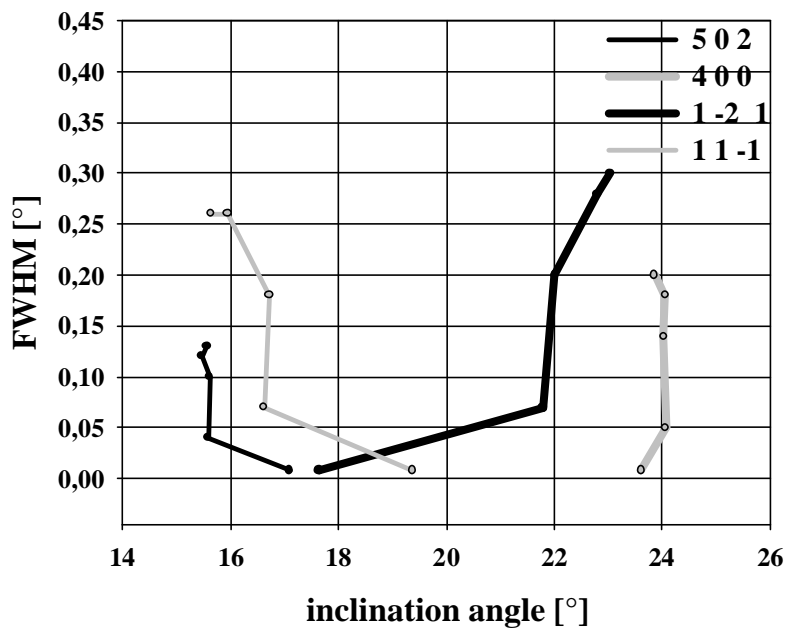


Fig. 3.21: The dependencies of FWHM of reflections of LNG from inclination angles.

The profiles of the reflections (h00), (h0l) and (hkl) ((400), (502), (1 -2 1) and (1 1 -1)) of trigonal LNG were measured at 10 different pressures. Fig.3.22 presents the dependence of FWHM of the reflection profiles as functions of pressure as a simple horizontal step plot. Each step corresponds to the FWHM observed at first-step pressure. The average value of the

initial FWHM for all reflections is 0.008° pointing out the extremely high crystal quality of our specimens. The FWHM of the reflection profiles increase at pressure 22.85GPa by factors of 15, 24 and 31 for reflections (h0l), (h00) and (hkl), respectively. Final average values of the FWHM for reflections (h0l), (h00) and (hkl) are 0.13° , 0.2° and 0.26° , at pressure 22.85GPa. For example, a deviation of the β -angle of monoclinic domains from 90° by approximately 0.02° might cause such a broadening of reflection profiles. Due to still narrow (0.2°) FWHM of reflection profiles it was possible to record integral reflection intensities assuming trigonal symmetry.

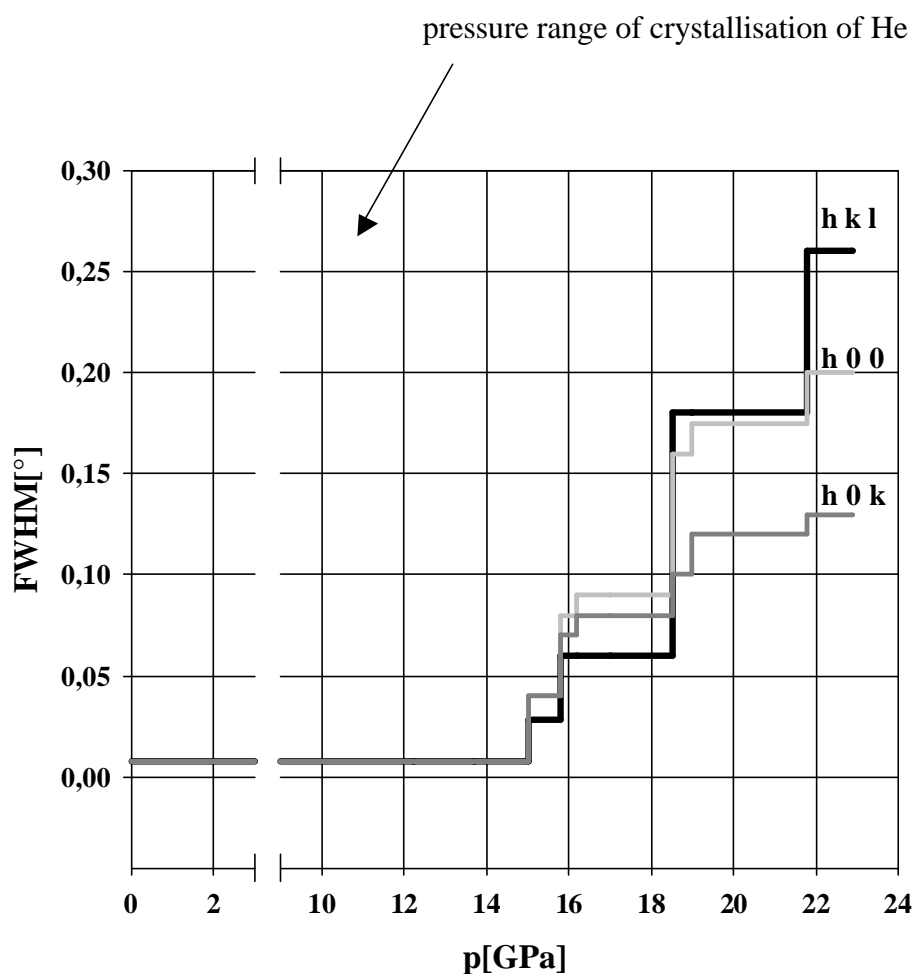


Fig. 3.22: FWHM of reflection profiles in ω -scans vs. pressure.

3.2 Temperature dependencies of the unit cell parameters of LNG, LTG and LGSZ

3.2.1. The thermal expansion of LNG and LTG lattices

The variations of unit cell parameters as function of temperature for LNG and LTG are depicted at Figures 3.23 and 3.24 [98]. As it can be seen the behaviour of unit cell parameters is almost the same for both compounds and do not display any anomalies. The Figures 3.25 and 3.26 show the thermal expansion of the cell dimensions $\Delta a/a_0$, $\Delta c/c_0$ and $\Delta V/V_0$. A least squares fit of a second order polynomial $\Delta L/L_0 = a + bt + ct^2$ to the experimental thermal expansion data yields the following parameters:

for LNG	$a \times 10^{-4}$	$b \times 10^{-6}$	$c \times 10^{-9}$
$\Delta a/a_0$	-1.7(5)	6.2(3)	2.1(3)
$\Delta c/c_0$	-5.4(7)	3.7(4)	2.5(4)
$\Delta V/V_0$	-4.0(11)	1.6(1)	7.0(11)
for LTG	$a \times 10^{-4}$	$b \times 10^{-6}$	$c \times 10^{-9}$
$\Delta a/a_0$	-2.2(10)	6.2(5)	1.7(6)
$\Delta c/c_0$	-2.1(10)	4.2(7)	1.5(6)
$\Delta V/V_0$	-7.6(13)	1.72(8)	4.8(9)

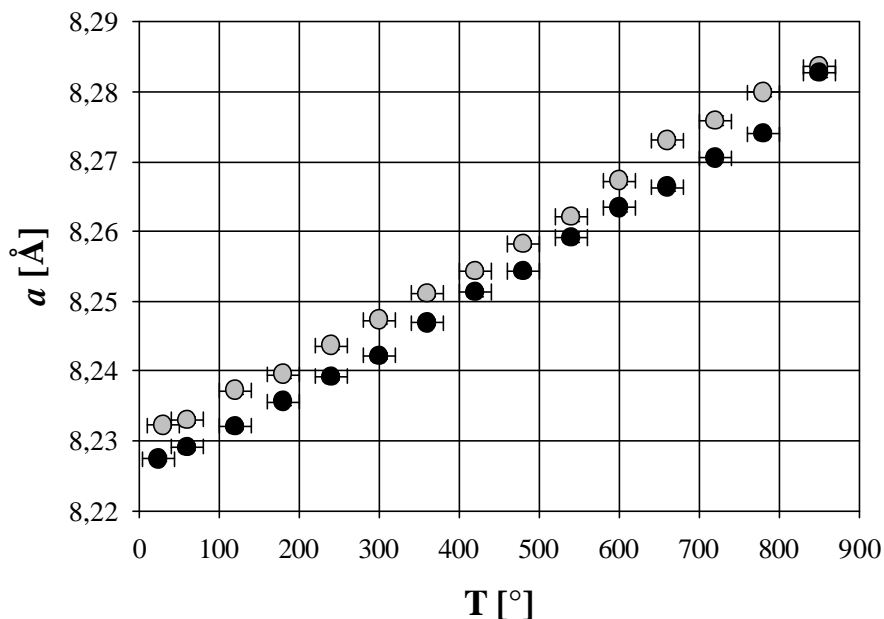


Fig. 3.23: The variation of a cell parameter of LNG (black symbols) and LTG (grey symbols) with temperature

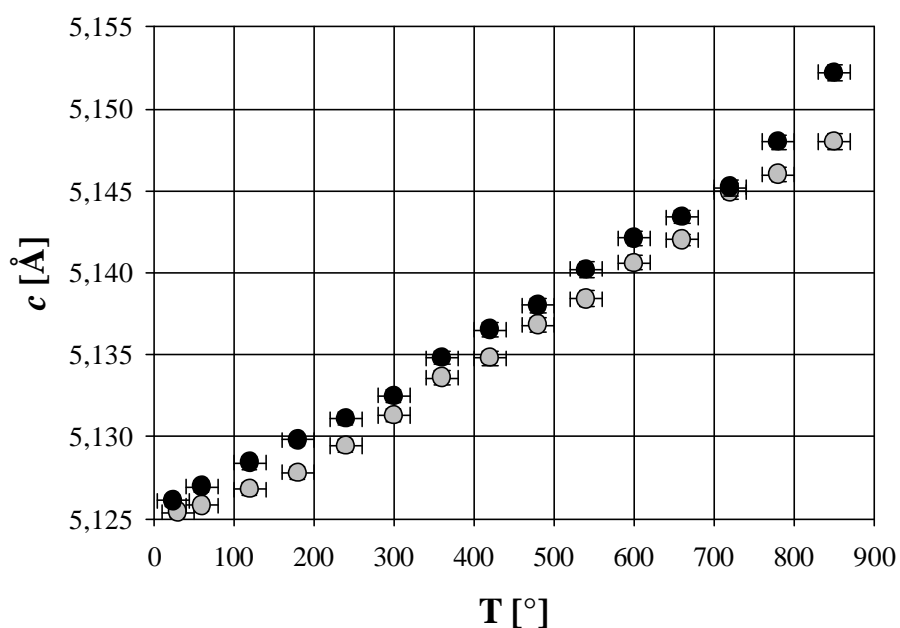


Fig. 3.24: The variation of c cell parameter of LNG (black symbols) and LTG (grey symbols) with temperature

The mean thermal expansion coefficients are presented in Table 3.14. As it can be seen the mean thermal expansion coefficients of unit cell parameters of LNG and LTG are similar. The thermal expansion of these compound is slightly anisotropic within the investigated temperature range, as the increase of the c -axis direction is slightly lower than that in the a -axis direction in both cases (see also Fig. 3.25 and Fig. 3.26).

Table 3.14. Mean thermal expansion coefficients of unit cell parameters of LNG and LTG

$a_L [^{\circ}\text{C}^{-1} \times 10^{-6}]$	LNG (24-850°C)	LTG (24-850°C)
a_a	8.141(4)	7.563(6)
a_c	6.162(5)	5.344(7)
a_v	22.563(7)	20.651(7)

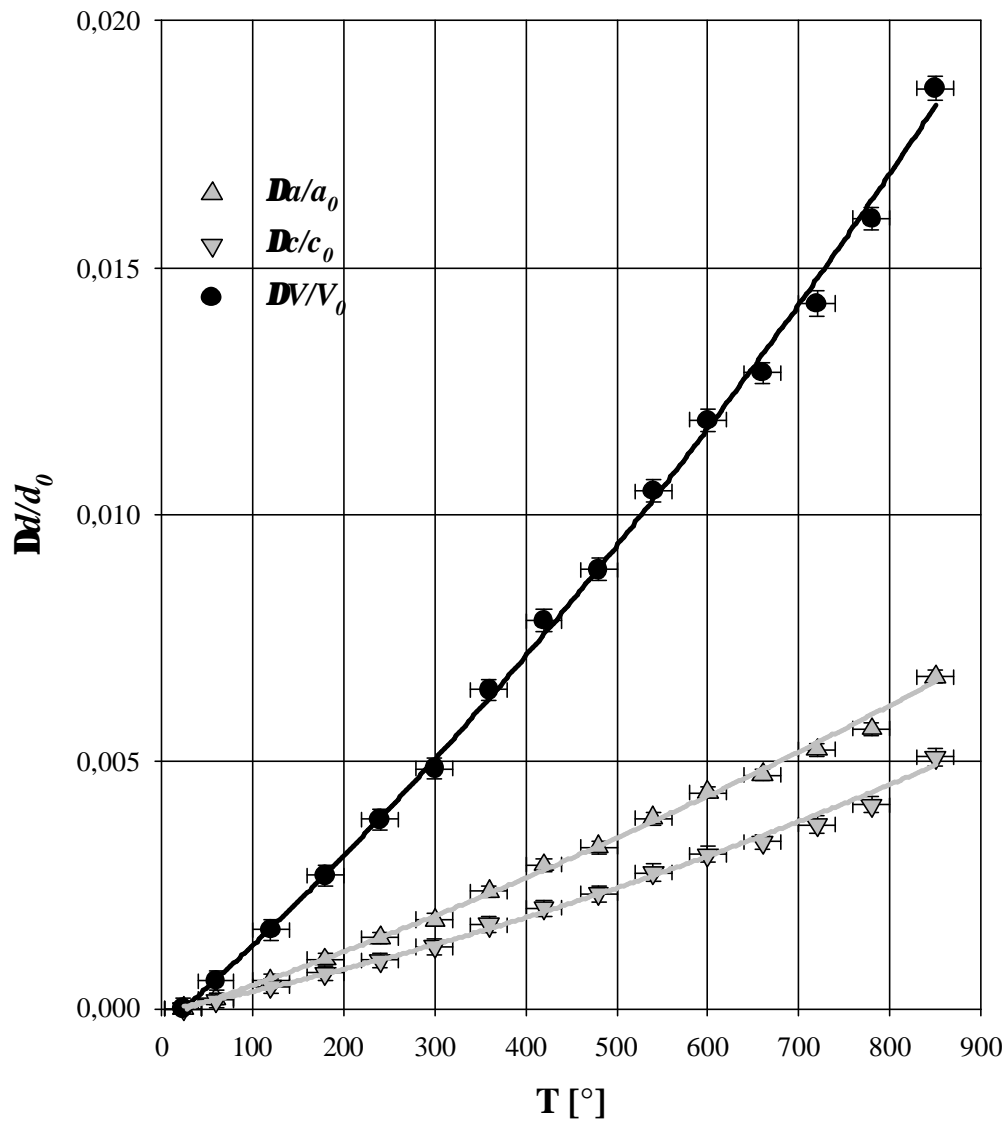


Fig. 3.25. Lattice expansion of LNG under elevated temperature.

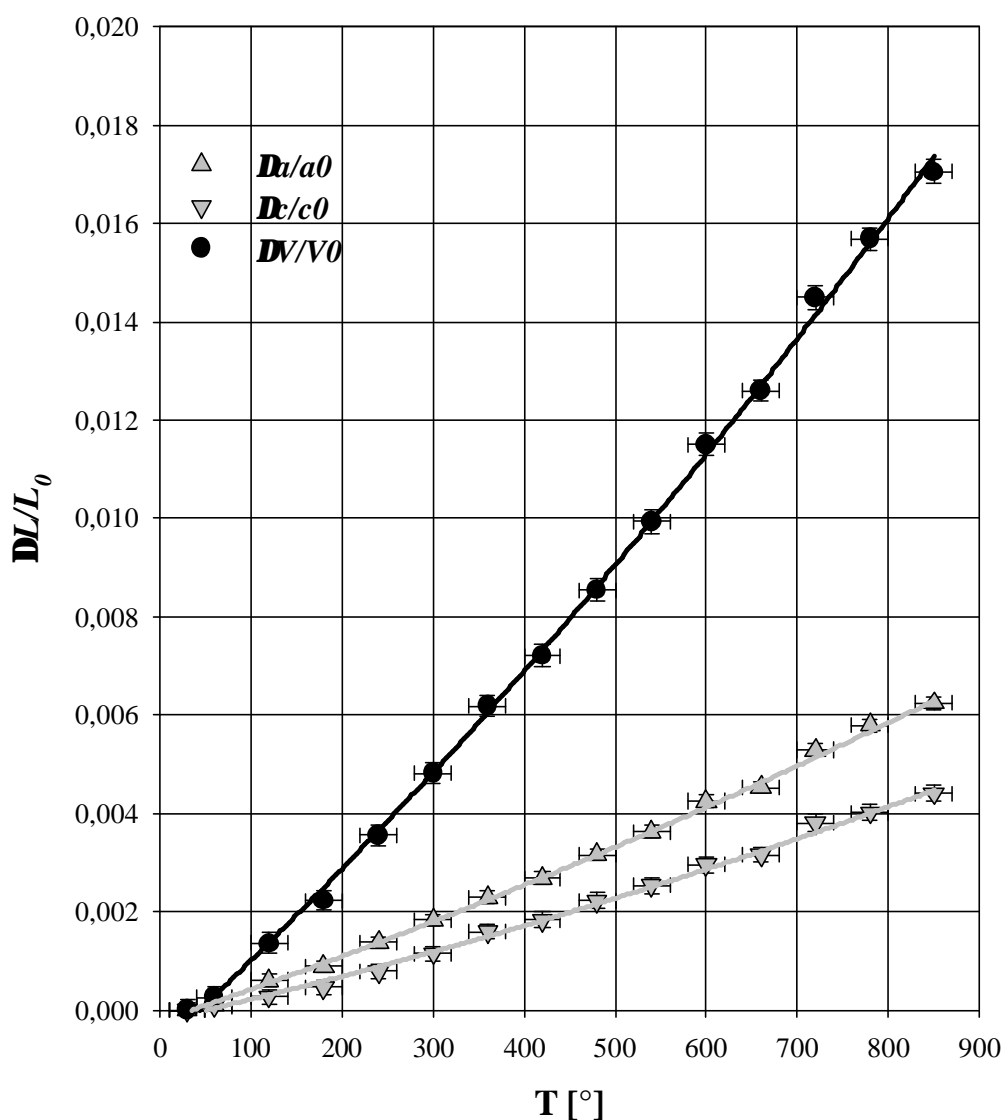


Fig. 3.26. Lattice expansion of LTG under elevated temperature.

It may be concluded that thermal expansions of trigonal cell parameters of LNG and LTG are the same in the investigated temperature range. Compared to the high pressure experiments the most prominent changes are again observed for *a*-axis (see Fig. 3.5). Therefore the behaviour of these compounds, which structures consist of polyhedral layers, under thermal expansion is anisotropic as well as under compression. This can be well explained by differing bond strength between (along *c*-axis direction) and within (along *a*-axis direction) the layers.

On the other side the heating and the compression cause differing changes within the crystal structures. In general the heating of inorganic compounds increases the energy of the crystals and structures may undergo phase transitions to higher symmetry. Due to high symmetry the crystal structure of LNG and LTG are very stable under elevated temperature, no phase transition was detected up to melting point ($T_m \sim 1460(10)^\circ\text{C}$) [11, 93]. The heating of these structures leads to increase volumes of the unit cell, which is probably accompanied by increase of volume and regularity of cation-anion polyhedra, whereas the compression of the crystal structures of LNG and LTG leads to decrease of the unit cell volumes and consequently results in decrease of volume of polyhedra. At pressures above 12(1)GPa both compounds transform to lower symmetry structures with excess of free-energy. Thus the high pressure polymorph of LNG or LTG is energetically more favourable at pressures above 12(1)GPa.

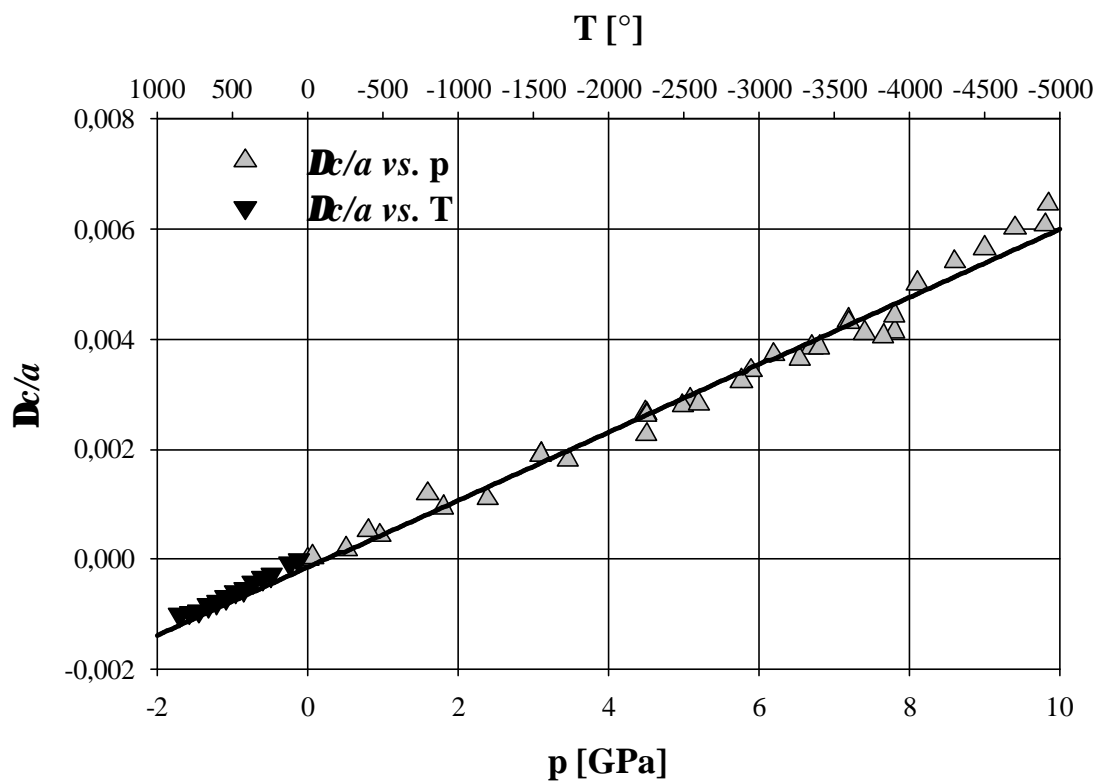


Fig. 3.27: The changes of the c/a ratio as compared to the initial value versus pressure.

In general the structural changes under increasing temperature and under increasing pressure are converse. It can be assumed, that the behaviour of the unit cell parameters under compression corresponds to that one under cooling. For comparison of the influence of pressure and temperature on the lattice parameters the linear fit to the data of the changes of c/a ratio of LNG under pressure and temperature was obtained (Fig. 3.27). Therefore, it can be suggested that the change of the unit cell parameters of LNG or LTG after cooling from 850°C down to room temperature corresponds to that one under increase of pressure of about 1.4GPa.

3.2.2. Thermal expansion of LSZG lattice

The compound $\text{La}_3\text{SbZn}_3\text{Ge}_2\text{O}_{14}$, which was investigated in this part of study, is a new member of the langasite family. The present structure model was proposed by B. Maximov [88]. It was proposed that LSZG crystallises in monoclinic symmetry, space group $A2$. Furthermore it is expected, that the crystal structure of this compound will turn to trigonal symmetry at temperature about 500° [88].

The temperature dependencies of the unit cell parameters of monoclinic crystal structure of LSZG, as determined by Rietveld analysis, are shown in Figure 3.28 [98]. As it can be seen, the changes of the unit cell parameters of LSZG with temperature reveal that a phase transition occurs at temperatures between 200°C and 300°C. Within this temperature interval there are significant discontinuities in the cell parameter evolutions, which suggests the first-order nature of phase transition. The b cell edge change at the phase transition has been estimated to $\Delta b \sim 0.28\%$, whereas the change of the c cell edge at the phase transition has been estimated to $\Delta c \sim -0.28\%$. Thus the changes of b - and c - axis parameters at 250(50)°C are the same in values but opposite in direction. This leads to the assumption that similar but reverse changes of the b - and c - axis parameters indicate the phase transition to trigonal symmetry with b equal to c . The a cell edge change at the phase transition is rather small and has been estimated to $\Delta a \sim 0.01\%$. The change of the monoclinic angle β at the temperature of phase transition (250(50)) has been estimated to $\Delta \beta \sim 0.10\%$.

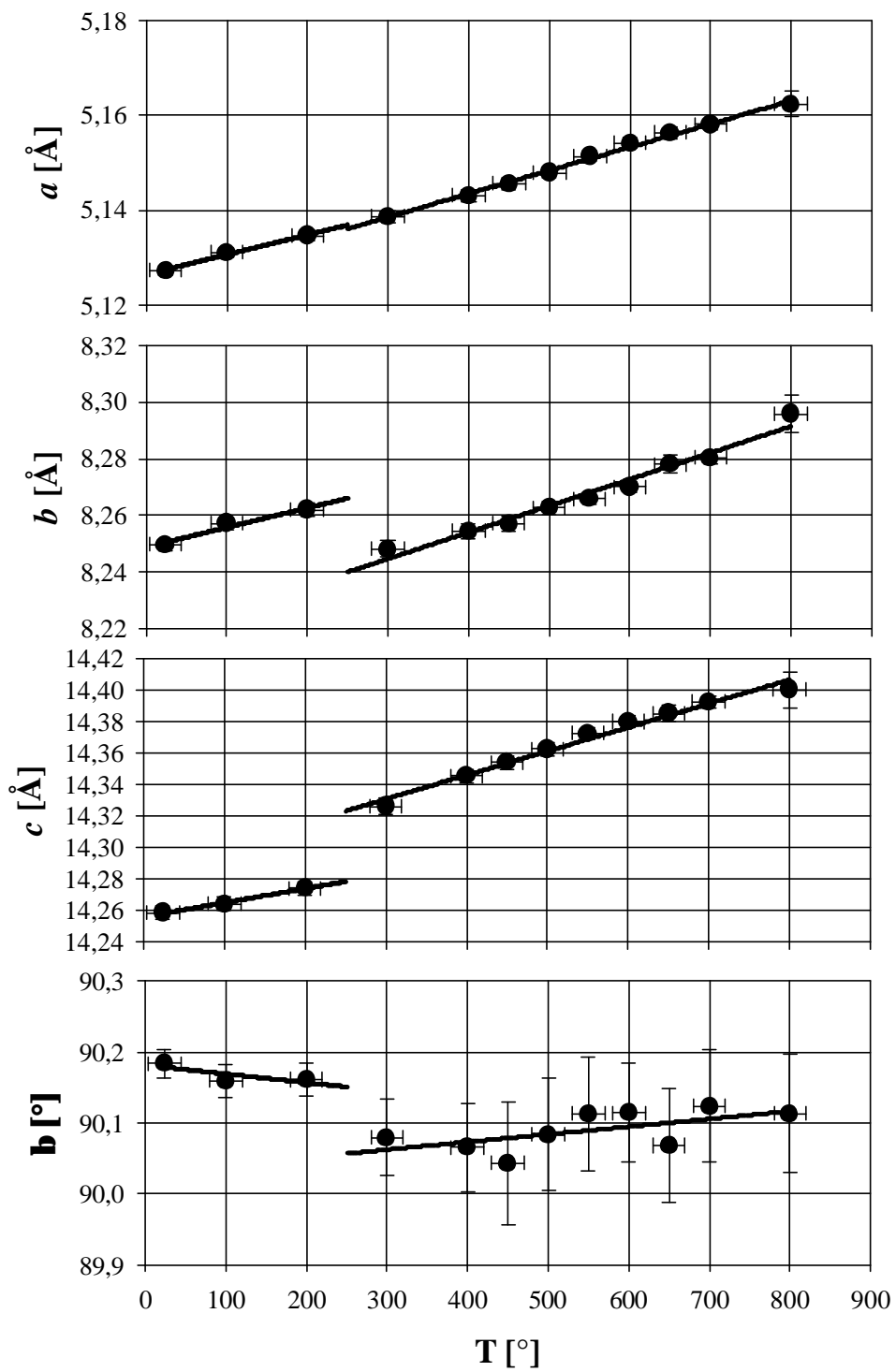


Fig. 3.28: The variation of monoclinic unit cell parameters of LSZG with temperature.

Examination of the mean thermal expansion coefficients of the monoclinic cell parameters at temperature ranges below the phase transition (Tab. 3.15) reveals slightly anisotropic behaviour of cell parameters. Thus $a_b > a_a > a_c$ in temperature range from room temperature up to 200°C.

Table 3.15. Mean thermal expansion coefficients of unit cell parameters of LSZG

$a_L [^{\circ}\text{C}^{-1} \times 10^{-6}]$	LSZG (24-200°C)
a_a	8.201(3)
a_b	8.471(5)
a_c	6.216(6)
a_v	23.40(6)
a_B	1.362(4)

Pointed above phenomena suggest, that under elevated temperature the crystal structure of LSGT undergoes the phase transition to higher symmetry.

The crystal structure of LSZG at normal condition is represented in Figure 3.29. As it can be seen the crystal structure of LSZG is similar to that one of monoclinic high pressure polymorph of LNG or LTG. Probably the substitution of Ga and Nb/Ta cations of LNG or LTG by large cations of Sb, Ge in case of LSZG leads to lower symmetry of the crystal structure of LSZG at normal condition as compared to that of LNG or LTG. The heating of the crystal structure of LSZG, leads to an increase of unit cell volume, combined with an increase of volume and regularity of polyhedra. This results in phase transition to higher symmetry at temperatures above 250(50)°C, which is similar to low pressure phase of LNG or LTG.

On the other hand, the compression of the crystal structure of LNG or LTG leads to decreasing of the unit cell volumes. Therefore the crystal structures of LNG and LTG under pressure turn to lower monoclinic symmetry, which is similar to the crystal structure of LSZG at normal condition. It can be assumed, that the low temperature structure of LSZG is equivalent to the monoclinic high pressure phase of LNG or LTG and conversely the high temperature phase of LSZG is equivalent to the low pressure phase of LNG or LTG.

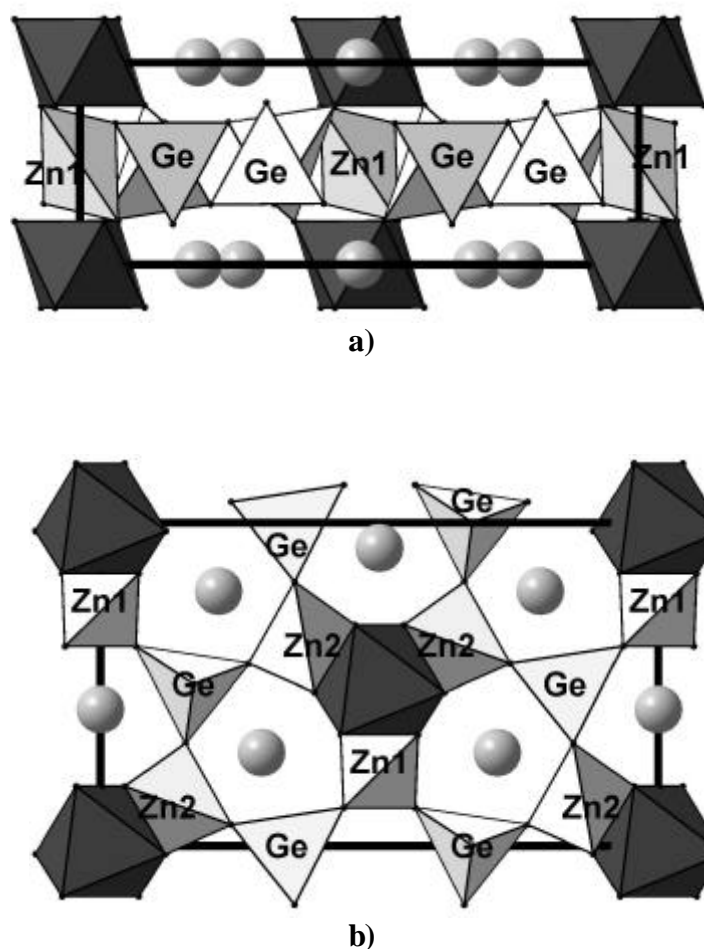
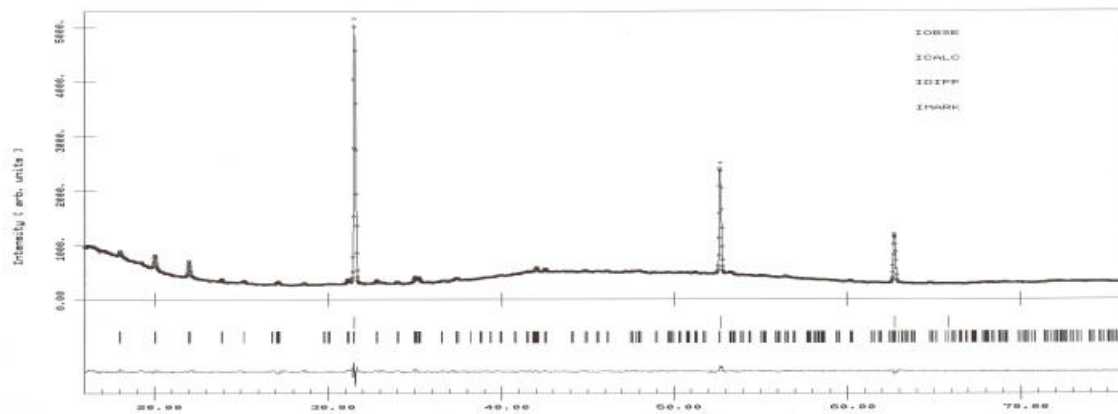
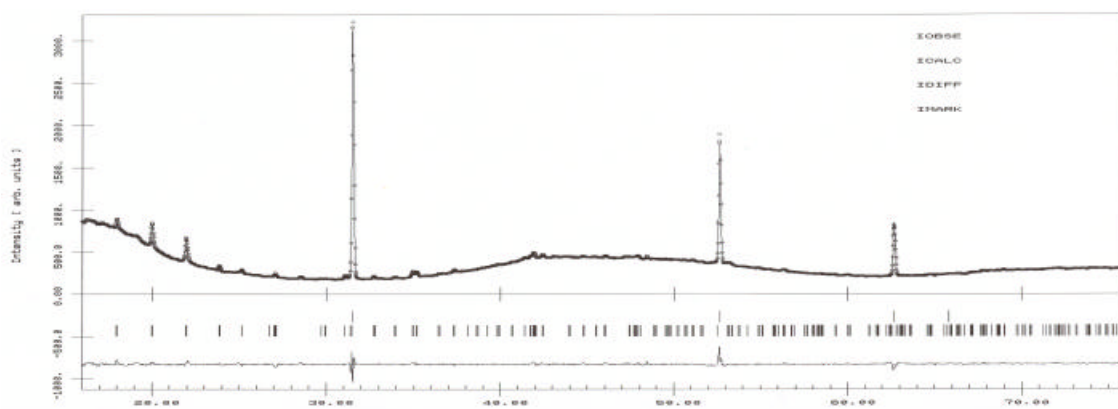


Fig. 3.29: Projection of the monoclinic unit cell of LSZG along the *b* (a) and *a* (b) axis at normal condition, the GeO_4 , ZnO_4 and SbO_6 polyhedra are shown:

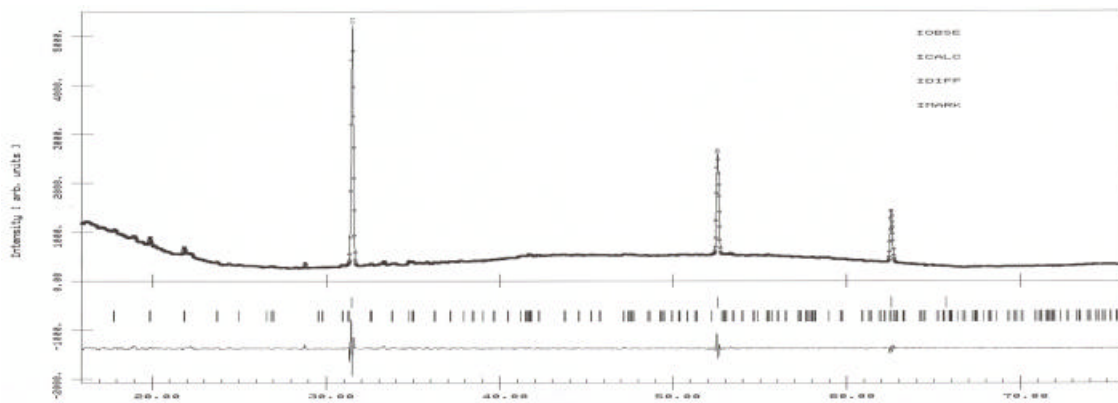
The Figure 3.30 depicts the observed and calculated patterns for monoclinic structure of LSZG at room temperature (a), at 300°C (b) and at 800°C (c) for monoclinic crystal structure of LSZG. Fortunately, the Rietveld analysis allows to obtain with good accuracy the temperature dependence of the cell parameters also from observed patterns with unfavourable background to reflection intensity ratios (Fig. 3.30, Fig. 3.31). This does not allow sufficient determination of atom positions. Furthermore the precision of the high temperature experiments with image plate (the scan step_{min} $\sim 0.01^\circ$) does not allow the analysis of separate reflection profiles at different temperatures (Fig. 3.31). Therefore for the more precise determination of the structural change (or changes) of LSZG at temperature the further experiments are required.



a)



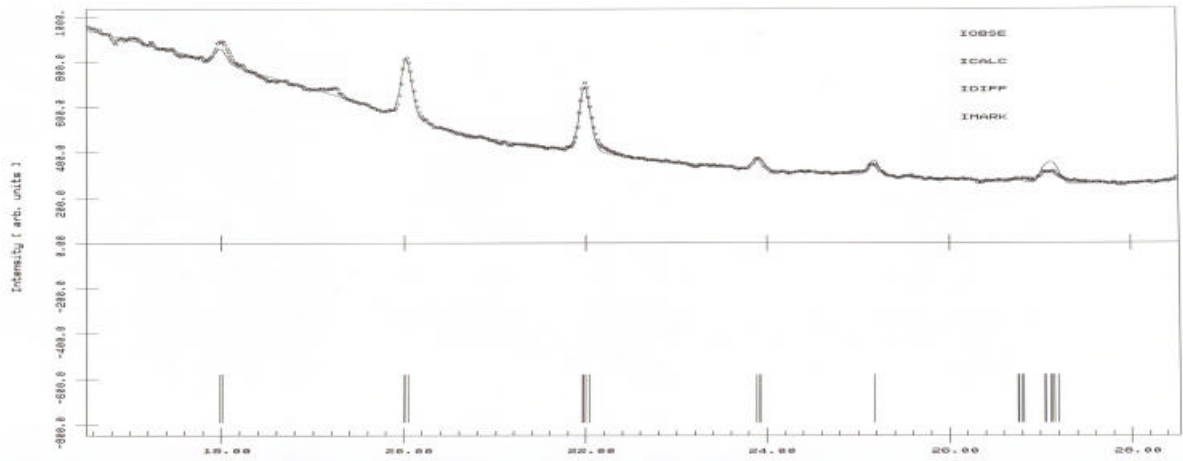
b)



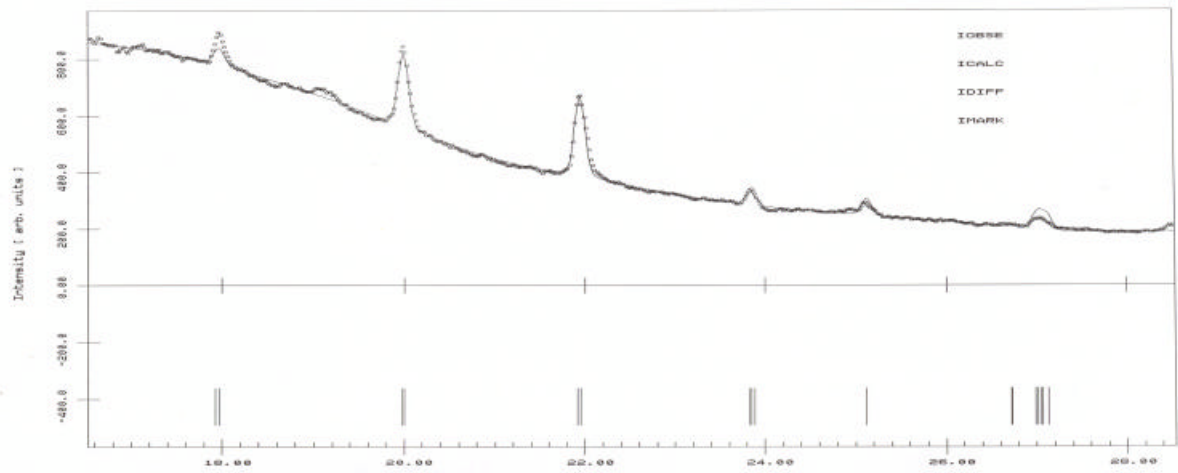
c)

Fig.⁵ 3.30: Observed and calculated difference pattern at room temperature (a), at 300°C (b) and at 800°C (c) of a two phase Rietveld refinement. The indicated reflection positions in first line belong to the diamond and the second one belong to the LSZG. The y-direction corresponds to Intensity, the x-direction corresponds to 2 θ .

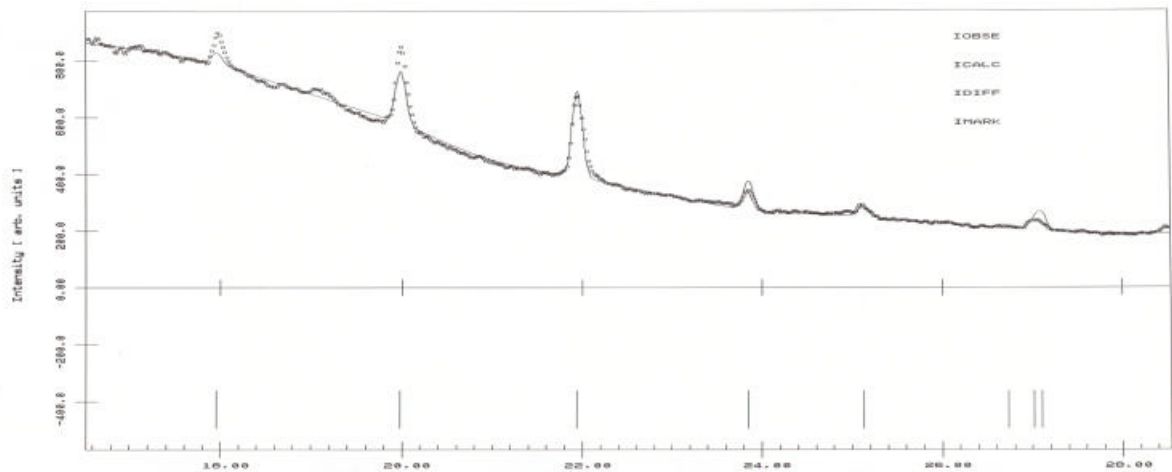
⁵ The diamond powder was applied in order to minimise the absorption effects



a)



b)



c)

Figure 3.31 Observed and calculated pattern at room temperature calculated for monoclinic structure of LSZG (a), at 300°C calculated for monoclinic structure of LSZG (b) and at 300°C calculated for trigonal structure of LSZG (c). The indicated reflection positions belong to the diamond (first row) and to the LSGZ (second row). The y-direction corresponds to Intensity, the x-direction corresponds to 2θ .

As pointed out above, according to the low pressure phase of LNG it was suggested that the monoclinic crystal structure of LSZG (space group *A2*) at temperature above 250(50)°C transforms to trigonal crystal structure (space group *P321*), the corresponding space groups being maximal non-isomorphic subgroups. Thus the monoclinic crystal structure of LSZG was transformed to trigonal crystal structure by following matrix with program Jana98:

$$\begin{vmatrix} 0 & 0 & 1 \\ 1/2 & 1/2 & 0 \\ -1/2 & 1/2 & 0 \end{vmatrix}$$

The refinements by Rietveld analysis of the trigonal cell parameters of LSZG (the atom positions were set accordingly to the transformed atom positions of monoclinic structure at room temperature) are represented in Table 3.16. As it can be seen, the refinements of the crystal structure of LSZG in trigonal space group *P321* do not improve the refinement parameters. This can be probably explained by unfavourable experimental conditions. In addition, the temperature dependencies of trigonal cell parameters of LSZG are depicted at Fig. 3.32.

Table 3.16. Results of Rietveld refinements of LSZG X-ray data at different temperatures

T [°]	R_{Bragg}		R_{wp}		SQRT GOOF	
	<i>A2</i>	<i>P321</i>	<i>A2</i>	<i>P321</i>	<i>A2</i>	<i>P321</i>
300	29.80	35.44	2.57	2.78	0.47	0.51
400	25.99	29.15	2.96	3.05	0.55	0.57
500	25.27	30.63	3.02	3.17	0.60	0.63
600	25.73	36.61	2.83	3.12	0.62	0.69
700	26.38	32.05	2.92	3.15	0.62	0.67
800	34.52	41.26	2.97	3.03	0.64	0.65

As it can be seen the thermal expansion of the cell dimensions $\Delta a/a_0$, $\Delta c/c_0$ and $\Delta V/V_0$ are linear. A least squares fit of a first order polynomial $\Delta L/L_0 = a + bt$ to the thermal expansion data obtained yields the following parameters:

for LSZG	$a \times 10^{-3}$	$b \times 10^{-5}$
$\Delta a/a_0$	-3.38(14)	1.14(3)
$\Delta c/c_0$	-2.4(2)	0.74(4)
$\Delta V/V_0$	-9.17(16)	3.04(3)

In conclusion it may be stated, that the low temperature structure of LSZG is equivalent to the monoclinic high pressure phase of LNG or LTG and conversely the high temperature phase of LSZG is comparable to the low pressure phase of LNG or LTG.

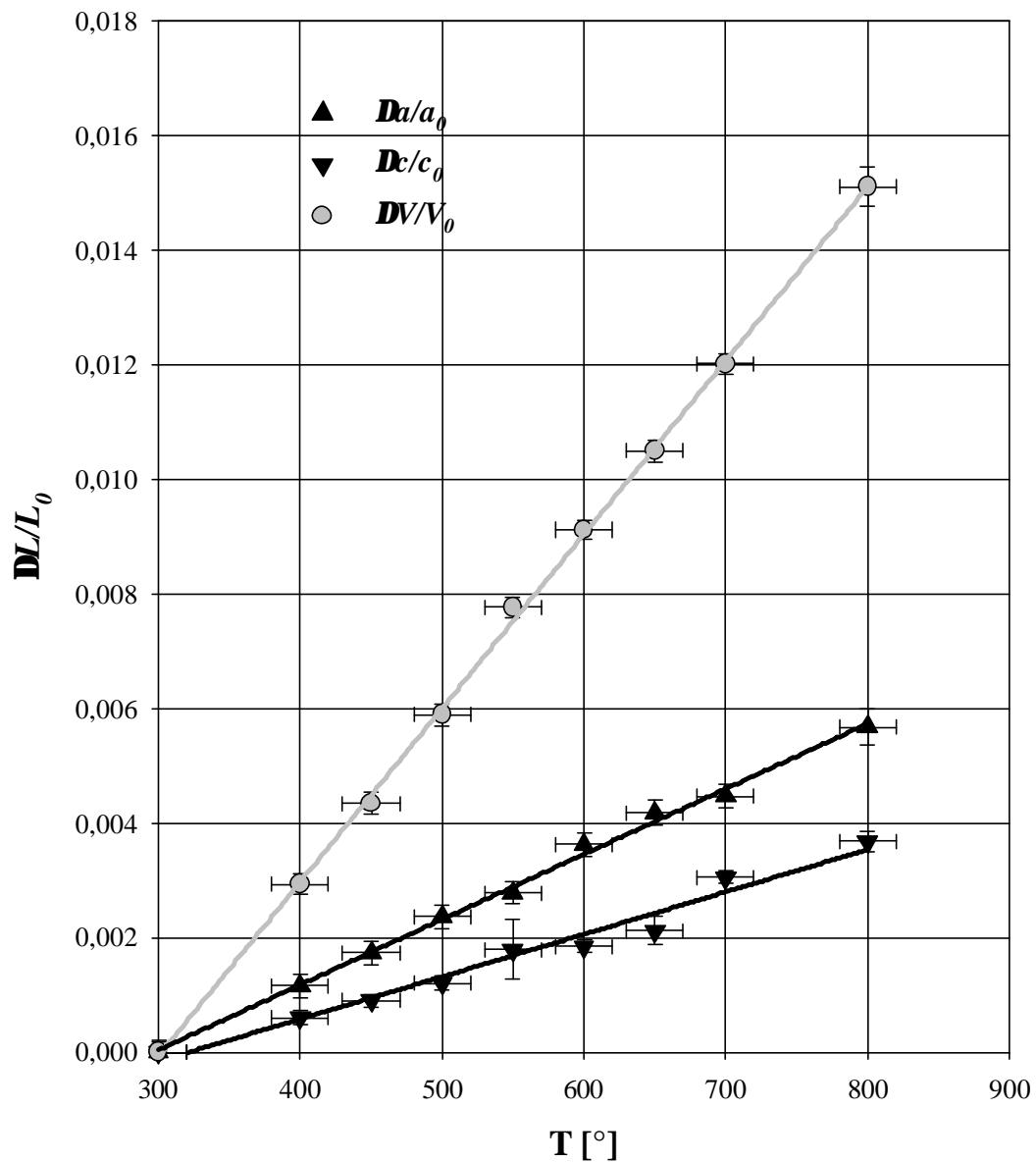


Fig. 3.32: Trigonal lattice expansion of LSGZ under elevated temperature.

4. CONCLUSIONS

4.1. High pressure experiments

It may be concluded that the high pressure behaviour of LNG and LTG is anisotropic as expected for layered compounds. The a axis is the most compressible direction for both compounds. This marked compressional anisotropy can be explained by the different character of interconnectivities across and within the layers. Thus, under hydrostatic pressure, the compression in c direction is rigid due to less flexible interconnectivities of polyhedra (shared edges). In contrast, the compression within the ab -plane is more rapid and it is achieved mainly due to decreasing volumes and distortions of anion-cation polyhedra.

The crystal structures of LNG and LTG undergo phase transitions at pressures of 12.4(3) GPa and 11.7(3) GPa, respectively. Above these pressures the crystal structures of LNG and LTG can be defined as monoclinic, the monoclinic angle β deviates slightly from 90° starting at 14 GPa. Thus, similar to GaPO₄ or α -quartz, the crystal structures of LNG and LTG undergo a trigonal to monoclinic phase transition, whereas the driving forces for these transitions are different. The compression of the crystal structure of GaPO₄, which consists of tetrahedral chains (GaO₄ and PO₄), leads to tilting and distortion of tetrahedra. At pressures above 7 GPa a phase transition from trigonal to monoclinic symmetry occurs due to large distortion of the GaO₄ tetrahedra. The existence of octahedra and dodecahedra, which are sharing their edges and (or) corners with neighbouring tetrahedra, causes the main difference between compression mechanisms of the crystal structures of LNG or LTG and of GaPO₄. Thus, the compressions of LNG and LTG are mainly achieved by decreasing volumina of polyhedra. But the tilting and distortion of polyhedra is hampered due to shared interconnectivities and high symmetry. This leads to increasing internal strains (especially within the layers of GaO₄ tetrahedra with atomic bonding). Finally, this results in break of high symmetry of the crystal structures of LNG and LTG.

Significant differences in the behaviour of the investigated compounds under pressure are observed only for high pressure phases, whereas the initial phases of LNG and LTG are similarly compressible. Therefore the substitution of Nb⁵⁺ against Ta⁵⁺ causes almost no difference of compressibilities of low pressure phases of LNG and LGT. The calculated bulk moduli for low pressure phases of LNG and LTG are 145(3) GPa and 144(2) GPa, respectively. The initial phase of LNG or LTG crystals is less compressible, than α -quartz and GaPO₄ with bulk moduli 37.12(9) GPa (B_0' =5.99(4)) and 39.9(9) GPa (B_0' =3.7(3)),

respectively. The lower compressibility of LNG or LTG as compared to α -quartz or GaPO₄ might be explained by closer packing of these compounds. Thus the packing coefficient (c_i) of LTG as well as of LNG is 0.63, due to the equal ionic radius of Nb and Ta (0.64Å). The c_i calculated for α -quartz and GaPO₄ at ambient conditions are 0.41 and 0.32, respectively. On the other hand, the difference between bulk moduli of α -quartz structures and LNG or LTG can be well explained by different interconnectivities of polyhedra of these structures. Thus the crystal structure of α -quartz or GaPO₄ consist of corner sharing tetrahedra. This allows higher compression of the low quartz structure as compared to that of LNG or LTG, which is rigid due to polyhedra sharing edges.

The high-pressure phase of LNG has a bulk modulus of 93(2) GPa ($B_0' = 1.9(9)$). The obtained bulk modulus for high-pressure phase of LTG is $B_0 = 128(12)$ GPa (B_0' was set to 1.9 according to the value of LNG). Thus a difference between compressibilities of investigated compounds appears only above pressures of the phase transitions. This difference may be caused by increase of polarisation of the oxygen arrangement by Nb⁵⁺ ions within the high pressure polymorph, whereas the octahedra formed by Ta⁵⁺ still stay almost regular. Furthermore, a higher compressibility of the high-pressure polymorph of LNG, as compared to the low-pressure phase, is clearly observed. An increase in compressibility is typical for polyhedral tilt. In most cases, the additional freedom due to symmetry breaking and thus increasing flexibility of individual structural rigid units within framework-type structures gives sufficient explanation for the (at first glance rather unexpected) higher compressibility of the high pressure polymorph. In addition, for various compounds, a higher compressibility of the high-pressure phase could be explained by anomalous elasticity.

On further increase of pressure (above 22 GPa), compression of monoclinic structure of LGN can lead to even more dramatic changes in the crystal structure with changes in the coordination number, most likely for the Ga³⁺ cations. Probably a similar processes will take place also in the case of LTG, but under again higher pressures.

4.2. High temperature experiments

The thermal expansions of trigonal cell parameters of LNG and LTG are the same in the investigated temperature range. The most prominent changes are again observed for a -axis. Therefore the behaviour of these isostructural compounds under thermal expansion is anisotropic as well as under compression. The absence of polarisation of the oxygen arrangement by Nb⁵⁺ or Ta⁵⁺ ions within the trigonal structure of LNG or LTG, leads to

similar behaviour of these compounds under elevated temperatures. Thus, the examination of the mean thermal expansion coefficients of the unit cell volumes a_V (24-850°C) of LNG and LTG results in almost the same values for investigated compounds 22.563(7) and 20.651(7) [$\times 10^{-6} \text{ }^\circ\text{C}^{-1}$], respectively.

On the other side the structural changes under heating and under compression are converse. It can be assumed, that the behaviour of the unit cell parameters under increase of pressure corresponds to that one under decrease of temperature. From the linear fit to the data of the changes of c/a ratio of LNG under pressure and temperature it follows that the change of the unit cell parameters of LNG or LTG after cooling from 850°C down to room temperature corresponds to that one under increase of pressure to about 1.4 GPa.

In addition, the heating of the monoclinic crystal structure of LSZG, which is comparable to the high pressure phase of LNG or LTG, results in a phase transition. The high temperature phase of LSZG is suggested to be trigonal, with respect to low pressure phase of LNG or LTG. In conclusion it may be stated, that the low temperature structure of LSZG is equivalent to the monoclinic high pressure phase of LNG or LTG and conversely the high temperature phase of LSZG is equivalent to the low pressure phase of LNG or LTG.

For a more precise description of the phase transition of the crystal structure of LSZG at elevated temperature further experiments are required.

4.3. Compilation of features with regard to advantageous technical applications

In addition, it will be useful to list the properties of LNG and LTG single crystals again:

6. Crystals of LNG and LTG can be grown by conventional Czochralski technique with rather high structural perfection.
7. The results of the DTA measurements show no anomalies in the behaviour of LNG or LTG up to 1400°C [5]. The phase identification by using powder X-ray diffraction analysis showed that the samples after DTA measurement have kept the initial phase. Results of X-ray diffraction experiments reported in this study confirm the absence of phase transitions at temperatures up to 800°C. Since LNG and LTG probably have no phase transitions up to their melting points at about 1470(30)°C, they are ideally suited for piezomechanical applications at high temperatures[3,5,11].
8. The hardness of LNG and LTG is almost the same as that of quartz.
9. Neither LNG nor LTG is insoluble in acids or bases.

10. The pass band width of LNG or LTG filter is three times wider than that of quartz. Therefore, LNG and LTG are by far superior materials for filter devices.

With regard to this study the following recommendations may be made:

5. In regard with high quality of these materials (the full width at half maximum of the reflections is about 0.0008°), it can be recommended to use these crystals as a test-crystal for adjustment of single-crystal diffractometers.
6. As well as α -quartz [58], these crystals can be used as internal pressure standard at high pressure single crystal experiments, due to large number of strong independent reflections. On the other side, the lower compressibility of LNG or LTG as compared to α -quartz, may lead to lower precisions of pressure measurements. This disadvantage can be compensated by high scattering power of these compounds.
7. LNG or LTG can be supplied as materials for pressure sensors up to very high pressure level (up to 11 GPa). The upper pressure is limited by phase transition to lower symmetry, which LNG and LTG undergo at pressures above 12(1) GPa.
8. The thermal stability of these materials was confirmed. Thus the temperature dependence of lattice parameters of these materials show no anomalies within the investigated temperature range (24°C - 850°C). In this way, LNG and LTG can be strongly recommended as a substrate material for temperature sensors.

ACKNOWLEDGEMENTS

I am very grateful to **Dr. S. Werner** for his guidance, for really good scientific support, for very useful discussion and in-depth answer for all my questions, and encouragement throughout the project, which made this thesis possible.

I would like to express my sincere gratitude to **Prof. Dr. W. Moritz, Dr. H. Boysen, Dr. J. Schneider** and **Prof. Dr. H. Schulz** for very interest and fruitful discussions, good ideas and questions at X-rays group seminars.

I would like to thank **Prof. B. Mill** and **Prof. B. Maksimov** for providing the sample material and useful discussion.

I am very grateful to **Dr. R. Boehler** for the opportunity to load the DACs with Xe and He, for help and support.

I would like to thank the **people at the workshop and electronical laboratory** for technical support.

I would like to thank **work group at beamlines D3 and B2** for technical assistances during my experiments at HASYLAB.

I am very grateful to **Dr. E. Weidner** for correcting the English language.

I would like to thank my **parents** and, especially, to my **husband**, for love, support and motivations.

The present study was supported by the Deutsche Forschungsgemeinschaft

6. REFERENCES

1. Mill, B. V.; Butashin, A. V.; Khodzhabagyan, G. G.; Belokoneva, E. L.; Belov, N. V.: Modified rare-earth gallates with $\text{Ca}_3\text{Ga}_2\text{Ge}_4\text{O}_{14}$ structure. *Sov. Phys. Dokl.* **27** (1982) 434.
2. Belokoneva, E.L.; Mill, B.V.: Crystal chemistry and isomorphism of compounds $\text{A}_3\text{B}_x\text{C}_{6-x}\text{O}_{14}$. *Crystal chemical systematics of minerals*; V.S.Urusov; ed. Moscow. Moscow St. Univ. (1985) 140-156.
3. Mill, B. V.; Pisarevsky, Y. V.: Langasite-type materials: from discovery to present state. *IEEE/EIA Int. Frequency Control Symp.* (2000) 133.
4. Silvestrova, I. M.; Pisarevskiy, Yu. V.; Kaminskiy, A. A. and Mill, B. V.: Elastic, piezoelectric, and dielectric properties of $\text{La}_3\text{Ga}_{5.5}\text{Nb}_{0.5}\text{O}_{14}$ crystals. *Fiz. Tverd. Tela (Leningrad)* **29** (1987) 1520-1522.
5. Takeda, H.; Shimamura, K.; Koho, T.; Fukuda, T.: Growth and characterization of $\text{La}_3\text{Ga}_{5.5}\text{Nb}_{0.5}\text{O}_{14}$ single crystals. *J. Crystal Growth.* **169** (1996) 503-508.
6. Kanawaka, H.; Takeda, H.; Shimamura, K.; Fukuda, T.: Growth and characterization of $\text{La}_3\text{Ga}_{5.5}\text{Ta}_{0.5}\text{O}_{14}$ single crystals. *J. Crystal Growth.* **183** (1998) 274-277.
7. Chai, B.; Qiu, Y. Y. and Lefaucher, J. L.: Growth of high quality single domain crystals of langasite family compounds. *IEEE Int. Frequency Control Symp.* (1999) 821-828.
8. Mateescu, I.; Pop, G.; Ghita, C.: A new theoretical approach for the coupling coefficient in the monolithic structures. *IEEE Int. Frequency Control Symp.* (1998) 580-586.
9. Sato, J.; Takeda, H.; Morikoshi, H.; Shimamura, K.; Rudolph, P; Fukuda, T.: Czochralski growth of $\text{RE}_3\text{Ga}_5\text{SiO}_{14}$ (RE = La, Pr, Nd) single crystals for the analysis of the influence of rare earth substitution on piezoelectricity. *J. Crystal Growth.* **191** (1998) 746-753.
10. Smythe, R. C.; Helmbold, R. C.; Hague, G. E. and Snow, K. A.: Langasite, langatite, and langatate resonators: resent results. *IEEE Int. Frequency Control Symp.* (1999) 816-820.
11. Bohm, J.; Heimann, R. B.; Hengst, M.; Roewer, R.; Schindler, J.: Czochralski growth and characterization of piezoelectric single crystals with langasite structure $\text{La}_3\text{Ga}_5\text{SiO}_{14}$ (LGS), $\text{La}_3\text{Ga}_{5.5}\text{Nb}_{0.5}\text{O}_{14}$ (LGN), and $\text{La}_3\text{Ga}_{5.5}\text{Ta}_{0.5}\text{O}_{14}$ (LGT). Part I. *J. Crystal Growth.* **204** (1999) 128-136.
12. Bohm, J.; Heimann, R. B.; Hengst, M.; Roewer, R.; Schindler, J.: Czochralski growth and characterization of piezoelectric single crystals with langasite structure $\text{La}_3\text{Ga}_5\text{SiO}_{14}$ (LGS), $\text{La}_3\text{Ga}_{5.5}\text{Nb}_{0.5}\text{O}_{14}$ (LGN), and $\text{La}_3\text{Ga}_{5.5}\text{Nb}_{0.5}\text{O}_{14}$ (LGT). Part II. *J. Crystal Growth.* **216** (2000) 293-298.

13. Hornsteiner, J., Born, E., Riha, H., Langasite for High Temperature Acoustic Wave Application, *Phys. Status solid A*(1997), **R3**, 163.
14. Weitzel, H.: Kristallstrukturverfeinerung von Wolframiten und Columbiten. *Z. Kristallogr.* **144** (1976) 238-258.
15. Malovichko, G.; Grachev, V.; Bykov, I.; et al.: Phase diagram of lithium niobate and tantalate in their lattices under anisotropic compression. *Sov. Phys. Solid State* **29** (1987) 244-246.
16. Voron'ko, Yu.; Kudryavtsev, A.; Osiko, V. et al.: Raman scattering study of phase transitions in lithium niobate and tantalate. *Sov. Phys. Solid State* **29** (1987) 771-775.
17. Bravina, S.; Kremenchugsky, L.; Morozovsky, N.; Strokach, A.: Low-temperature pyroelectric effect in uniaxial displacement-type ferroelectrics. *Ukrayins'kyi Fizychnyi Zhurnal* **33** (1988) 1065-1072.
18. Neumann, T.; Scharfschwerdt, C.; Neumann, M.: Electronic structure of KNbO_3 and KTaO_3 . *Phys. Rev. B* **46** (1992) 10623-8.
19. Kitamura, M.; Chen, H.: Electronic structures and the phase stability of perovskite-type oxides KNbO_3 and KTaO_3 . *Ferroel.* **206** (1998) 55-67.
20. Sepliarsky, M.; Stachiotti, M.; Migoni, R.: Model potential for the ferroelectric ABO_3 perovskites. *Ferroel.* **186** (1996) 69-72.
21. Darlington, C. N. W.; Magaw, H. D.: The low-temperature phase transition of sodium niobate and the structure of the low-temperature phase, *N. Acta Cryst.* **29** (1973) 2171.
22. Molchanov, V. N.; Maksimov, B. N.; Kondakov, A. F.; Chernaya, T. S.; Pisarevsky, Yu.V.; Simonov, M. I.: Crystal structure and optical activity of langasite family $\text{La}_3\text{Nb}_{0.5}\text{Ga}_{5.5}\text{O}_{14}$ and $\text{Sr}_3\text{Ga}_2\text{Ge}_4\text{O}_{14}$ single crystals. *Pis'ma ZHETF.* **74** (2001) 244-247.
23. Takeda, H. K.; Sugiyama, K.; Inaba, K.; Shimamura, T.; Fukuda, T.: Crystal growth and structural characterization of new piezoelectric material $\text{La}_3\text{Ta}_{0.5}\text{Ga}_{5.5}\text{O}_{14}$. *Jpn. J. Appl. Phys.* **36** (1997) 919-921.
24. Hazen, R. M.; Finger, L. W.: Crystals at high pressure. *Scientific Am.* **252** (1985) 84-91.
25. Hazen, R. M. and Finger, L. W.: Polyhedra Tilting: A common type of pure displacive phase transition and its relationship to analcite at high pressure. *Phase Transit.* **1** (1979) 1-22.
26. Hazen, M. and Hexiong Yang.: Increased compressibility of pseudobrookite – type MgTi_2O_5 caused by cation disorder. *SCIENCE* **277** (1997) 1965-1967.
27. Cauble, R.; Perry, T.S.; Bach, D.R. et al.: Absolute equation of state data in the 10-40 Mbar (1-4 Tpa) regime. *Phys. Rev. Lett.* **80** (1998) 1248-1251.

28. Sowa, H.: The crystal structure of GaPO₄ at high pressure. *Z. Kristallogr.* **209** (1994) 954-960.
29. Murashov, V. V.: Pressure-induced phase transition of quartz-type GaPO₄. *Phys. Rev. B* **53** (1995) 107-110.
30. Peters, M. J.; Grimsditch, M.; Polian, A.: High-pressure Raman scattering from GaPO₄. *Sol. St. Communic.* **114** (2000) 335-340.
31. Krempf, P.; Scheinzer, G.; Wallnofer, W.: Gallium phosphate, GaPO₄: a new piezoelectric crystal material for high-temperature sensorics. *Sensors and Actuators A (Physical)* **A61** (1997) 361-363.
32. Bardo, J.; Itie, J. P.; Polian, A.: On the high-pressure phase transition in GaPO₄. *Europ. Phys. J. B.* **1** (1998) 265-8.
33. Mariathasan, J. W. E.; Finger, L. W.; Hazen, R. M.: High-pressure behaviour of LaNbO₄ (crystal structure) *Acta Cryst. Section B (Structural Science)* **B41** (1985) 179-184.
34. Jornada, J. A. H.; Block, S.; Mauer, F. A.; Piermarini, G. J.: Phase transition and compression of LiNbO₃ under static high pressure. *J. Appl. Phys.* **57** (1985) 842-844.
35. Avanesyan, G. T.: Equilibrium structure of lithium niobate and tantalate crystals. *Sov. Phys. Solid State* **29** (1987) 1080-1081.
36. Sepliarsky, M.; Stachiotti, M. G.; Migoni, R. L.: Structural instabilities in KTaO₃ and KNbO₃ described by the nonlinear oxygen polarizability model. *Phys. Rev. B.* **52** (1995) 4044-4049.
37. Bardo, J.; Gillet, Ph.; McMillan, P. F.; Polian, A. and Itie, J.-P.: A combined XAS study of the high-pressure behaviour of GaAsO₄ berlinite. *Europhys. Let.* **40** (1997) 533-538.
38. Carpenter, M. A. and Salje, E. K. H.: Elastic anomalies in minerals due to the structural phase transitions. *Eur. J. Mineral.* **10** (1998) 693-812.
39. Carpenter, M. A.; Salje, E. K. H.; Graeme-Barber, A.: Spontaneous strains as determinant of thermodynamic properties for phase transitions in minerals. *Eur. J. Mineral.* **10** (1998) 621-691.
40. Transformation Processes in Minerals. *Rev. in Min. & Geochem.* **39** (2000).
41. Sil'vestrova, I. M.; Pisarevskii, Yu. V.; Senyushchenkov, P. A. and Krupnyi A. I.: Temperature dependences of the elastic properties of La₃Ga₅SiO₁₄ single crystals. *Fiz. Tverd. Tela (Leningrad)* **28** (1986) 2875-2878.
42. Sorokin, B. P.; Turchin, P. P. and Glushkov, D. A.: Elastic nonlinearity and propagation of volume acoustic waves under conditions of homogenous mechanical stresses in a La₃Ga₅SiO₁₄ single crystals. *Fiz. Tverd. Tela (St. Petersburg)* **36** (1994) 2907-2915.

43. Dove, M. T.: Theory of displacive phase transitions in minerals. *Am. Min.* **82** (1997) 213-244.
44. Hazen, R. M. and Finger, L. W.: High-temperature and high-pressure crystal chemistry. *High-pres. Res. In Geosc.* (1982) 151-176.
45. High-pressure techniques in chemistry and physics. Oxford University Press (1997).
46. Miletich, R., private communication.
47. Merrell, L.; Bassett, W. A.: Miniature diamond anvil cell for single crystal X-ray diffraction studies. *Rev. Sci. Instr.* **45** (1974) 290-294.
48. Werner, S.; Kim-Zajonz, J.; Wittlinger, J.; Schulz, H.: Single crystal diffraction under hydrostatic pressure up to 35GPa. In: *Proc. German-Japanese Workshop on the Use of Ultra-short Wavelength Photons and GAMMA-rays for High-Precision, High-Resolution Analysis of Electronic States of Solids, HASYLAB.* (1996) 26-29.
49. Kim-Zajonz, J.: (1997) Dissertation, Ludwig-Maximilians-Universität München.
50. Eremets, M.: High pressure experimental methods. Oxford Science Publications (1996).
51. Carlson, F.: High pressure structural investigations using single crystal techniques. *Dep. Of Struc. Chem. Strockholm University, Dissertation* (1998).
52. Wittlineg, J.; Fischer, R.; Werner, S.; Schneider, J. and Schulz, H.: High-pressure study of *h. c. p.*- Argon. *Acta Cryst.* **B53** (1997) 745-749.
53. Asuami, K.; Ruolff, A.L.: Nature of the state of stress production by xenon and smome alkali iodides when used as pressure media. *Phys. Rew. B* **33** (1986) 5633-5636.
54. Bell, P. M. and Mao, H. K.: Degrees of Hydrostaticity in He, Ne, and Ar pressure-transmitting media. *Yb. Carnegie Inst. Washington Yearb.* (1981) 404-406.
55. Forman, R. A.; Piermarini, G. J.; Barnett, J. D. and Block , S.: *Science* **176** (1972) 284-285.
56. Piermarini, G. J.; Block, S.; Barnett, J. D.; Forman, R. D.: Calibration of the pressure dependence of the R_1 ruby fluorescence line to 195kbar. *J. Appl. Phys.* **46** (1975) 2774-2780.
57. Mao, H. K.; Xu, J.; Bell, P. M.: Calibration of the ruby pressure gauge to 800kbar under quasi-hydrostatic conditions. *J. Geophys. Res.* **91** (1986) 4673-4676.
58. Angel, R. J.; Allan, D. R.; Miletich, R.; Finger, L.W.: The use of quartz as an internal pressure standard in high - pressure crystallography. *J. Appl. Cryst.* **30** (1997) 461-466.
59. Ross, M. and Young, D. A.: Theory of the equation of state at high pressure. *Annu. Rev. Phys. Chem.* **44** (1993) 61-87.

60. Bass, J. D.; Liebermann, R. C.; Weidner, D. J.; Finch, S. J.: Elastic properties from acoustic and volume compression experiments. *Phys. Earth Planet. Inter.* **25** (1981) 140-158.
61. King, Jr.; H. E.; Figer, L.: Diffracted beam crystal centering and its application to high-pressure crystallography. *J. Appl. Cryst.* **12** (1979) 374-378.
62. Wittlinger, J.; Werner, S.; Schulz, H.: Pressure-Induces Order-Disorder Phase Transition of Spinel Single Crystals, *Acta Cryst* **B54** (1998) 716.
63. Petricek, V.: *Crystallographic Computing System*, Praha: Institute of Physics Academy of Sciences of the Czech Republic (1997).
64. Sasaki, S., Numerical tables of anomalous scattering factors calculated by the Cromer and Liberman's method. KEK Report. **88-14** (1989) 1-136
65. Sasaki, S., X-ray absorption coefficient of the elements (LI TO BI, U). KEK Report. **90-16** (1990) 1-143.
66. Sheldrick, G.(1997). Program for crystal structure determination SHELX97, University of Cambridge.
67. Finger, L. W.: VOLCAL, Programm to calculate polyhedral volumes and distortions. Carnegie Inst. Of Washington Geophys. Lab. (1971).
68. Hazen, R. M. and Finger, L. W.: *Comparative Crystal Chemistry*. A Wiley-Interscience Publication (1982).
69. Aleksandrov, I. V.; Goncharov, A. F.; Zisman, A.N.; Stishov, S.M.: Diamond at high pressures: Raman scattering of light, equation of state, and high-pressure scale. *Sov. Phys. JETP.* **66** (1987) 680-691.
70. Takemura, K.: Evaluation of the hydrostaticity of a helium-pressure medium with powder x-ray diffraction techniques. *J. Appl. Phys.* **89** (2001) 662-668.
71. Pavlovska, A.; Werner, S. and Boehler, R.: Influence of high hydrostatic pressure on lattice parameters of a single crystals of LGN. Accepted for publication in *Z. Kristallogr.*
72. Pavlovska, A.; Werner, S.; Maksimov, B. and Mill, B.: Pressure-induced phase transitions of piezoelectric single crystals from langasite family: $\text{La}_3\text{Ga}_{5.5}\text{Nb}_{0.5}\text{O}_{14}$ and $\text{La}_3\text{Ga}_{5.5}\text{Ta}_{0.5}\text{O}_{14}$. Submitted to *Acta Cryst. B*.
73. Eysel, W.; Lambert, U.; Mayer, B. E.; Renkenberger, C.: Crystal structures and crystal chemistry of compounds $\text{M}_{5-p}\text{T}_{4+p}\text{O}_{14}$. *Z. Kristallogr.* **201** (1992) 235-251.
74. Giacovazzo, C. et al.: *Fundamentals of Crystallography*. Oxford University Press (1995) 429.

75. *International Tables for Crystallography Vol. A*, Dordrecht, Boston, London: ed. by Theo Hahn (1989).
76. *International Tables for Crystallography Vol. C*, Dordrecht, Boston, London: ed. by Wilson (1992).
77. Karki, B. B.; Ackland, G. J. and Grain, J.: Elastic instabilities in crystal from *ab initio* stress-strain relations. *J. Phys.: Condens. Matter.* **9** (1997) 8579-8589.
78. Belokoneva, E.L.; Stefanovich, S. Yu.; Pisarevskii, Yu. V. and Mosunov, A.V.: Refined structures of $\text{La}_3\text{Ga}_5\text{SiO}_{14}$ and $\text{Pb}_3\text{Ga}_2\text{Ge}_4\text{O}_{14}$ and the crystal-chemical regularities in the structure and properties of compounds of the langasite family. *Rus. J. Inorg. Chem.* **45** (2000) 1642-1651.
79. Hainess, J.; Leger, J.M.; Gorelli, F. and Hanfland, M.: Crystalline post-quartz phase in silica at high pressure. *Phys. Rev. Lett.* **87** (2001) 155503/1-155503/4.
80. Hemley, R.G.; Jephcoat, A. P.; Mao, H. K.; Ming, L.C.; Manghanani, M.H.: Pressure induced amorphization of crystalline silica. *Nature* **334** (1988) 52-54.
81. Kingma, K. J.; Hemley, R. J.; Mao, H. K. and Veblen, D. R.: New high-pressure transformation in α -quartz. *Phys. Rev. Lett.* **70** (1993) 3927.
82. Kim-Zajonz, J.; Werner, S. and Schulz, H.: High pressure single crystal X-ray diffraction study on α -quartz. *Z.Kristallogr.* **214** (1999) 324-330.
83. Hazen, R. M. and Prewitt, C. T.: Effects of Temperature and pressure on interatomic distances in oxygen-based minerals. *Amer. Miner.* **64** (1977) 309-315.
84. Hazen, R. M. & Finger, L.W.: Bulk modulus-volume relationship for cation-anion polyhedra. *J. Geophys. Res.* **64** (1979) 196-201.
85. Löchner, U.; Pennartz, P. U.; Mieke, G. and Fuess, H.: Synchrotron Powder Diffractometry at HASYLAB/DORIS-Reviewed. *Z. Kristallogr.* **204** (1993) 1-41.
86. Wölfel, E. R.: A new method for quantitative X-ray analysis of multiphase mixtures. *J. Appl. Crystallogr.* **16** (1983) 341-348.
87. Schneider, J.; Frey, F.; Johnson, N. and Laschke K.: Structure refinements of $\beta\text{-Si}_3\text{N}_4$ at temperatures up to 1360°C by X-ray powder investigation. *Z. Crystallogr.* **209** (1993) 328-333.
88. Maximov, B., private communication.
89. Schneider, J.: Profile refinement on IBM-PC's. *Int. Workshop on the rietveld Method, Petten* (1989) 71.
90. Pathak, P. D. and Vasavada N. G.: Thermal expansion of NaCl, KCl and CsBr by X-ray diffraction and the law of corresponding states. *Acta Cryst.* **A26** (1970) 655-658.

91. Cameron, M.; Sueno, S.; Prewitt, C. T. and Papike, J. J.: High-temperature crystal chemistry of acmite, diopside, hedenbergite, jadeite, spodumene and ureyite. *Am. Min.* **58** (1973) 594-618.
92. King, H. E. and Prewitt, L. W.: Improved pressure calibration system using the ruby R_1 fluorescence. *Rev. Scien. Instrum.* **51** (1980) 1037-1039.
93. Honal, M.; Fachberger, R.; Holzheu, T.; Riha, E.; Born, E.; Pontogratz, P.; Bausewein, A.: Langasite surface acoustic wave sensors for high temperatures IEEE/EIA Int. Frequency Control Symp. (2000) 113-118.
94. Chan, K. S.; Huang, T. L.; Grzybowski, T. A.; Whetten, T. J.; Ruoff, A. L.: Pressure concentrations due to plastic deformation of thin films of gaskets between anvils. *J. Appl. Phys.* **53** (1982) 6607-6612.
95. Liebenberg, D.H.: A new hydrostatic medium for diamond anvill cells to 300kbar pressure. *Phys. Lett. A* **73** (1979) 74-76.
96. LeSar, R.; Ekberg, S. A.; Jones, L. H.; Mills, R. L.; Schwabe, L. A.; Schifer, D.: Raman spectroscopy of solid nitrogen up to 374Kbar. *Solid State Commun.* **32** (1979) 131.134.
97. Asaumi, K.: High-pressure X-ray diffraction study of solid xenon and ist equation of state in relation to metallization transition. *Phys. Rev. B* **29** (1984) 7026-7029.
98. Pavlovska, A.; Maximov, B.; Schneider, J.; Werner, S.; Mill, B.: In preparation.

7. APPENDICES

7.1. APPENDIX A

Table 7.1. Cell dimensions of LGT and LGN materials at normal conditions as determined by different research groups

Who	<i>La3Ga5.5Nb0.5O14</i>			<i>La3Ga5.5Ta0.5O14</i>		
	<i>a</i> [Å]	<i>c</i> [Å]	<i>V</i> [Å ³]	<i>a</i> [Å]	<i>c</i> [Å]	<i>V</i> [Å ³]
Takeda¹ <i>et. al.</i> [23]	-	-	-	8.228(2)	5.124(2)	300.41
Bohm² <i>et. al.</i> [11]	8.233	5.129	299.25	8.236	5.128	301.23
Molchanov³ <i>et. al.</i> [22]	8.235(5)	5.129(2)	301.216	-	-	-
This study⁴	8.236(2)	5.130(1)	301.35(12)	8.235(3)	5.131(2)	301.34(25)

The results listed in Table 7.1 were obtained by following methods:

1) Single crystal X-ray diffraction, cell dimensions were determined by a least-squares fit to θ values ($20^\circ < \theta < 30^\circ$) of automatically centred 30 reflections. The e-mails of authors:

kawachu@lexus.imr.tohoku.ac.jp

hirodx@lexus.imr.tohoku.ac.jp

2) X-ray powder diffraction.

The e-mail of the leader of the research group:

heimann@mineral.tu-freiberg.de

3) Single crystal X-ray diffraction method. Cell parameters were calculated from angle position of 25 reflections within the θ range 27° - 32° . The e-mails of authors:

maximov@ns.crys.ras.ru

mill@plms.phys.msu.su

4) Single crystal X-ray diffraction method. Cell parameters were obtained by a least-squares fit to θ values ($25^\circ < \theta < 32^\circ$) of 16-24 reflections automatically centred in 4 different setup.

7.2. APPENDIX B

Table 7.2. The atomic coordinates of $\text{La}_3\text{Nb}_{0.5}\text{Ga}_{5.5}\text{O}_{14}$ at normal conditions

Atom	Wyck. pos.	q	x	y	z
La	3e	1.0	0.42459(2)	0.0	0.0
Ga:Nb=1:1	1a	0.5	0.0	0.0	0.0
Ga2	2d	1.0	0.33333	0.66667	0.53124(7)
Ga3	3f	1.0	0.76176(4)	0.0	0.5
O1	2d	1.0	0.33333	0.66667	0.1784(5)
O2	6g	1.0	0.4563(3)	0.3088(3)	0.3054(3)
O3	6g	1.0	0.2188(3)	0.0773(3)	0.7627(3)

Table 7.3. The interatomic distances [\AA] within the polyhedra of $\text{La}_3\text{Nb}_{0.5}\text{Ga}_{5.5}\text{O}_{14}$ at normal conditions

LaO₈-dodecahedra				Ga/NbO₆-octahedra	GaO₄-tetrahedra		GaO₄-tetrahedra	
La-O3 x2	La-O1 x2	La-O2 x2	La-O2' x2	Ga,Nb-O3 x6	Ga2-O1 x1	Ga2-O2 x3	Ga3-O3 x2	Ga3-O2 x2
2.413(3)	2.619(1)	2.464(2)	2.882(2)	1.995(2)	1.809(3)	1.840(2)	1.832(2)	1.873(2)

7.3. APPENDIX C

Table 7.4. The atomic coordinates of $\text{La}_3\text{Ta}_{0.5}\text{Ga}_{5.5}\text{O}_{14}$ at normal conditions

Atom	Wyck. pos.	q	x	y	z
La	3e	1.0	0.42492(7)	0.0	0.0
Ga:Ta 0.56:0.46	1a	0.5	0.0	0.0	0.0
Ga2	2d	1.0	0.33333	0.66667	0.4689(2)
Ga3	3f	1.0	0.7617(1)	0.0	0.5
O1	2d	1.0	0.33333	0.66667	0.822(2)
O2	6g	1.0	0.4568(7)	0.3089(8)	0.694(1)
O3	6g	1.0	0.2194(8)	0.0787(8)	0.241(1)

Table 7.5. The interatomic distances [\AA] within the polyhedra of $\text{La}_3\text{Ta}_{0.5}\text{Ga}_{5.5}\text{O}_{14}$ at normal conditions

LaO₈-dodecahedra				Ga/TaO₆-octahedra	GaO₄-tetrahedra		GaO₄-tetrahedra	
La-O3 x2	La-O1 x2	La-O2 x2	La-O2' x2	Ga,Ta-O3 x6	Ga2-O1 x1	Ga2-O2 x3	Ga3-O3 x2	Ga3-O2 x2
2.428(7)	2.618(3)	2.464(6)	2.885(6)	2.007(6)	1.810(8)	1.836(6)	1.819(6)	1.874(6)

7.4 APPENDIX D

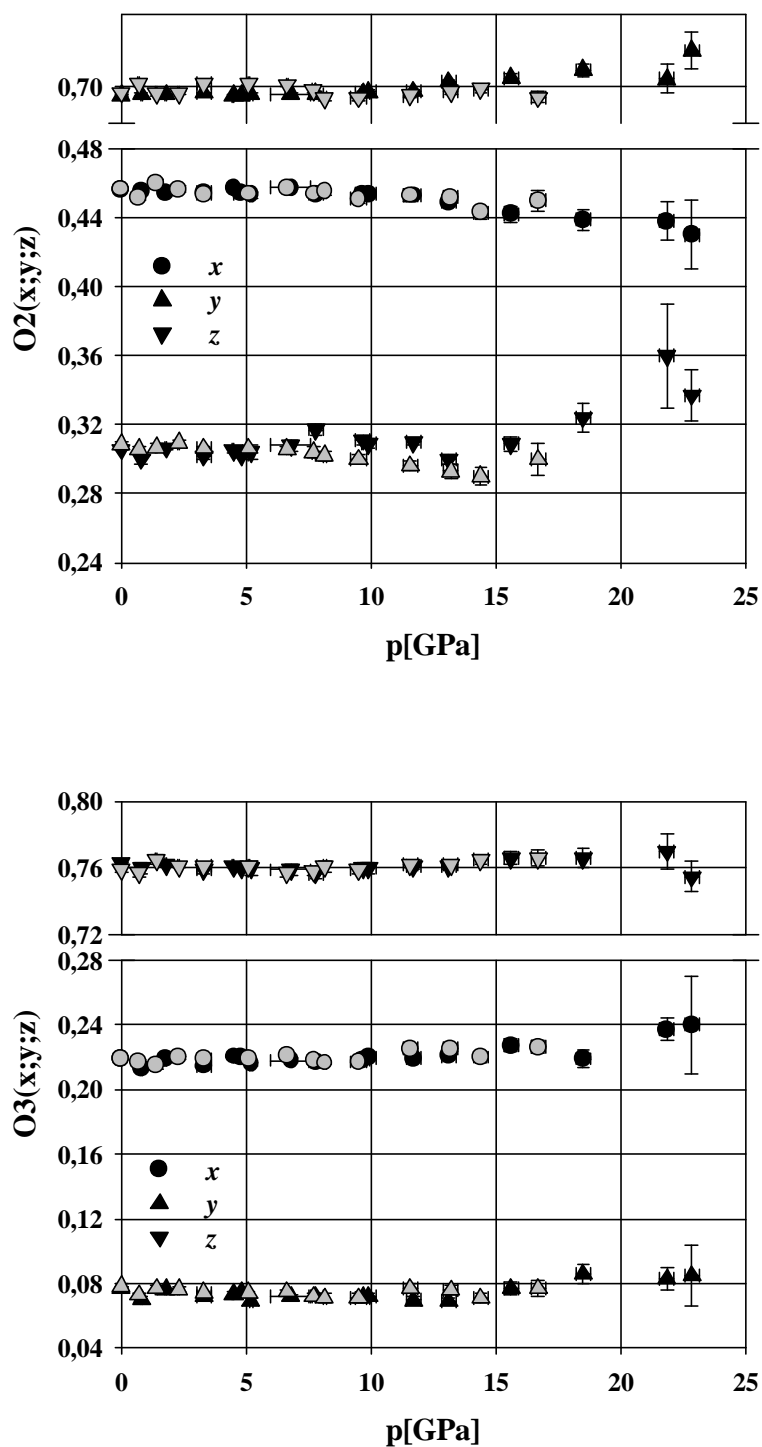


Fig. 7.1: Pressure dependencies of positional parameters of oxygen O(2), O(3) of LNG (black symbols) and LTG (grey symbols) refined in trigonal symmetry (space group $P321$)

7.5. APPENDIX E

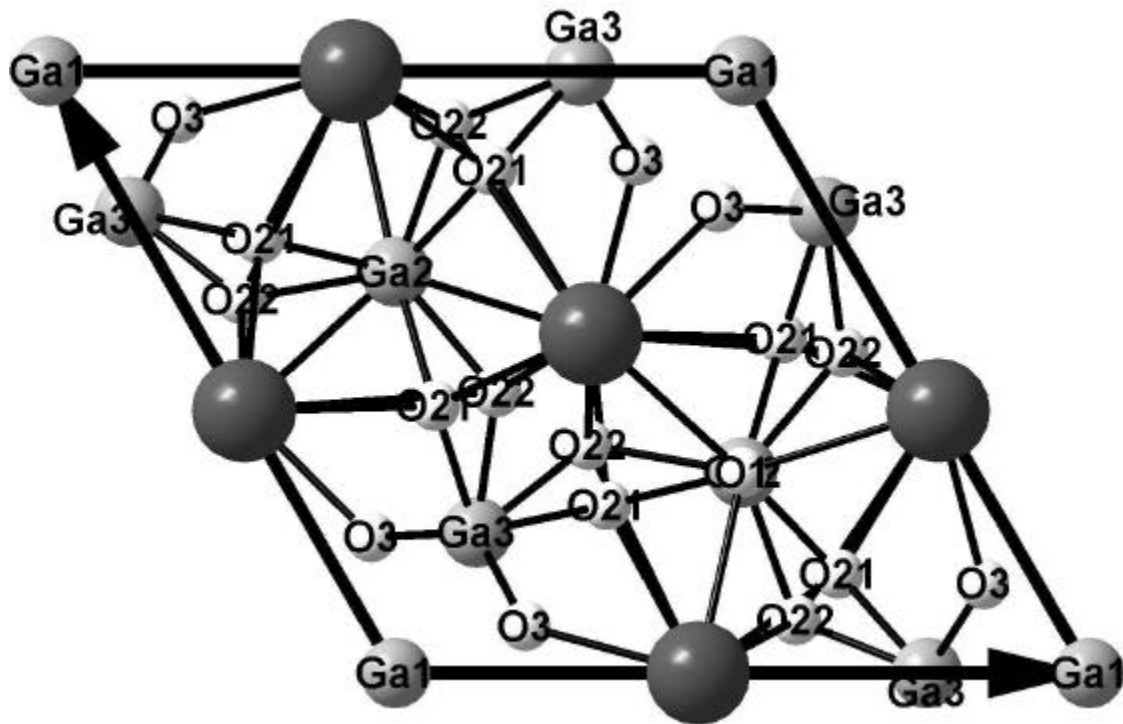


Fig. 7.2: Structural model of LNG at pressure 15.6GPa refined in space group $P321$ with split positions for O2(O21-O22).

7.6. APPENDIX F

Table⁶ 7.6. The difference between observed and calculated structure factors ($F^2_c - F^2_o$) for the reflections of LNG at pressure 15.6 GPa with the largest differences between calculated structure factors ($F^2_{c1} - F^2_{c2}$) for refinements in *P321* and *A2* space groups.

?	<i>h k l</i>	$F^2_{c1} - F^2_{c2}$	$F^2_{o1} - F^2_{c1}$	$F^2_{o2} - F^2_{c2}$
1	-3 0 8	205,00	62,54	18,41
2	2 0 16	196,14	76,41	28,39
3	7 2 22	172,06	92,06	77,85
4	0 8 8	117,28	52,62	6,69
5	-2 -8 18	99,75	45,76	11,06
6	7 -5 19	94,84	89,84	79,70
7	1 -1 17	94,51	60,74	21,71
8	-5 6 16	88,57	67,89	37,93
9	1 1 17	82,29	16,39	56,23
10	1 3 25	79,51	26,00	84,46
11	0 -8 8	68,54	62,51	34,51
12	-1 -8 24	68,02	85,13	74,38
13	0 0 16	65,81	77,44	61,64
14	2 -1 17	57,62	55,64	28,32
15	-2 5 21	55,51	10,86	49,45
16	5 2 22	54,02	61,45	39,14
17	1 -3 25	53,933	34,68	69,15
18	-4 1 3	53,30	28,35	13,85
19	2 1 17	50,46	47,62	19,21
20	1 -4 26	49,55	30,35	6,78
21	7 -2 22	47,36	88,80	83,09
22	6 0 24	47,15	41,23	11,35
23	3 0 22	46,97	35,10	2,22
24	-3 8 18	45,72	46,77	18,32
25	1 5 23	45,63	42,87	20,37
26	0 -1 17	45,35	37,41	6,74
27	-1 10 4	45,22	44,00	15,71
28	-1 1 17	44,44	8,53	35,44
29	7 5 19	41,06	66,75	51,93
30	-4 7 17	40,10	43,07	12,14
$\sum_{30}^{n=1}$			1538,88	1076,21

⁶ F_{c1} and F_{c2} calculated structure factors for refinements in *P321* and *A2*, respectively. F_o - observed structure factors.

Table⁷ 7.7. The difference between observed and calculated structure factors ($F^2_c - F^2_o$) for the reflections of LNG at pressure 0.8 GPa with the largest differences between calculated structure factors ($F^2_{c1} - F^2_{c2}$) for refinements in *P321* and *A2* space groups.

?	<i>h k l</i>	$F^2_{c1} - F^2_{c2}$	$F^2_{o1} - F^2_{c1}$	$F^2_{o2} - F^2_{c2}$
1	-4 8 6	42,70	32,66	4,47
2	0 -2 18	40,28	30,32	4,88
3	1 -5 17	40,15	7,55	26,62
4	0 2 18	38,48	25,66	1,49
5	2 -7 9	36,03	9,36	15,61
6	-4 -6 4	34,60	3,99	6
7	2 7 9	33,98	0,39	23,21
8	0 -7 15	32,95	2,24	19,10
9	0 7 15	32,59	7,73	30,54
10	-4 -7 9	32,40	51,84	42,10
11	-4 6 4	32,22	12,66	4,93
12	-1 3 19	32,03	13,30	4,25
13	0 3 19	31,97	26,07	10,37
14	-2 5 17	31,85	0,14	19,38
15	-2 -5 17	31,78	13,49	3,33
16	0 -3 19	31,64	1,82	18,56
17	0 7 17	31,12	0,70	19,83
18	-1 0 20	31,03	15,43	0,58
19	-1 -7 17	31,02	15,78	0,23
20	-1 7 17	30,45	0,21	18,31
21	1 -7 17	30,11	1,47	19,76
22	-1 -9 13	29,82	3,48	12,34
23	-1 -3 19	29,80	16,69	2,99
24	1 7 17	29,77	2,39	20,19
25	0 -7 17	29,54	5,90	23,21
26	0 -4 16	29,28	0,13	17,19
27	0 -8 14	29,23	7,40	8,03
28	1 -3 15	29,17	5,66	22,21
29	0 4 16	29,11	1,52	15,35
30	0 -5 17	29,05	22,23	10,64
$\sum_{30}^{n=1}$			338,26	449,21

⁷ F_{c1} and F_{c2} calculated structure factors for refinements in *P321* and *A2*, respectively. F_o - observed structure factors.

7.6. APPENDIX G

Table 7.8. Coordinates of atoms of $\text{La}_3\text{Sb}_1\text{Zn}_3\text{Ge}_2\text{O}_{14}$ and their isotropic thermal parameters at normal conditions.

atom	Positio n	x	y	z	B_j
La1	2a	0.0	0.422656	0.0	0.76
La2	4c	0.00031(4)	0.28863(5)	0.28857(2)	0.88
Sb	2a	0.0	0.00043(7)	0.0	0.46
Zn1	2b	0.5	0.25979(10)	0.5	0.56
Zn2	4c	0.50013(9)	0.12017(9)	0.12011(4)	0.66
Ge	4c	0.46139(9)	0.00006(8)	0.33338(8)	0.38
O1	4c	0.2123(6)	0.4748(4)	0.3836(2)	1.46
O2	4c	0.8008(6)	0.0010(5)	0.3336(2)	1.23
O3	4c	0.7860(7)	0.3435(4)	0.4312(3)	1.56
O4	4c	0.2147(6)	0.1836(4)	0.0437(2)	1.78
O5	4c	0.3017(10)	0.1172(7)	0.4164(2)	1.21
O6	4c	0.2970(10)	0.0645(7)	0.2341(4)	1.54
O7	4c	0.7012(9)	0.3173(6)	0.1520(3)	1.67

Lebenslauf

Name	Anzhela Pavlovska
Geburtsdatum	1.06.74
Geburtsort	Belowa (Rußland)
Familienstand	verheiratet
1981-1988	Schule, St. Leningradski (Rußland)
1988-1991	Schule, St. Makarov (Ukraine)
1991-1997	Studium der Physik von Metallen an der Nationalen Technischen Universität der Ukraine
1997	Diplom in Physik von Metallen, Thema der Diplomarbeit: <i>„Phasenübergang bei Nitrieren von Fe-V Legierungen in Sinterkörpern“</i>
1997-1999	Wissenschaftliche Mitarbeiterin an der Nationalen Technischen Universität der Ukraine
seit 1999	Wissenschaftliche Mitarbeiterin am Institut für Kristallographie und Angewandte Mineralogie, Universität München